The Exeter Partnerships:
An Insider's Comments on Effectiveness

Energy-aware Approaches for Energy Harvesting Powered Wireless Sensor Systems

Submitted by Tingwen Ruan to the University of Exeter
as a thesis for the degree of
Doctor of Philosophy in Engineering
In May 2019

I certify that all material in this thesis which is not my own work has been identified and that no material has previously been submitted and approved for the award of a degree by this or any other University.

Tingwen Ruan

Signature: ……..

ABSTRACT

Energy harvesting (EH) powered wireless sensor systems (WSSs) are gaining increasing popularity since they enable the system to be self-powering, long-lasting, almost maintenance-free, and environmentally friendly. However, the mismatch between energy generated by harvesters and energy demanded by WSS to perform the required tasks is always a bottleneck as the ambient environmental energy is limited, and the WSS is power hunger.

Therefore, the thesis has proposed, designed, implemented, and tested the energy-aware approaches for wireless sensor motes (WSMs) and wireless sensor networks (WSNs), including hardware energy-aware interface (EAI), software EAI, sensing EAI and network energy-aware approaches to address this mismatch.

The main contributions of this thesis to the research community are designing the energy-aware approaches for EH Powered WSMs and WSNs which enables a >30 times reduction in sleep power consumption of WSNs for successful EH powering WSNs without a start-up issue in the condition of mismatch between the energy generated by harvesters and energy demanded by WSSs in both mote and network systems.

For EH powered WSM systems, the energy-aware approaches have (1) enabled the harvested energy to be accumulated in energy storage devices to deal with the mismatch for the operation of the WSMs without the start-up issue, (2) enabled a commercial available WSMs with a reduced sleep current from 28.3 µA to 0.95 µA for the developed WSM, (3) thus enabled the WSM operations for

a long active time of about 1.15 s in every 7.79 s to sample and transmit a large number of data (e.g., 388 bytes), rather than a few ten milliseconds and a few bytes.

For EH powered WSN systems, on top of energy-aware approached for EH powered WSM, the network energy-aware approaches have presented additional capabilities for network joining process for energy-saving and enabled EH powered WSNs. Once the EH powered WSM with the network energy-aware approach is powered up and began the network joining process, energy, as an example of 48.23 mJ for a tested case, has been saved in the case of the attempt to join the network unsuccessfully. Once the EH-WSM has joined the network successfully, the smart programme applications that incorporate the software EAI, sensing EAI and hardware EAI allow the EH powered WSM to achieve (4) asynchronous operation or (5) synchronised operation based on the energy available after the WSM has joined the network.

Through designs, implementations, and analyses, it has been shown that the developed energy-aware approaches have provided an enabled capability for EH successfully powering WSS technologies in the condition of energy mismatch, and it has the potential to be used for wide industrial applications.

Index Terms— Energy-aware approaches, hardware energy-aware interface, software energy-aware interface, sensing energy-aware interface, network energy-aware approaches, energy harvesting powered wireless sensor system (WSS), wireless sensor mote (WSM), wireless sensor network (WSN)

ACKNOWLEDGMENTS

This is an excellent opportunity to express my gratitude and respect to all the people who supported me while I was doing my PHD. They all contributed to this work in their way. A special gratitude I give to my supervisor Professor Meiling Zhu, who has guided, advised and helped me to go through the whole PhD study in many ways.

I would like to express my great appreciation to my colleges, Dr. Zheng Jun Chew and Dr. Yang Kuang, for guiding and inspiring me during my research period and for showing me what the research is about.

I would like to give my thanks to the financial support from the Innovate UK grant: "SENTIENT: *SENsors To Inform & Enable wireless Networks"* for developing self-powered wireless sensor motes for integrated vehicle health management using vibration energy harvested. Also, I would like to thank Professor Meiling Zhu for giving me an excellent opportunity to work in the EPSRC grants of: "SMARTER: *Smart Multifunctional ARchitecture & Technology for Energy aware wireless sensoRs"* and "En-ComE: *Energy Harvesting Powered Wireless Monitoring Systems Based on Integrated Smart Composite Structures and Energy-Aware Architecture"*.

I would also like to thank my friends. I appreciate all the knowledge we exchanged and all the laughs we shared together. My deepest thanks I would like to give to my parents, your love, support and tolerance have always been my source of courage and momentum to keep going.

Contents

List of Figures

List of Tables

Nomenclature

Acronyms & Abbreviations

AAM	Asynchronous Acceleration Measurements
AC	Alternating Current
A/D	Analog-to-digital
ADC	Analog to Digital Converter
API	Integrated Peripherals Application Programming Interface
ARM	Advanced RISC Machine
ASN	Absolute Slot Number
BLE	Bluetooth Low Energy
CPU	Central Processing Unit
CTCA	Cooperative Topology Control with Adaptation
DAC	Digital Converter to Analog
DC	Direct Current
Dest. PAN ID	Destination Personal Area Network identifier
Dest. Address	Destination Address
DIO	Input / Output
DTV	Digital Television
EAI	Energy-aware Interface
EH	Energy Harvesting
FCS	Frame Check Sequence
FFD	Full Function Devices
GPIO	General Purpose Input/Output
GSM	Global System for Mobile Communications
IDE	Integrated Development Environment
JTAG	Joint Test Action Group
LoRa	Long Range Radio
LPWAN	Low-power Wide-area Network
MAC	Media Access Control
MCU	Microcontroller Unit
MFC	Macro-fibre Composite
MFR	Media Access Control Footer
MHR	Media Access Control Header
MQAM	M-ary Quadrature Amplitude Modulation
N-MOSFET	N-Metal Oxide Semiconductor Field-Effect Transistor
NPLC	Number of Power Line Cycles
PAN	Personal Area Network
PMM	Power Management Module
PMMT	Maximum Power Point Tracking
P-MOSFET	P-Metal Oxide Semiconductor Field-Effect Transistor
P2P	Peer-to-peer

RC	Resistor and Capacitor
RF	Radio Frequency
RFD	Reduced Function Devices
RFID	Radio Frequency Identification
RH	Relative Humidity
RISC	Reduced Instruction Set Computing
RX	Receive
SAM	Synchronous Acceleration Measurements
SDK	Software Developer’s Kit
TEG	Thermoelectric Generator
TSCH	Time Slotted Channel Hopping
TX	Transmission
UTC	Coordinated Universal Time
UWB	Ultra-wide Band
WSM	Wireless Sensor Motes
WSN	Wireless Sensor Network
WSS	Wireless Sensor System
3G	Third Generation
et al	and others
Fig.	Figure
Tab.	Table

Symbols

cm^2	centimetres squared
dBm	power ratio in decibels of the measured power referenced to one milliwatt.
g	gravitational acceleration
GHz	gigahertz
Hz	hertz
KB	kilobyte
kbps	kilobits per second
kg	kilogram
kHz	kilohertz
km/h	kilometers per hour
m	metres
mA	milliampere
Mbps	megabit per second
MHz	megahertz
mm^2	millimetres squared
mJ	millijoule
mJ/Mb	millijoule of transmitting 1 Mb data
mW	milliwatt
m/s	metre per second
nW	nanowatt

s	second
W	watt
µA	microampere
µW	microwatt
µε	microstrain
Ø	Diameter
°C	Temperature

Variables

a	the number of bytes of the WSM transmission data
b	the pre-set number of bytes of the WSM transmission data
C	the capacitance of the energy storage capacitor
C_S	the energy storage device
E_{b-samp}	the energy required for the WSM to complete the basic sampling task including sampling, transmitting and resetting the hardware EAI
E_{con}	the remaining energy in the capacitor
$E_{connected}$	the average energy required for the WSM to complete the connecting process
E_{CS}	the total energy that has been outputted by the PMM from the time beginning at t_i to the end at t_n
$E_{\text{effective}}$	the effective energy stored in the capacitor
$E_{max-low}$	the maximum consumed energy of the WSM by staying in the low-voltage search process
E_{nego}	the average energy required for the WSM to complete the negotiating process
$E_{required}$	the energy required for the next operation of the WSM
E_{reset}	the energy required for resetting the voltage supervisor
E_s	the accumulated energy stored in the storage device
E_{samp-1}	the energy required for sampling one byte of data
$E_{tx-samp}$	the energy required for taking one pre-set cycle sensor reading and transmitting all the data
E_{tx-1}	the energy required for transmitting one byte of data
E_w	the whole energy consumption of the WSM in a period of time
I_{ave}	the average current of the WSM measured within a fixed timeframe of T
I_{CS}	the input current to the storage device
I_{w}	the current through the WSM
M	the number of the WSM sampling cycles
n	the number of data points
P_{ave}	the average power over the time period T
P_{low-v}	the average power consumed by the WSM in the low-voltage search process
P_w	the instantaneous power consumption of the WSM
T	a fixed timeframe for calculating I_{ave} and V_{ave}

$T_{\max-\text{low}}$	the maximum time that the WSM is able to stay in the low-voltage search process
T_{reportms}	the pre-set time for the WSM synchronously repeating acceleration measurements in the SAM application
T_{sec}	the number of seconds since midnight of January 1, 1970, represented in the SAM application
T_{usec}	the number of microseconds since the beginning of the current second in the SAM application
T_{waitms}	the waiting time for the WSM start the next acceleration measurements in the SAM application
t_i	beginning time when calculate E_w
t_k	The instantaneous time
t_n	end time when calculate E_w
V_{ave}	the average voltage of the WSM measured within a fixed timeframe of T
V_{CS}	voltage across the storage device
$V_{\text{cs}-\text{sample}}$	the measured voltage across the super-capacitor after WSM completing the accelerometer sampling function in the basic sampling application
$V_{\text{cs}-\text{schedule}}$	the measured voltage across the super-capacitor after WSM synchronously transmit the data to the network manager in the SAM application
V_{END}	the voltage that is used to judge whether the capacitor has enough effective energy to supply the WSM to perform the next tasks
V_{H-on}	defined turn-on threshold voltage of the voltage supervisor circuit
V_{H-off}	defined turn-off threshold voltage of the voltage supervisor circuit
V_{judge}	a pre-set voltage to determine if WSM does the next sampling process at Chapter 6
V_{MIN}	the minimum operating voltage of the WSM
$V_{\min}$	the pre-set minimum operating voltage of the WSM
$V_{\min-\text{schedule}}$	the minimum voltage across the super-capacitor to meet the energy requirement for the WSM implementing one measurement cycle
V_{S-off}	the voltage that is used to judge whether the capacitor has enough effective energy to supply the WSM to perform the next tasks
V_{w}	the voltage across the WSM
Δt	the sampling time interval set by the source meter

Chapter 1 Introduction

1.1 Background

Traditionally, sensors are wired where cables are essential for their power supply and data transmission. As the technologies advance, in the last decade there has been an increasing interest in the development of wireless sensor systems (WSSs), since they offer an attractive wireless solution to various monitoring applications for many industrial sectors, such as: aerospace [1], agriculture [2], building automation [3], health and medical cares [4], industrial process control [5], infrastructure and structures [6], oil and gas [7], and railway [8].

The significant advantage of WSSs over wired systems is that WSSs are easier, more flexible, and cheaper to be installed due to without the need for cables, and therefore, there are much fewer restrictions on the WSS installations[9]. The benefits of using WSS in industrial applications can be: reducing the weight and installation complexity by eliminating extensive cabling, reducing the chance of an entire system failure due to a common cable fault, enabled predictive maintenance as more sensors can be easily installed, and allowed more measurements to take.

The WSSs can be typically classified into wireless sensor motes (WSMs) and wireless sensor networks (WSNs). Generally, a WSM consists of three basic blocks: (1) a microcontroller unit for controlling the system and processing data, (2) a sensing unit for sampling data from one or more sensors, and (3) a wireless communication unit for communicating and sending data to the base station; a

WSN system is composed of a number of WSMs and a network manager for receiving data and managing the network.

One of the significant problems WSS facing industries today is their energy supply [9, 10, 11] since once the energy supply of the WSS is depleted, it will no longer play its role in the application unless either the energy supply is replaced or EH devices are built in the system. Currently, the energy source used by most of the WSS is batteries, but there are many problems associated with them. Firstly, the batteries have a limited capacity and need to be replaced. Secondly, the leakage current of the batteries cannot be ignored. Batteries will gradually discharge even if they are not used. Thirdly, the damage on the batteries, whether caused by internal problems such as short circuits or external problems such as extreme weather conditions, can lead to chemical leaks that cause various environmental problems. Finally, due to the limited energy capacity of the batteries, it may hinder the long-term operation of the WSS [12]. In most WSS application scenarios, the lifetime of each WSM is required to range from several months to several years, but often their operations have to end prematurely due to depleted batteries. Moreover, if the deployment of the WSMs is in hostile and challenging terrain or the large number of WSMs is deployed, it is challenging, sometimes impossible, to recharge or replace the batteries.

There are, therefore, significant demands of exploring a new type of power source to solve the problems above. Energy harvesting (EH) technologies have emerged to be a potential solution for the perpetual operation of WSS and can be used to generate energy through harvesting ambient surroundings energy of WSS to provide power supply for one specific WSM system or the overall WSMs in a

WSN system. The EH sources of ambient surroundings generally include radio frequency (RF), solar, thermal, flow, mechanical-based, and human-based EH sources.

Ambient sources such as solar, thermal, and wind flow are readily available in the environment at almost no cost [13]. On the other hand, energy sources such as mechanical vibration, structural stress-strain energy, and human motion energy are deployed explicitly in the structures and humans, which can be harnessed for EH purposes [14].

Compared with batteries, the EH technologies use the ambient energy sources without the need of batteries and, therefore, without replacement of batteries, to provide energy that is renewable and more environmentally friendly. They can harvest the ambient energy that is being wasted, such as vibration, radio waves, or simply mechanical energy from people in motion. Moreover, from the point of view of the actual applications and working environments of WSS, the EH technologies are more suitable than the batteries powered WSS in most cases. For example, the embedded WSSs are expected to work in a closed environment for several years, so replacing the battery is no longer an option [9].

Therefore, all of the above factors encourage the use of EH technologies in WSS, since it enables WSS to be self-powering, long-lasting, almost maintenance-free, and also environmentally friendly. However, to date, there are just a few implementations of EH-WSS e.g., [14, 15, 16, 17, 18]. The main reason is that the energy generated by energy harvesters is not high enough for powering the WSS as commercially available WSS is power hungry. This means there is a

mismatch between the energy generated by the harvesters and the energy demanded by the WSS to perform the required tasks. Therefore, there is a need to deal with this mismatch by increasing the amount of power that can be harvested and/or extracted to WSS and reducing the power consumption of WSS.

To increase the energy harvested to power the WSS, there has been a large number of research interests in the world in designing energy harvesters to improve the amount of harvested energy, e.g., [19, 20, 21, 22, 23]. Another practical approach is to place an efficient and effective power management module (PMM) in between the energy harvester and the WSS to deliver as much power as possible from the energy harvester to WSS under various conditions [24].

To reduce the power consumption of WSS is extremely important for EH enabled WSS. It is essential to understand the power consumption characteristics of a WSM operating in every process, especially for the sampling and transmission processes, but there are just a few types of research working on this, e.g., [25] and [26]. Systematic energy consumption analyses of a WSM is, therefore, one of the target research in the thesis.

There is a growing consensus that a comprehensive approach is needed, one that addresses all levels of the system [27]. One of the useful approaches is to incorporate energy awareness into the energy harvesting powered wireless sensor systems (EH-WSS), which enables the energy-constrained WSM to work appropriately with low power consumption in the system [28]. The energy-aware approaches are a suite of techniques that is able to reduce the power

consumption and perform energy usage optimisation based on the energy level while targeting all stages of EH-WSS from the underlying hardware components to the application software and communication protocols [28]. For example, in addition to using low power consumption hardware components in the EH-WSS system, the energy-constrained WSM is required to have the capacity to estimate the energy requirement of an application that has to be executed and make subsequent decisions about its processing ability based on the energy it has at that moment.

This thesis focuses on developing the energy-aware approaches for EH powered WSS, and the energy-aware approaches will be realised by the use of combined hardware and software methods. The thesis will use commercially available WSMs for the research. The developments of energy harvesters and power management solutions are out of the scope of the thesis.

1.2 Aim and Objectives

1.2.1 Aim

The research aim is to develop smart energy-aware approaches for EH powered WSMs or WSNs, enabled the motes and the networks to be powered by EH. The research purpose is to achieve self-powered and battery-free WSS for a wide range of industry applications, including structural and environmental monitoring.

1.2.2 Objectives

- To develop an understanding of WSM power consumption for the development of EH powered WSMs;

- To identify key issues of EH directly powered WSMs and develop smart energy-aware approaches to solve the identified issues, enabled successful EH powered WSMs in one-way communication operations;
- To analyse the energy of network behaviour in EH powered WSN and identify issues in the network joining process.
- To develop network energy-aware approaches to reduce the energy consumption of the WSM joining the network for EH powered WSNs enabled successful EH powered WSMs in network two-way communication operations.
- To enable EH powered WSNs for structural and environmental monitoring applications.

1.2.3 Results of the Research

The author has proposed, designed, implemented, and tested the energy-aware approaches, including hardware energy-aware interface (EAI), software EAI, sensing EAI, and network energy-aware approaches to address the EH powered WSM and WSN challenges, enabling their successful operations. The main contributions of this thesis to the research community are the **smart mote and network energy-aware approaches –** which enables a >30 times reduction in sleep power consumption of WSNs for successful EH powering WSNs without the start-up issue in the condition of mismatch between the energy generated by harvesters and demanded by WSNs in both mote and network systems. For EH powered WSM systems, the energy-aware approaches have (1) enabled the harvested energy to be accumulated in the energy storage device to deal with the mismatch for the operation of the WSM; (2) solved the start-up issue and enabled a commercial available WSM with a reduced sleep current from 28.3 µA to 0.95 µA; (3) enabled the WSM operations for a long active time of about

1.15 s in every 7.79 s to sample and transmit a large number of data (e.g., 388 bytes), rather than a few ten milliseconds and a few bytes. Moreover, for EH powered WSN systems, on top of energy-aware approached for EH powered WSM, the network energy-aware approaches have additional capabilities for network joining process. The capabilities are explained here. Once the EH powered WSM with the network energy-aware algorithm is powered up and began the network joining process, energy, as an example of 48.23 mJ for a tested case, can be saved when the attempt to join the network failed. Once the EH powered WSM has joined the network successfully, the different programme applications that incorporate the software EAI, sensing EAI, and hardware EAI allow the EH powered WSM to achieve asynchronous operation or synchronised operation based on the energy level left after the WSM has joined the network.

1.3 Research Methodology

A key research question of EH powered WSS is the mismatch between the energy generated by the harvesters and the energy demanded by the WSS, as the energy harvested is limited, and the WSS is power hungry. Therefore, the thesis is proposed to address this mismatch by using the following research methodologies via three steps:

1. **Background investigations**

- Through (1) reviewing the EH techniques that can be used to extract energy from different available sources, focusing on the power output that can be harvested by the different available energy sources to date; (2)

reviewing the wireless communication technologies and the off-the-shelf commercial chips, focusing on the energy consumption of transmission and receive processes, (3) comparing the energy generated by the harvesters and the energy demanded by the WSS, a key research question of EH powered WSS is proposed, which is the mismatch between the energy generated by the harvesters and the energy demanded by the WSS, as the energy harvested is limited, and the WSS is power hungry;

- Determine reducing the energy consumption of WSS to deal with the mismatch and then determine the scope of thesis is energy-aware approaches for EH powered WSS by reviewing the energy-saving mechanisms for WSS;

- By reviewing the energy-aware approaches for EH powered WSS, the detailed research gaps to be addressed in the thesis are analysed.

  a) Lack of available information focusing on energy consumption of EH powered WSM and WSN;
  b) Lack of an interface between EH and WSS able to be efficient energy management and energy storage in the context of track condition monitoring user cases;
  c) Lack of the energy-saving approaches that focus on enabling the EH powered WSS to sample, transmission, commutation, and joining the network with the limited energy, since most of the previous energy-saving approaches on the WSM and WSN are powered by batteries;

d) Lack of a comprehensive energy-aware approach that considers energy-saving or maximum energy utilisation during the active phase of the EH powered WSS;

e) Lack of energy efficient hardware and software approaches to decrease current consumption for sleeping and for transmission in computing, sensing and communication to achieve ultra-low-power consumptions for implementation of EH powered WSS.

2. Preliminary experiments and analyse the causes of issues

- Through reviewing the energy consumption of wireless communication technologies and the off-the-shelf commercial chips, select the suitable commercially available wireless commutation, microcontrollers, wireless transceivers and sensors for the development of EH powered WSS. The choices are mainly based on the low energy consumption, especially in the transmission and receive processes;

- Implement a battery powered WSM with one-way communication and analyse the energy consumption of the WSM through the experimental testing to develop an understanding of power consumption of every process of the WSM;

- Replace the battery with EH power supply, and analyse the causes of issues that the WSM is not able to be powered to wake up: (1) the mismatch between the energy generated by the harvesters and the energy demanded by the WSMs to carry out required tasks and (2) the WSM start-up issue;

- Develop EH powered WSN systems with two-way communication, analyse the energy consumption of the developed system and analyse the causes of issues of the network joining process in power demanding, especially for search processes, and in randomness that the undetermined energy consumption of WSM joining the network.

3. Propose the approaches to solve the issues based on the analysed causes

- Propose energy-aware concepts and implement the energy-aware approaches for EH powered WSM, including hardware EAI, software EAI and sensing EAI, which aim to manage the energy flow from the energy storage capacitor to the WSMs to deal with the mismatch and the start-up issues;

- In order to solve the problem of the uncertainty of the EH powered WSM joining the network in the EH powered WSN, network energy-aware approaches are designed to trace the energy consumption of every EH powered WSM in the EH powered WSN during the targeted joining network processes especially for those with high power consumption and a long, uncertain time.

1.4 Paper Publications

Journal Articles:

1. **Ruan T.**, Chew Z. J. & Zhu M. (2017). Energy-aware approaches for energy harvesting powered wireless sensor nodes. *IEEE Sensors Journal*, 17(7), 2165–2173.

    - **Ruan T**: propose, design, implement and test the energy-aware approaches;
    - Chew Z. J: Propose, design, implement the PMM circuit.

    - One of the 25 most downloaded IEEE Sensors Journal papers in the months of March 2017, August, September, October, November and December 2018, and January 2019.

2. Chew Z. J, **Ruan T.** & Zhu M (2018). Power Management Circuit for Wireless Sensor Nodes Powered by Energy Harvesting: On the Synergy of Harvester and Load. *IEEE Transactions on Power Electronics* (Volume: 34, Issue: 9, Sept. 2019，Page(s): 8671 - 8681).

    - **Ruan T**: propose, design, and implement the energy-aware approaches;
    - Chew Z. J: propose, design, implement the PMM circuit and test its performance.

3. Chew Z. J, **Ruan T.** & Zhu M (2017). Strain Energy Harvesting Powered Wireless Sensor System Using Adaptive and Energy-Aware Interface for Enhanced Performance. *IEEE Transactions on Industrial Informatics* (Volume: 13, Issue: 6, Dec. 2017，Page(s): 3006 - 3016).

    - **Ruan T**: propose, design, implement energy-aware approaches and test the system with the energy-aware approaches；
    - Chew Z. J: propose, design, implement the PMM circuit and test the performance of whole system from energy harvester to WSM.

4. Chew Z. J, **Ruan T.**, Zhu M, Bafleur M. & Dilhac J.-M (2017). Single piezoelectric transducer as strain sensor and energy harvester using time-multiplexing operation. *IEEE Transactions on Industrial Electronics* (Volume: 64, Issue: 12, Dec. 2017, Page(s): 9646 - 9656).

    - **Ruan T**: propose, design and implement energy-aware approaches.
    - Chew Z. J: propose, design, implement the PMM circuit and design the sensor algorithm.

5. Kuang Y., **Ruan T.**, Chew Z. J. & Zhu M. (2017). Energy harvesting during human walking to power a wireless sensor node. *Sensors & Actuators A: Physical*, 254, 69–77.

    - **Ruan T**: propose, design and implement energy-aware approaches;
    - Chew Z. J: propose, design, implement the PMM circuit;
    - Kuang Y: design and implement the energy harvester.

Conference Papers:

1. Chew Z. J, **Ruan T.** & Zhu M (2019). Energy Harvesting Powered Wireless Sensor Nodes With Energy Efficient Network Joining Strategies. For IEEE International Conference on Industrial Informatics, INDIN'19

2. Chew Z. J., **Ruan T.**, Zhu M., Bafleur M. & Dilhac J-M. (2017). "A multifunctional device as both strain sensor and energy harvester for structural health monitoring". *IEEE Sensors 2016*, Orlando, Florida, USA, 30 October–3 November, DOI:10.1109/ICSENS.2016.7808554.

3. Kuang Y., **Ruan T.**, Chew Z. J. & Zhu M. (2016). Energy autonomous wireless sensing system enabled by energy generated during human walking. *Journal of Physics: Conference Series*, 773(1), 012050.

4. Chew Z. J., **Ruan T.** & Zhu M. (2016). Strain energy harvesting powered wireless sensor node for aircraft structural health monitoring. *Procedia Engineering*, 168, 1717–1720.

5. Somov, A., Chew, Z. J., **Ruan, T.**, Li, Q., & Zhu, M. (2016, April). Piezoelectric energy harvesting powered WSN for aircraft structural health monitoring. In *Information Processing in Sensor Networks (IPSN), 2016 15th ACM/IEEE International Conference on* (pp. 1-2). IEEE.

6. Somov, A., Chew, Z. J., **Ruan, T.**, Zhu, M., & Platt, S. P. (2016, October). Ultra-low-power RADFET sensing circuit for wireless sensor networks powered by energy harvesting. In *SENSORS, 2016 IEEE* (pp. 1-3). IEEE.

1.5 Thesis Structure

The thesis consists of seven chapters in total. This section provides a general overview of the thesis and summarises the content of each chapter.

Chapter 1 gives an introduction to this thesis. This chapter opens by describing the background and motivation of the thesis. Following this, the aim and objectives, and the thesis structure are described.

Chapter 2 presents the literature review, which begins by reviewing the EH techniques that can be used to extract energy from different available sources and focusing on the power output that can be harvested by the different available energy sources to date. After that, wireless communication technologies, protocols, and the off-the-shelf commercial chips are reviewed and compared in performance for the EH powered WSS requirements, especially in the energy consumption of transmission and receive processes. Based on the reviews of the EH and wireless sensor technologies, a research challenge in the mismatch between energy harvested by harvesting methods and energy demanded by wireless sensor technology is identified. After that, the energy-saving mechanisms in the WSS are reviewed with a particular focus on the energy-aware approach.

Chapter 3 presents the experimental study of a battery powered WSM for understanding energy consumption. The chapter opens by describing a typical battery powered WSM system and the implementations of the hardware,

software, and communication implementation, followed by describing the testing set-up and methods. The experimental results are then presented in multiple cycles of the WSM operation and one cycle of the WSM operation. The former is to analyse the overall energy consumption during active and sleep time, and the latter is to analyse the energy consumption during the active time accurately. The chapter ends with a discussion and conclusions of the work.

Chapter 4 is about the development of energy-aware approaches for EH powered WSM. It begins by describing a typical EH powered WSM system and then identifying the key issues of the EH powered WSM system through the experimental measurements using the custom developed piezoelectric vibration powered EH powered WSM system. The experimental results are then presented with a focus on the discussions on the start-up issue and the energy mismatch issue in the system. Following this, energy-aware approach concepts are proposed, and the implementation methods are developed to solve the problems above, including hardware EAI, software EAI and sensing EAI. After that, a description of how these combined energy-aware approaches were tested by the use of the same piezoelectric vibration powered EH powered WSM system as mentioned above. The experimental results on the system performance were presented, discussed, and concluded. Finally, this chapter ends with a conclusion.

Chapter 5 presents the study of energy analyses of the WSM during the network joining process in the EH powered WSN. It begins by describing the studied star structure of EH powered WSNs. After that, the implementation, the overview, and the operation of the studied WSN are given. And then, an experimental analysis

of the energy consumption during the WSM network joining process is given. Furthermore, the effects of duty cycle and storage capacitor size on the EH powered WSM joining the network process are studied. The results are then presented, and discussed and a critical issue of uncertainty in the energy consumption of the network joining process is identified.

Chapter 6 presents the development of the network energy-aware approach for EH powered WSNs to trace and manage the available energy in the WSM to solve the uncertainty problem identified in **Chapter 5**. It begins by describing the proposed network energy-aware approaches concepts and algorithms. After that, the implementation and experimental study of the network energy-aware methods using the developed WSN system powered by multiple EH sources are described. The results on the system performance were presented, discussed and concluded.

Chapter 7 presents a summary of the research performed in this thesis. The structure of the discussion follows the objectives set out by this thesis. It explains how each objective is achieved with its primary outcomes and the resulting contributions to the research community. Following this, the thesis is concluded. Finally, based on the limitations of this thesis, recommendations for further work are suggested.

Chapter 2 Literature Review

This Chapter provides background and state-of-the-art researches that are related to this thesis. Section 2.1 describes an overview of the power output capability of standard EH techniques for EH powered WSS. Section 2.2 presents typical wireless communication technologies and compares the performance of wireless communication protocols that have the potential to suit EH powered WSS. Section 2.3 overviews the energy-saving mechanisms in the literature that may be suitable for the EH powered WSS. Section 2.4 overviews the energy-aware approaches that have been studied for the EH powered WSS. Section 2.5 concludes the chapter with a summary of the key findings.

2.1 Energy Harvesting Techniques

For EH powered WSS, the energy generated by the energy harvesters is important to determine whether or not the chosen energy harvesters can provide the required power output for the WSM or WSN. The power output capability of RF, solar, thermal, and mechanical EH methods are presented below.

2.1.1 Radio Frequency Energy Harvesting

Radio frequency EH converts RF signals into electrical energy using the antenna. The frequency range of the radio signals is usually from 3 kHz to 300 GHz [29]. However, RF EH typically has low output power. For example, there are five typical frequency bands for Digital television (DTV), Global system for mobile communications (GSM) 900, GSM 1800, 3G, and Wi-Fi, and they are 470-610MHz, 925-960 MHz, 1805-1880 MHz, 2110-2170 MHz, and 2400-2500MHz

frequencies, respectively around 270 London Underground stations have been measured and analysed [30]. The average power density generated by RF is 0.89 nW / cm^2, 36 nW / cm^2, 84 nW / cm^2, 12 nW / cm^2 and 0.18 nW / cm^2, respectively.

2.1.2 Solar Energy Harvesting

Solar EH is one of the most established techniques [31]. It can generate energy from microwatt to milliwatt range per square millimetre, depending on the surface area of the solar cell and the amount of illumination [32]. For example, it has been reported that the solar system is able to produce a typical power density of 75 mW/mm^2 for outdoor solar cell operation and a typical power density of 100 µW/mm^2 for indoor lighting [33]. There is much more potential for solar EH technology to improve as currently solar cells only have an efficiency of around 2 to 15%. If the technology of solar cells can be further improved and matured, more power will be available to the WSS.

2.1.3 Thermal Energy Harvesting

Thermal EH relies on the temperature gradient between the two surfaces of thermoelectric generators and converts it into electrical energy using a thermoelectric generator (TEG) that operates based on Seebeck effect that is a phenomenon in which a temperature difference between two dissimilar electrical conductors or semiconductors produces a voltage difference between the two substances. The output power of TEG can be very high if the temperature gradient is considerable. For example, by using a TEG with an area of 3136 mm^2,

an output power of 10.3 W can be obtained at a temperature gradient of 200 ^{o}C [34].

Even at a lower temperature gradient, an output power of milliwatt range can be obtained. For instance, some designers have obtained about 23.9 mW power at a 22.5 °C temperature difference with a flexible thermoelectric generator using special N-type and P-type thermoelectric materials [35]. However, TEG has a low efficiency of about 5-6% [36].

2.1.4 Mechanical Energy Harvesting

Mechanical EH has the most varied EH sources and methods. Energy sources that can be considered as mechanical energy can be fluid flow, vibrations, pressure, stress-strain, and motions from virtually anything, including humans.

Due to the breadth of a variety of mechanical EH sources and methods, the range of power that can be harvested is widely dispersed. The choice of transducer design mainly depends on the environment of the application. For example, harvesting energy from fluid flow using an electromagnetic mechanism is likely to obtain more power. The output power from fluid flow EH using cantilever based piezoelectric transducer and electromagnetic transducer are in the microwatt range [37] and milliwatt range [38], respectively. Other types of transducer designs, such as the turbine, could provide a high output power of around 26 mW to 140 mW at an air speed of 10 to 18 m/s [39]. On the other hand, piezoelectric or electrostatic generators are able to provide the highest density of power for the pressure variations [14]. Patch type piezoelectric transducers that were bonded

on the surfaces of structures have been used to directly convert the strain experienced by the structures into electrical energy, with the power of 3.2 mW power generated by a piezoelectric energy harvester under an emulated aircraft wing strain loading of 600 με at 10 Hz [40].

Energy can also be harvested from humans in a variety of ways, such as through locomotion or changes in finger position, walking, and knee-joint. In some cases, power can reach watt levels. For example, a backpack instrumented with an electromagnetic generator that is driven by a rack and pinion gear is able to generate a maximum power of approximately 7.37 W [41]. At body parts such as fingers and knee, smaller transducers based on piezoelectric mechanisms may be more common due to their more compact size than electromagnetic transducers. For example, a polyvinylidene fluoride film attached to a curved substrate in a piezoelectric shell shape is able to generate an output power of 0.21 mW from the slow and irregular motion of elbow and fingers [42]. Another example is a magnetically plucked piezoelectric bimorph knee-joint energy harvester, which is able to generate an average power of 2.72 mW when the wearer was walking at a speed of 4km/h [43].

2.1.5 Summary

A summary of the power output generated from different EH is given in Table 2.1 [21-35]. It can be seen that the power output varied a lot, depending on the energy sources and transduction mechanisms. It should also be noted that the power output from energy harvesters is not the exact amount of power that is usable by a WSS. The energy output will be conditioned by the power management circuit and stored in energy storage devices. Therefore, the realistic amount of power

for use by the WSS is much lower than the energy harvested as the power management consumes energy.

Table 2.1: The output power from different energy harvesting techniques [21-35]

EH Techniques	Performance	Energy Harvester	Conditions
RF	0.18 nW / cm^2	Antenna	Wi-Fi (2400-2500MHz)
RF	84 nW / cm^2	Antenna	GSM 1800(1805-1880 MHz)
Solar	75 mW/mm^2	Solar cell	Outdoor solar
Solar	100 μW/mm^2	Solar cell	Indoor lighting
Thermal	10.3 W with3136 mm^2	Thermoelectric generator	200 °C temperature difference
Thermal	23.9 mW	Thermoelectric generator	22.5 °C temperature difference
Mechanical	26 mW to 140 mW	Turbine	Air speed of 10 to 18 m/s
Mechanical	3.2 mW	Patch type piezoelectric transducers	An emulated aircraft wing strain loading of 600 με at 10 Hz
Mechanical	7.37 W	A backpack instrumented with an electromagnetic generator	Walked at speeds ranging from 2.5 to 4.0 mph while carrying 38kg loads when walking up a 10% incline
Mechanical	0.21 mW	A polyvinylidene fluoride film attached to a curved substrate in a piezoelectric shell shape	The slow and irregular motion of elbow and fingers
Mechanical	2.72 mW	A magnetically plucked piezoelectric bimorph knee-joint	Walked at a speed of 4km/h

2.2 Wireless Communication Technologies

The standardised wireless transmission technologies have shown a potential for development of EH powered WSS, and they mainly comprise ZigBee, Bluetooth low energy (BLE), Ultra-wide band (UWB), and Long Range Radio (LoRa). The power consumption of WSS mainly depends upon the intended applications, which define requirements for the wireless transmission technologies such as transmission rate and distance required to complete the tasks. Currently, there are several commercially available modules based on different wireless communication technologies for developing EH powered WSS. Due to differences in applications and advances in fabrication technologies used, the modules may exhibit different performances in terms of energy usages even if they are using the same communication technology. Therefore, this section reviews these low-power wireless communication technologies to understand their operation, which directly relates to energy requirements and compares different popular wireless communication modules concerning different parameters, especially for the energy consumption of transmission and receive process.

2.2.1 ZigBee

ZigBee is a wireless technology developed as an open standard to address the requirements of low-cost, low-power devices [44, 45]. ZigBee defines the upper layer communication protocols based on the IEEE 802.15.4 standard. It has three types of devices. The first is the ZigBee end-device that corresponds to an IEEE Reduced Function Devices (RFD) or Full Function Devices (FFD), acting as a

simple device. The second is the ZigBee router, which is an FFD with routing capabilities. The third is the ZigBee coordinator, which is the Personal Area Network (PAN) coordinator to manage the whole network. It is able to support three main network topologies: star, tree, and mesh network topologies, as shown in Fig. 2.1, and to connect hundreds to thousands of devices [46].

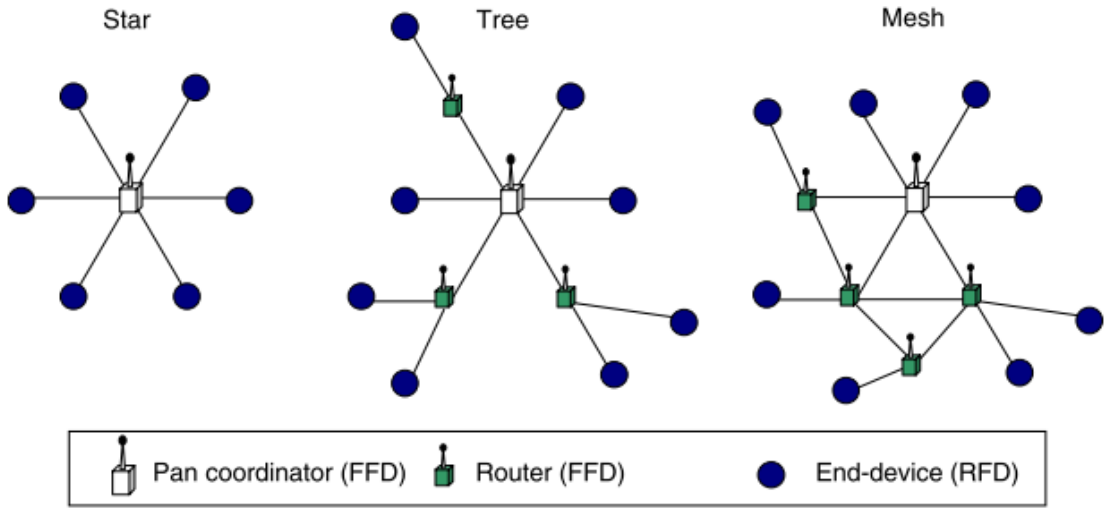

Figure 2.1: Network topologies in ZigBee [46]

A star network consists of an FDD and several RFDs. The FDD is used to manage and control all functions of the network and all the RFDs directly connected to an FDD, which are used to collect data from the environments and then transmit it to the FDD. The RFDs are not able to communicate with each other. A tree network is a hybrid network topology in which star networks are interconnected via the bus network, which is the network topology in which motes directly connected to a standard linear. Tree networks are hierarchical, and each FDD can have an arbitrary number of child motes (FFDs or RFDs). Mesh topology is a more complex and expensive network than the star network, where all motes cooperate to distribute data amongst each other. It consists of a self-forming multi-hop mesh of motes and an access point mote that connects the motes to

the network manager. Motes are capable of two way communication and collect and relay data. The data is propagated along a path by hopping from one mote to another mote until it reaches its destination.

It should be noted that, in every network topologies, an RFD may connect to a cluster tree network as a leave mote at the end of a branch, because it may only associate with one FFD at a time. Any of the FFDs may act as a coordinator and provide synchronisation services to other devices or other coordinators. Only one of these coordinators can be the overall PAN coordinator, which may have more significant computational resources than any other device in the PAN.

Table 2.2 presents four popular ZigBee wireless communication modules: JN5148 [47] from NXP, EM260 [48] from Ember, CC2430 [49] from Texas Instruments, and XBee-S1 [50] from Digi International. XBee-S1 has the highest current consumption of transmission and receiver processes, which are about 45 mA and 50 mA, respectively. JN5148 has the lowest current consumption of transmission and receiver processes, which are about 15 mA and 17.5 mA, respectively. The current consumption of EM260 and CC2430 for both transmission and receiving are about the same at around 27 mA. JN5148 has a 32-bit processor with 128 kB RAM, which has enough capacity to store sampled data. EM 260 has a 16-bit processor while CC2430 and XBee-S1 have an 8-bit processor. These three modules have relatively low RAM, which is no more than 8 kB.

It should be noted that, the sleep mode, mentioned in the Chapter 2, means that the devices turn off most functions, including the radio and internal regulator, and leave only the critical chip functions powered, including RAM retention.

Furthermore, all output signals are maintained in a frozen state and upon waking from sleep mode, the internal regulator is re-enabled. The devices can wake on both an internal timer and an external signal from the sleep mode. Therefore, the sleep mode result in the low current consumption.

Moreover, the devices are able to control enabling and configuration of the oscillator sources to optimize energy consumption in sleep mode by minimizing power dissipation in unused peripherals and oscillators. In detail, the clock system of the devices normally has three kinds of oscillator sources: (1) a high frequency Resistor and Capacitor (RC) oscillator, which is available for the clock system, when crystal accuracy is not required. (2) a low frequency 32.768 kHz RC oscillator for low power operation where high accuracy is not required; (3) an ultra-low frequency 1 kHz RC oscillator which is available to provide a timing reference at the lowest energy consumption in the sleep mode. It should be noted that, compared with the low accuracy of oscillator sources, the clock system normally has two kinds of crystals: (1) the high-frequency crystal oscillator and integrated 38.4 MHz crystal, which provide a precise timing reference for the MCU and radio; (2) the low-frequency crystal oscillator and integrated 32.768 kHz crystal, which provide an accurate timing reference for low energy modes and the real-time-clock circuits.

Therefore, when all these modules go to sleep, the current consumption is typically less than 10 μA. In detail, JN5148 has 1.3 μA current consumption in sleep mode with 32.753 kHz RC oscillator. EM260 has about 1 μA in sleep mode with 1 kHz RC oscillator. CC2430 has about 0.5 μA in sleep mode with 32.753

kHz RC oscillator. XBee-S1 has less than 10 µA in sleep mode with 32.753 kHz RC oscillator.

Table 2.2: Typical IEEE 802.15.4 and ZigBee wireless communication modules and parameters

Chipset	JN5148 [47]	EM 260 [48]	CC2430 [49]	XBee-S1 [50]
Manufacturer	NXP	Ember	Texas Instruments	Digi International
Testing Conditions	3.0V supply at 25°C of ambient temperature	3.0V supply at 25°C of ambient temperature	3.0V supply at 25°C of ambient temperature	3.3V supply at 25°C of ambient temperature
Supply Voltage	2.3-3.6 V	2.1-3.6 V	2.0-3.6 V	2.8-3.4 V
MCU	32-bit	16-bit	8-bit	8-bit
RAM	128 KB	5 KB	8 KB	4 KB
TX	15 mA at +2.5 dBm	24 mA at +0 dBm	27 mA at +0 dBm	45 mA at +0 dBm
RX	17.5 mA	28 mA	27 mA	50 mA
Data rates	250 kbps	250 kbps	250 kbps	250 kbps
Sleep	1.3 µA	1 µA	0.5 µA	<10 µA

2.2.2 Bluetooth Low Energy

Bluetooth Low Energy (BLE) [51] is a developed energy-efficient short-range wireless communication protocol and is an extension of the Bluetooth technology that allows communication on every major operating system that enables development for a broad range of connected devices. The transmission distance of BLE is normally within 10 m but is able to go up to 100 m. Furthermore, BLE devices can operate either in a master role that is able to control other devices or a slave role that advertises and waits for connections [52]. A master can manage multiple simultaneous connections with a number of slave devices and provide the synchronisation reference. Moreover, a device is able to be a slave or a

master to another operating Bluetooth network in the surroundings, which means it able to be a mote or a base station. Master and slaves have a common clock and frequency hopping pattern.

Table 2.3 presents three typical BLE wireless communication modules: BGM13P [53] from Silicon Labs, CC2540F256 [54] from Texas Instruments, and RN4871 [55] from Microchip. BGM13P has the lowest current consumption of the receiver process which is about 9.6 mA at +0 dBm while has the lowest current consumption of receiver process, which is about 9.9 mA. CC2540F256 has the highest current consumption of transmission, which is about 13 mA at +0 dBm. In addition, BGM13P has a 32-bit processor with 64 kB RAM, which has enough capacity to store sampled data. CC2540F256 and RN4871 have an 8-bit processor. These two modules have relatively low RAM, which is no more than 8 kB.

In sleep mode, BGM13P integrates an low frequency 32.768 kHz RC oscillator and an ultra-low frequency 1 kHz RC oscillator to control system clocks to optimize energy consumption in any specific application by minimizing power dissipation in unused peripherals and oscillators. Where the high accuracy is not required, it is able to have about 1.5 μA current consumption with RAM retention and running from 32.768 kHz RC oscillator. Moreover, BGM13P is able to have as low as 1.14 μA current consumption with full RAM retention and running from 1 kHz RC oscillator. CC2540F256 has about 0.9 μA current consumption in sleep mode with RAM retention and running from 32.768 kHz RC oscillator. Moreover, it has a special sleep mode for quickly wake up the system through keeping the digital regular on, which is able to wake up the system with about 4 μs, compared

with about 120 μs wake up time with the digital regular off. But the current consumption of this quick wake up mode is about 235 μA, which is much higher than the normal sleep mode. Similarly, RN4871 has about 2.9 μA in sleep mode with 32.768 kHz RC oscillator thus reducing power consumption, which is higher than 1.5 μA current consumption and 0.9 μA current consumption in the BGM13P and CC2540F256 with the same RC oscillator.

Table 2.3: Typical BLE wireless communication modules and parameters

Chipset Manufacturer	BGM13P [53] Silicon Laboratories	CC2540F256 [54] Texas Instruments	RN4871 [55] Microchip
Testing Conditions	3.3 V supply at 25°C of ambient temperature	3.0 V supply at 25°C of ambient temperature	3.0 V supply at 25°C of ambient temperature
Supply Voltage	1.8-3.8 V	2 V–3.6 V	1.9-3.6 V
MCU	32-bit Processor	8-bit processor	8-bit processor
RAM	64 KB	8 KB	8 KB
TX	9.6 mA at +0 dBm	21 mA at +0 dBm	13 mA at +0 dBm
RX	9.9 mA	15.8 mA	13 mA
Data rates	2 Mbps	1 Mbps	10 kbps
Sleep	1.5 μA, 1.14 μA	235 μA, 0.9 μA	2.9 μA

2.2.3 Ultra-wide Band

Ultra-wide band (UWB) [56] is a radio technology that aims to be used for short-range, high-bandwidth communications over a large portion of the radio spectrum with a very low energy level, which belongs to the standardisation group IEEE 802.15.3a. This standard is able to provide data rates from 11 to 55 Mbps at distances of greater than 70 m. In addition, this standard is designed to provide simple, ad-hoc connectivity that allows devices to exchange information without

a direct intervention of users automatically. Typically, the individual essential cells of the UWB for more complex network structures is Peer-to-peer (P2P), which is a networking distributed application architecture that partitions tasks or workloads among peers [57].

Table 2.4 presents the two most common UWB wireless communication transceiver modules: DWM1000 [58] from Decawave and XS110 from Freescale [57, 59]. Both of them have high current consumption of transmission and receiver process. DWM1000 consumes about 140 mA at +9.3 dBm current for transmission and 160 mA for receiving. XS110 consumes about 227 mA at +20 dBm for transmission and 227 mA for receiving. Despite the lower current consumption, DWM1000 has a much superior transmission distance of up to 300 m than XS110 that can only transmit up to 10 m. However, the data rate of DWM1000 is only up to 6.8 Mbps, while XS110 can go up to 114 Mbps.

Table 2.4: Typical UWB wireless commutation transceiver modules and parameters

Chipset	DWM1000 [58]	XS110 [57],[59]
Manufacturer	Decawave	Freescale
Testing Conditions	3.3V supply at 25°C of ambient temperature	3.3V supply at 25°C of ambient temperature
TX	140 mA at +9.3 dBm	227 mA at +20 dBm
RX	160 mA	227 mA
Data rates	110 kbps, 850 kbps, 6.8 Mbps	29, 57, 86 and 114 Mbps
Transmission Distance	up to 300 m	10 m

2.2.4 LoRa

LoRa is a low-power wide-area network (LPWAN) protocol for Internet of Things applications based on spread spectrum technology with a broader band, which is defined by the LoRa Alliance [60]. The main advantage is that demodulation is possible with a noise level of less than 20dB, which allows LoRa to achieve a long transmission distance of up to a few kilometre ranges. LoRa transceivers use sub-GHz frequencies for their communication, which include 433 MHz, 868 MHz (Europe), and 915 MHz (North America) industrial, scientific, and medical (ISM) radio bands [61]. The LoRa modulation between the physical and Media Access Control (MAC) layer [62] is a Semtech proprietary technology that includes two basic techniques: forward error correction techniques of code rate to further increase the receiver sensitivity and multiple orthogonal spreading factors to provide a trade-off between data rate and range. Moreover, LoRa utilizes a wider band, usually of 125 kHz or more, to broadcast the signal, which allows the usage of scalable bandwidth of 125 kHz, 250 kHz, or 500 kHz [63].

The basic network architecture of a LoRaWAN consists of LoRa end devices, LoRa gateways, and a LoRa network server [64], as shown in Fig. 2.2. The network makes use of star topology in which LoRa gateways are transparent bridges.

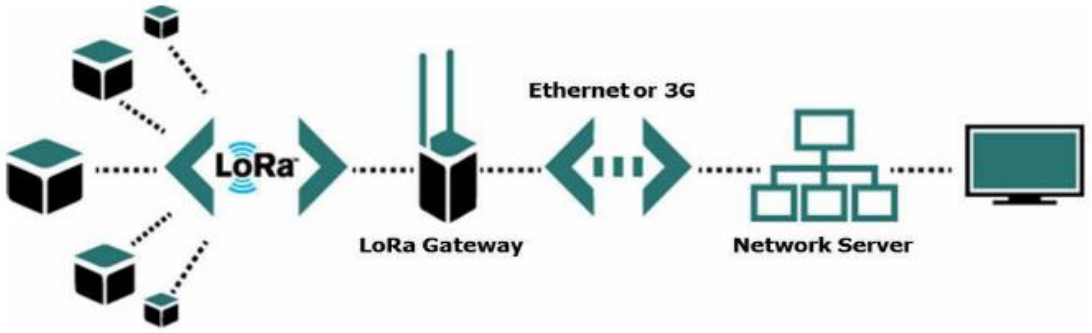

Figure 2.2: LoRa network architecture [64]

The LoRa end devices communicate with gateways that employ LoRa with LoRaWAN. LoRa gateways pass raw LoRaWAN packets from the end devices to a LoRa network server with a high throughput based on the backhaul interface, which is typically the third generation (3G) of a wireless mobile telecommunications network or Ethernet. LoRa gateways also act as a bidirectional communication or protocol adapter with the LoRa network server. In this case, the LoRa network server takes charge of decoding the data packets transmitted by the LoRa devices and creates the frames that would be directed back to the devices. The LoRa gateway collects data from LoRa motes to construct the topology of a star network and may communicate with a cloud server over a long communication range and with high scalability.

Table 2.5 presents three typical LoRa wireless communication transceiver modules: RN2483 [65] from Microchip, SX1273 [66] from SEMTECH, and eRIC-LoRa [67] from LPRS. Both SX1273 and eRIC-LoRa have the same current consumption for its transmission with the output power of +20 dBm and +17 dBm at 125 mA and 90 mA, respectively. RN2483 has a limited transmission power of no more than+15 dBm. The maximum current consumption for its transmission is 38.9 mA at +14.1 dBm. However, its current consumption for transmitting at +6.9

dBm is 30.0 mA, which is much higher than that of SX1273 at 18 mA when transmitting at +7 dBm. SX1273 and eRIC-LoRa both have about 10 mA current consumption for receiving, which is lower than that of RN2483 as well (14.2 mA). The maximum effective data rates of RN2483, SX1273, and eRIC-LoRa are 10.937 kbps, 37.5 kbps, and 37.5 kbps, respectively. Although all of them have high current consumption of transmission and lower data rates than other technologies, they have a long transmission distance, which can be more than 10 km.

Table 2.5: Typical LoRa wireless communication transceiver modules and parameters

Chipset	RN2483 [65]	SX1273 [66]	eRIC-LoRa [67]
Manufacturer	Microchip	SEMTECH	LPRS
Testing Conditions	3.3 V supply at 25°C of ambient temperature	3.3 V supply at 25°C of ambient temperature	5.0 V supply at 20°C of ambient temperature
Supply Voltage	2.1-3.6 V	1.8-3.7 V	2.5-6.0 V
TX	38.9 mA at +14.1dBm; 33.7 mA at +10.4 dBm; 30.0 mA at +6.9 dBm.	125 mA at +20 dBm; 90 mA at +17 dBm; 18 mA at +7 dBm.	125 mA at +20 dBm; 90 mA at +17 dBm; 40 mA at +10 dBm.
RX	14.2 mA	10 mA	10 mA
Effective Data rate	Up to 10.937 kbps	0.24 - 37.5 kbps	Up to 37.5 kbps
Transmission Distance	Up to 15 km coverage at suburban; up to 5 km coverage at urban area	Line of sight range of up to 48 km; more than 3 km in dense urban environments	Line of sight range of up to 10 km

2.2.5 Performance Comparison of Wireless Communication Protocols

Table 2.6 summaries and compares the aforementioned wireless communication technologies of ZigBee, Bluetooth, UWB, and LoRa based on the literature reviewed [36-62]. It can be seen that ZigBee, Bluetooth, UWB wireless protocols are suitable for working with short range, where the transmission distance is up to 100 m, whereas LoRa wireless protocol is considered for long range communication since it is able to communicate over a distance of more than 48 km in some cases. UWB has the highest transmission data rate, which is up to 110 Mb/s while the maximum transmission data rates of ZigBee, Bluetooth, and LoRa are 250 kbps, 2 Mb/s, and 50 kbps, respectively. ZigBee has higher network elasticity than Bluetooth, UWB, and LoRa since the basic network topologies of it are able to be star, tree, and mesh, which permits the formation of various network topologies.

Table 2.6: Comparison of different wireless communication technologies [36-62]

Wireless communication technologies	ZigBee	Bluetooth	UWB	LoRa
Standard	IEEE 802.15.4	IEEE 802.15.1	IEEE 802.15.3a	IEEE 802.15.4g
Frequency band	868/915 MHz and 2.4 GHz	2.4 GHz	3.1–10.6 GHz	433/869/915 MHz
Channel bandwidth	0.3/0.6 MHz;2 MHz	Up to 2 MHz	500 MHz-7.5 GHz	<500 KHz
Data rate	20, 40, and 250 kbps	2 Mb/s	110 Mb/s	50 kbps
Communication range	Up to 100 m	Up to 100 m	Up to 100 m	Up to kilometre
Max number of cell motes	> 65000	8 and BLE have more	8	10000
Basic Network Topologies	Star, tree, mesh	Scatternet	P2P	Star-of-stars

Moreover, Table 2.7 summaries and compares the energy consumption of those mentioned above off-the-shelf commercially available wireless chips based on the communication technologies of ZigBee, Bluetooth, UWB, and LoRa [36-62]. It should be noted that all the data of Table 2.7 is based on the datasheet in the given ideal manufacturers' test environment. Furthermore, JN5148 that uses ZigBee, RN4871 that uses BLE, DWM1000 that uses UWB and SX1273 that uses have been specifically chosen for comparison since they have the best performance in terms of current consumption for their wireless communication among their competitors. It should be noted that SX1273 will be compared in two different modes, which are with short transmission distance and long transmission distance.

The power consumption for transmission and receiving of ZigBee, BLE, and LoRa in short range is comparable. However, ZigBee and BLE are better than LoRa for their much superior data rates. If long distance communication in the range is required, LoRa wireless protocol is the only option. It preserves the same data rate but consumes a much higher power for its transmission. On the other hand, UWB is suitable for high data rate because of its low normalised energy consumption, but the power consumption of both transmission and receiving processes are much higher than ZigBee and BLE. Therefore, ZigBee and BLE are suitable for applications with limited power supply due to their low power consumption and adequate data rate.

Table 2.7: Energy consumption of chipsets for each protocol [36-62]

Standard	ZigBee	Bluetooth	UWB	LoRa	LoRa
Chipset	JN5148	RN4871	DWM1000	SX1273	SX1273
Range (m)	Up to 100 m	Up to 100 m	Up to 100 m	Up to 100 m	More than 30 km
Supply Voltage (V)	3	3.3	3.3	3.3	3.3
Transmission (TX) (mA)	15	13	160	18	125
Receive (RX) (mA)	17.5	13	140	10	10
TX (mW)	45	42.9	528	59.4	412.5
RX (mW)	52.5	42.9	462	33	33
Maximum Data rate (Mb/s)	0.25	1	6.8	0.0375	0.0375
The average energy consumption of transmitting 1 Mb data (mJ/Mb)	180	42.9	77.65	158.4	1100

2.2.6 Selected Wireless Communication Module for Thesis

Based on the above studies, ZigBee and BLE are considered to be appropriate candidates for the development of EH powered WSN. However, the network elasticity of ZigBee makes it a better choice. Therefore, the wireless MCU of Jennic JN5148-001-M00 that comes with an integrated 2.4 GHz IEEE802.15.4 transceiver communicating using ZigBee protocol was chosen as the studied case in this thesis. Also, JN5148 has high performances and low power consumption [47]. In detail, it features an enhanced 32-bit Reduced Instruction Set Computing (RISC) processor offering high coding efficiency through variable width instructions, a multistage instruction pipeline and low power operation with programmable clock speeds. It also includes 128kB RAM, 4Mbit flash memory, and 4-input 12-bit ADC pins, which enables the WSMs to have enough data storage memory and 4 channels of sampling output from the sensors. The current consumption of the MCU for keeping on and sleeping with active sleep timer is

about 7 mA and 2.6 μA, respectively. The current consumption of transmitting and receiving data is about 17.5 mA and 15 mA, respectively, which is lower than other state-of-the-art wireless chips. Moreover, the JN5148 chip is a viable choice for the implementation of EH powered WSM, where it was used as a WSM microcontroller powered by an aero-acoustic EH device, meant to be installed on an aircraft outside skin [69]. The task was to measure the temperature and send the data every 6 s, while consuming a mean power of 181 μW.

Moreover, the 2.4 GHz IEEE802.15.4 wireless LTC5800 chip also features a highly-integrated and low power radio design [70], which is considered to use in Chapter 5 and Chapter 6. It has an enhanced ARM Cortex-M3 32-bit microprocessor, 72 kB SRAM, 512 kB flash memory, and four input 12-bit ADC pins. The current consumption of transmitting at 8 dBm and receiving a packet is about 9.7 mA and 4.5 mA, respectively [70].

2.3 Energy-saving mechanisms for Wireless Sensor Systems

Based on the above studies, it can be known that there is a mismatch between the energy required by the WSS and the energy that can be provided by energy harvesters. Increment of the output power of energy harvesters might require innovation in the materials, mechanical designs, and electronic circuits, which involves a vast breadth of expertise in the multidisciplinary field and, last but not least, more energy from the ambient environments, which is beyond our control. One the other hand, manipulation of a WSS in terms of the software and hardware to achieve energy saving is more approachable and likely to benefit the

wider community as the energy harvesters have to be specific to the environment or applications while the WSS could be applied everywhere with different EH technologies to perform the sensing and monitoring tasks.

Several energy saving mechanisms for WSS have been proposed in recent years. These include sleep/wakeup schemes, data-driven, radio optimisation, and energy-efficient routing [11, 27]. In this section, these approaches that exist in literature will be reviewed to identify suitable schemes that are suitable for EH powered WSS.

2.3.1 Sleep/Wakeup Schemes

Sleep/wakeup schemes aim to adapt mote activities to save energy by placing the WSM in low power sleep mode since idle states of the WSM where the transceiver is active but without any communication activities are major sources of energy consumption especially for keeping the radio component on. The main approaches of the Sleep/wakeup schemes include adaptive duty cycling, passive wake-up radios, and topology control protocol technology.

Duty cycling is a mainly focused method for energy-saving mechanism during the operation of WSMs powered by batteries and EH methods. It is the fraction of one period in which a signal or system is active. The most efficient power-saving operation is to place the radio transceiver in a low-power sleep mode when no communication is required. For example, an adaptive duty cycling algorithm has been proposed where it attempts to predict the future energy availability so that EH powered sensor motes can autonomously adjust their duty cycle according to the predicted energy availability in the environment through periodically sampling

of the power from the energy harvester and consumed by the mote [71]. In terms of hardware-only implementation, an energy-aware hardware interface that controls the WSM to be active only when the voltage across its energy storage exceeds a fixed turn-on voltage threshold has also been presented [72].

Similarly, passive wake-up radios aim to make the WSM wakes up only when it is required to transmit or receive the data to reduce the energy wastage during the idle states. However, the implementation is slightly different from duty cycling, where another circuit such as an RF identification (RFID) tag is used as a wake-up receiver [73]. The RFID harvests the energy from transmitted signals and produces a wake-up signal to trigger an interruption that wakes up the mote. However, the energy cost of the wake-up transmitter is high, which makes it challenging to implement in networks that involve a multi-hop scheme, and the wake-up range is short.

The topology control protocol aims to reduce redundancy of coverage area by dynamically adjust the connectivity among the motes so that the number of active motes in the same coverage area can be minimised while maintaining a maximum area coverage A set number is assigned to each mote by the network coordinator. The motes are grouped into different sets based on the criteria that all the sets are able to maintain the desired area of coverage when their motes become active. Only the motes with the same set number will be activated at a time while other motes go to sleep to save energy. The different sets of motes will take turn to sleep or become active [74].

2.3.2 Data-driven

Data-driven approaches aim to reduce the amount of sampled and transmitted data by keeping the sensing accuracy just within an acceptable level for the application to reduce the energy consumption of WSS since the sampling and transmission processes are entirely power hungry, as can be seen in Section 2.2.

Event-driven methods aim to enable the WSM to automatically change the amount of sampled data and determine whether to transmit the data based on current event requirements [11]. For example, apart from the normal operating mode, an emergency mode for a solar-powered WSM system has been designed [75]. The WSM reports a sensed data to the base station with a certain time interval in the normal mode when the WSM is active. In this case, the WSM does not have to send a lot of data every time, which reduces the power requirement. Once the WSM detects an emergency event such as a fire nearby, it enters the emergency mode, where the WSM continuously samples the data and transmits it until the supply energy is depleted. Some other examples include an EH powered WSM system that only begins sampling and transmitting the data to the base station when there is an earthquake [76], and a vibration EH powered WSM system that autonomously monitors the amplitude of vibration of interest when it reaches a pre-set threshold, and wirelessly transmits an alarm signal when the vibration lasts for a considerable period of time [77]. Moreover, more energy is expected to be generated during these alarming events, which can take advantage to power and support the more frequent data transmission rate of the WSS.

Transmission data reduction aims to reduce the amount of transmitted data to reduce the energy consumption of transmission. It should be noted that this method does not reduce the number of samples or sampled data, but focuses on transmitting the least amount of data through analysing the sampled data based on the application requirements. Transmission data reduction can be achieved through data aggregation techniques [78] and data comparison techniques [79]. Data aggregation techniques [78] are aimed to gather and aggregate data in an energy-efficient method to reduce energy consumption during the transmission process. In a data aggregation scheme, the mote is required to analyse the sampled data and then chooses the critical information to transmit to the base station. For example, a mote may only send the average data or maximum of sampled data. However, data aggregation techniques may reduce the accuracy of the data collected. In fact, depending on the aggregation function, the receiver may not be able to recover the original data where information accuracy may be lost. Data compression techniques are aimed to reduce the size of transmitted packets through information coding performed in the WSM to save energy [79]. The information decoding can be performed in the base station. However, existing compression algorithms are not applicable to sensor nodes because of their limited resources. Therefore, specific techniques are required to be further developed to adapt to the limited computational and power capabilities of wireless motes [79].

2.3.3 Radio Optimisation

Radio optimisation approaches aim to reduce energy dissipation due to wireless communications through optimising the radio parameters such as coding and modulation schemes, power transmission and antenna direction since the radio

module is the main component that causes energy depletion of WSS. The main approaches of radio optimisation include modulation optimisation, cooperative communication schemes, transmission power control method, and directional antennas technology.

Modulation optimisation aims to find the optimal modulation parameters that result in the minimum energy consumption of the radio. For instance, energy depletion is caused by the circuit power consumption and the power consumption of the transmitted signal. For short distances, circuit consumption is higher than the transmission power, while for longer ranges, the signal power becomes dominant. Existing research tries to find a good trade-off between the constellation size (number of symbols used), the information rate (number of information bits per symbol), the transmission time, the distance between the motes and the noise. Cui et al. [80] reported that the system that optimises the transmission time and the modulation parameters is able to save up to 80% energy consumption compared to the non-optimised systems. Costa and Ochiai [81] studied the energy efficiency of different modulation schemes and reported that selecting the suitable modulation scheme is able to reduce the energy consumption of transmission. For example, M-ary Quadrature Amplitude Modulation (MQAM) which is a modulation scheme that conveys data by modulating the data transmission onto the amplitude via two carrier signals has poor performance for long distances, since it consumes much energy on the circuit while has better performance for short distances, since it consumes much energy on signal.

Cooperative communication schemes improve the quality of received signals by exploiting several collaborated single-antenna devices to create a virtual multi-antenna transmitter, which is to reduce the energy wastage caused by overheard from neighboring motes [67, 68].

Transmission power control methods enhance energy efficiency at the physical layer by adjusting the radio transmission power [82, 83]. An algorithm known as cooperative topology control with adaptation (CTCA) has been proposed to regularly adjust the transmission power of every mote in order to take the uneven energy consumption profile of the sensors into consideration [84]. A mote with higher remaining energy may increase its transmission power, which will potentially enable other motes to decrease their transmission power for saving energy. However, transmission power control strategy has an effect not only on energy but also on delays, link quality, interference, and connectivity. When transmission power decreases, the risk of interference also decreases as fewer nearby nodes are subjected to overhearing. On the contrary, the delay is potentially increased, because more hops will be needed to forward a packet. Therefore, alternating the transmission power will influence the network because the potential connectivity between sensors will vary.

Conventional antennas are omnidirectional, where signals are transmitted in all the directions. In contrast, directional antennas send a signal in a unidirectional manner towards the intended target, and therefore require less power for a given range [85, 86]. The use of directional antennas also improves transmission range and throughput and limits overhearing. However, if the antennas were not properly oriented, some problems that are specific to directional antennas have

to be considered such as deafness, in which the transmitter fails to communicate with its intended target and signal interference, in which collision occurred when more than one signals were sent in a path [87].

2.3.4 Energy-efficient Routing

Energy-efficient routing approaches are primarily designed for motes in a multi-hop scheme that is closer to the path because they have to route more packets, which results in more energy. Cluster architectures are used to organise the network into clusters, where each cluster will have a cluster head to manage and coordinate activities and communications of slaved motes, with the aim to reduce the energy consumption of transmission by reducing the communication range of the slaved motes inside the cluster and limiting the number of transmissions by performing data aggregation and/or fusion [88, 89]. The cluster heads, which are the motes with the highest energy resources, will then relay the data among them until the data is sent to the PAN. A new mote in each cluster will be elected as the new cluster head after a predefined number of transmission rounds so that the energy of the motes that were acting as the cluster head will not be quickly drained.

2.3.5 Discussions

Sleep/wakeup schemes aim to reduce the energy consumption of WSS by adapting mote activity. However, passive wake-up radio is not suitable for the EH powered WSS since it has a short wake-up range. This means each mote has to be equipped with a transmitter, which requires a lot of energy to be able to relay the signal across the network. Most EH powered WSNs are likely to have low redundancy in a given area since the activation of each mote is determined by the energy availability from the environment. Therefore, the topology control protocol is not suitable as well. The adaptive duty cycle is a suitable solution for EH powered WSS because it enables WSM to reduce the energy consumption controlled by itself rather than other motes such as network managers. Moreover, the energy-aware approaches enable the energy harvested is able to accumulate in the storage device, since it avoids the energy consumption of the WSM during the voltage across the storage device is charged up to the stable operating voltage of the WSM.

Data-driven approaches aim to reduce the energy consumption of WSS in the sampling and transmission of processes. Radio optimisation approaches aim to reduce energy dissipation due to wireless communications through optimising the different radio parameters which are specific to the applications in most cases. Both of them are suitable for EH powered WSS to reduce the energy consumption of WSS. However, they are developed based on the requirements and environment of the specific application, such as with the given range of transmission distance in most cases.

Energy-efficient routing approaches are primarily designed for motes in a multi-hop scheme, which are suitable for complex and expensive networks. However, the complex and expensive networks, especially for multi-hop networks, need several motes to be in the active state at the same time, which is difficult in the EH powered WSN system since the active time of the motes is unpredictable and very limited due to energy limitation. In most cases, only a few motes are active and remain in the network for a short time. Moreover, in a multi-hop network, the motes have to undertake not only the tasks of sampling and communicating directly with the network manager, but also need to communicate with other motes, which cost more energy than the motes where the network manager controls the network function. Therefore, star topology is considered here to be able to meet better the condition of EH powered WSN.

The advantage of star topology is that all the complexity in the network is given to a network manager, so all the other motes only need to perform a given task and communicate in their given time or frequency slot, which is helpful to reduce their energy consumption. In addition, it is able to reduce the impact of a transmission line failure by independently connecting each mote to the network manager. The failure of a transmission line linking any mote to the network manager will result in the isolation of that mote from all others, but the rest of the network will be unaffected. Therefore, energy-efficient routing approaches are not considered in the thesis.

Therefore, among the different proposed energy-saving mechanisms for WSS, energy-aware approaches are the most appropriate method for EH powered WSS, which will be further discussed in the next section.

2.4 Energy-aware Approaches for Energy Harvesting Powered Wireless Sensor Systems

Energy-aware approaches can be implemented via software and hardware. However, the hardware EAI between the WSS and energy harvesters or power management module (PMM) circuit in the EH powered WSS plays a more prominent role since it enables the generated energy to be stored in the storage device and system to have a low sleep power. A system without the hardware EAI will never provide the WSS with the required voltage supply to work properly in most cases [72].

Detailed power consumption measurements of the WSM are very important for reducing the energy consumption of the EH powered WSS, by designing the suitable energy-aware approaches based on a full picture of the WSM behaviour at different modes, including wake-up, active, sampling and transmission modes [90]. The WSM will consume more energy and behave unpredictably when the supply voltage is below its specified voltage range [72]. This increased power usage would cause a drop in the voltage of the energy storage devices such as super-capacitors. Furthermore, the energy storage devices will turn off the microcontroller again since the voltage drop. The voltage across the energy storage devices will never reach the stable operating voltage of the microcontroller. The experimental results show that without the cold start circuit, the super-capacitor could only be charged to 0.9 V, and the system never became fully functional, shown in Fig. 2.3. Therefore, a cold start circuit, which used a Torex XC61C voltage level detector to control an N-MOSFET switch to control the power supply to the microcontroller, as shown in Fig. 2.4. The cold start circuit was designed to ensure that the microcontroller will only begin to draw power

once a certain minimum supply voltage has been reached. When the voltage across the super-capacitor reaches a pre-set threshold of 2 V, the voltage level detector generates a high signal to connect the negative terminal of the microcontroller to the ground to form a closed circuit so that the microcontroller is able to draw the energy from the super-capacitor.

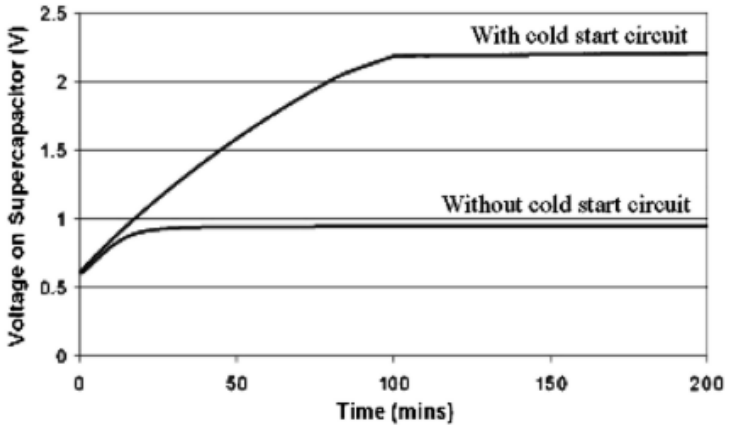

Figure 2.3: Super-capacitor voltage with and without cold start circuit [72]

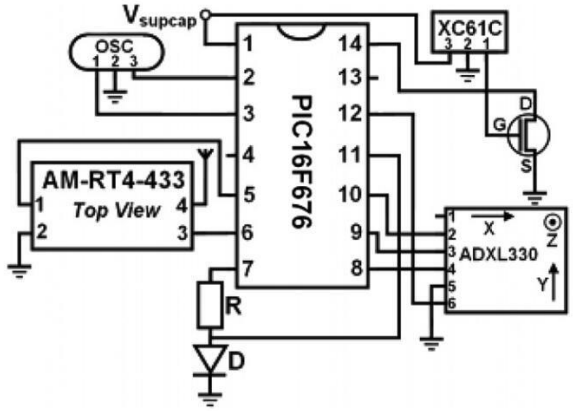

Figure 2.4: WSM subsystem schematic in the system [72]

To save the energy during the active time, software-based energy-aware approach is used where the microcontroller is programmed to operate in a low power sleep mode where it periodically samples the super-capacitor voltage until the super-capacitor voltage reaches 2.2 V. Once this threshold is reached, indicating that sufficient power is available, the microcontroller switches on the accelerometer. The microcontroller then takes 16 measurements at a sampling

rate of 1.25 kHz from the accelerometer and records the peak acceleration value. The transmitter module is then switched on to transmit a 17 bit packet consisting of a synchronisation bit, 8 identification bits and the 8 bit acceleration data value. It should be noted that there are many hardware interfaces with similar designs or functionality in terms of the control to start up the EH powered WSS that have been reported [72, 75, 28, 91, 92, 93]. The main purpose of these interfaces is to allow energy to be accumulated in the super-capacitor as it is clear that the output power from energy harvesters is insufficient to power a WSM directly [91, 92]. Energy-aware approaches that combine both the software and hardware implementation will be further discussed.

Similar cold start interface between the super-capacitor and the WSM, as shown in Fig. 2.5 has also been proposed [75]. The cold start interface is built with a BD4835G voltage detector IC series circuit [94]. If the voltage level of the super-capacitor is less than 3.5 V, the BD4835G IC will shut down the WSM to avoid the unexpected behaviour of the microcontroller. If the super-capacitor voltage level becomes 3.675 V, the reset IC restarts the WSM.

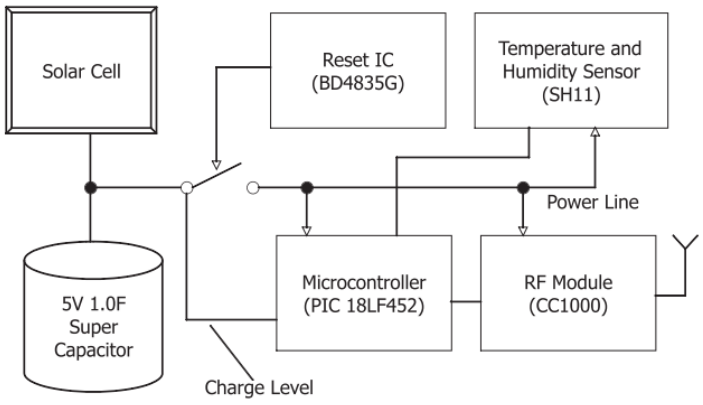

Figure 2.5: Block diagram of the solar biscuit WSM [75]

Moreover, three operational modes, namely the bootstrap mode, ordinary mode, and emergency mode, were designed as the basic states for the WSM,

depending on its energy level. When the voltage across the super-capacitor is below 3.675 V, the system is in bootstrap mode, which means the WSM is turned off by the cold start interface. In ordinary mode, the microcontroller wakes up at 3.675 V and then enters sleep mode until the supply voltage level increase to the pre-set voltage threshold of 4 V before enabling the WSM to perform the sensing and communicational tasks. When the WSM detects an emergency event, it enters emergency mode. In this mode, the WSM continuously sample the data and then transmit it until the supply voltage drops to 3.5 V, and then go to bootstrap mode as controlled by the cold start interface.

Another similar EAI to manage the energy flow between the storage capacitor and the WSM was also proposed [28]. The EAI is built with a voltage monitoring circuit which is used to monitor the voltage across the storage capacitor. The output of the energy-aware interface may be connected to an N-MOSFET for similar operation as previously discussed or to the RESET pin of a microcontroller, acting as an external interrupt to wake up the microcontroller from deep sleep mode when the voltage across the storage capacitor reaches the turn-on threshold, as shown in Fig. 2.6. However, if the supply voltage is outside of the specified voltage range, the deep sleep mode is not allowed in the microcontroller since it is a software-controlled mechanism that requires a valid operating condition to function properly. Therefore, the microcontroller will still consume energy during the deep sleep mode and is not able to avoid the unpredictable behaviour in this case.

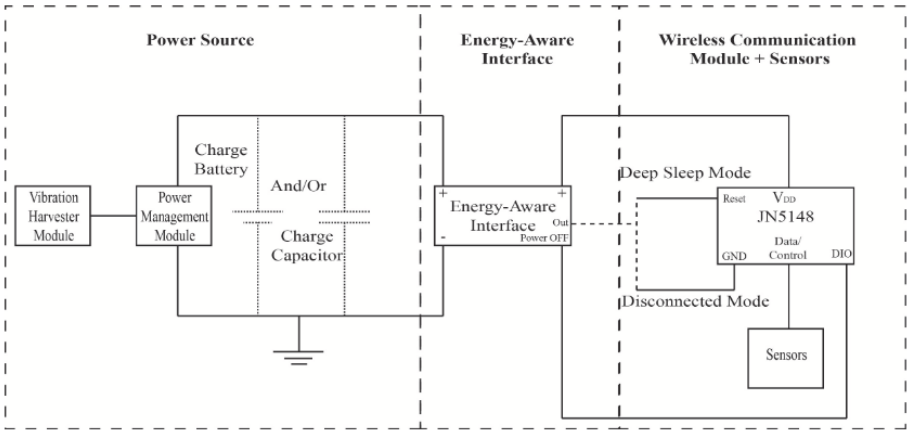

Figure 2.6: Block diagram of the vibration EH powered WSM with the EAI [28]

Some EAIs have been designed in different architectures and serve other purposes too. For example, apart from the usual monitoring of the threshold voltage of the energy storage capacitor for powering the WSM, the EAI is also used to disconnect the energy harvester from the power management circuit to prevent charging the capacitor to a high voltage level that exceeds the voltage rating of the capacitor [91]. Some designs eliminate the need of an additional voltage monitoring circuit for the implementation of the hardware EAI, achieved by using the inherent function within the power management chips.

For example, a Seiko S-882Z charge pump DC-DC converter was used to collect the low voltage from a micro electromagnetic generator and enable the harvested energy to be accumulated in the super-capacitor until it reaches the turn-on threshold of Seiko S-882Z itself [92]. Then, the super-capacitor will be discharged by an external load that was connected to the output of Seiko S-882Z, which in this case, is the MAX757CPA DC-DC boost converter, as shown in Fig. 2.7. The MAX757CPA provides a steady 3.3 V output the load, which is a WSM until the S-882Z turns off its output as the capacitor voltage reaches the turn-off threshold of S-882Z. Although an additional voltage monitoring circuit is eliminated, two

DC-DC converters are required for the charging and discharging purposes as shown in the energy flow chart in Fig. 2.8. It may not save energy during the discharging phase of the system as the MAX757CPA DC-DC boost converters requires about 10 mA of high current consumption when it becomes active.

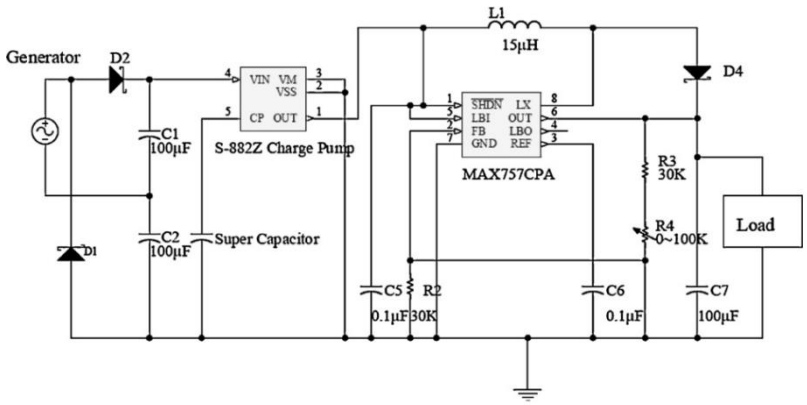

Figure 2.7: Schematic diagram of the power management circuits [92]

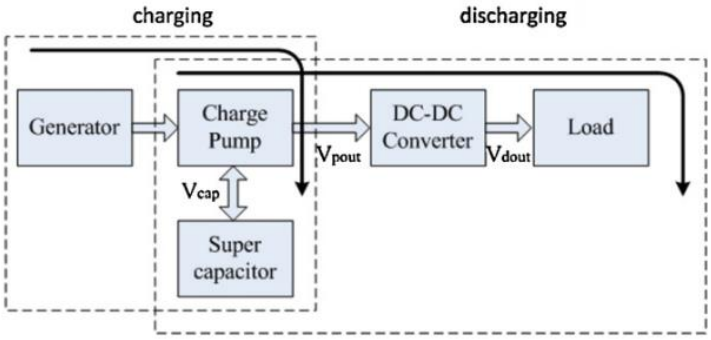

Figure 2.8: The energy flows during the charging process, and discharging process in the EH powered WSM system [92]

Another design relies on the “PGOOD” pin of the LTC3588 power management circuit to achieve the energy-aware functionality in a WSN that is powered by a piezoelectric patch bonded to a low-frequency vibrating beam [93]. The LTC3588 circuit integrates a full-wave bridge rectifier, a DC-DC converter, and a voltage comparator into a single chip where the PGOOD pin is controlled by the voltage comparator, as shown in Fig. 2.9. The PGOOD pin outputs a HIGH signal when the output voltage of the LTC3588 circuit is more than 92% of the target value [95]. An ISL43L210 switching circuit was used to manage the energy flow from

the LTC3588 circuit to the WSM. The switching circuit is directly controlled by the PGOOD signal, as shown in Fig. 2.10, where it will turn on the WSM when PGOOD is HIGH and turn off the WSM when PGOOD is LOW.

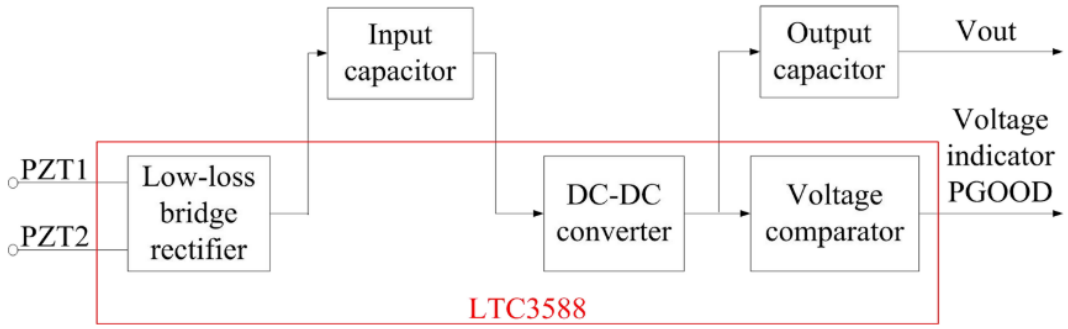

Figure 2.9: Block diagram of the EH module based on the LTC3588 and output capacitor [93]

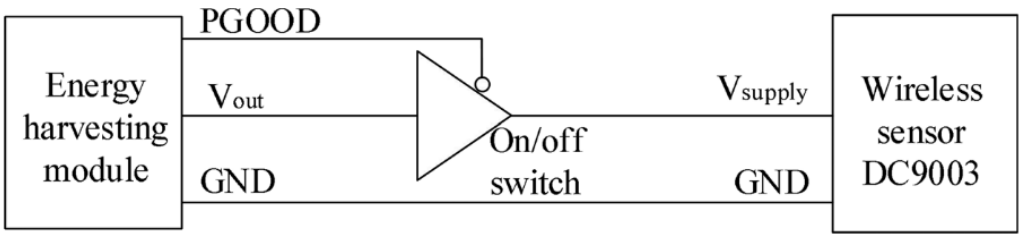

Figure 2.10: The switching interface between the EH module and a WSM [93]

In [96], the piezoelectric energy harvester is used to power the storage capacitor through the rectified circuit. As shown in Fig. 2.11, the charge management and regulation circuit is used to give a 2.5 V regulated supply voltage to the WSM. Moreover, the buck regulator and comparator LTC1540 circuit are used to turn on the WSM when the voltage across the storage capacitor reaches the pre-set threshold (5.3 V) and turn off the WSM when the voltage across the storage capacitor reaches falling threshold voltage varies between 2.8 V and 3 V, depending on the instantaneous current drawn. This is because the power saving quiescent current of the buck converter is much smaller than the current of WSM keeping on.

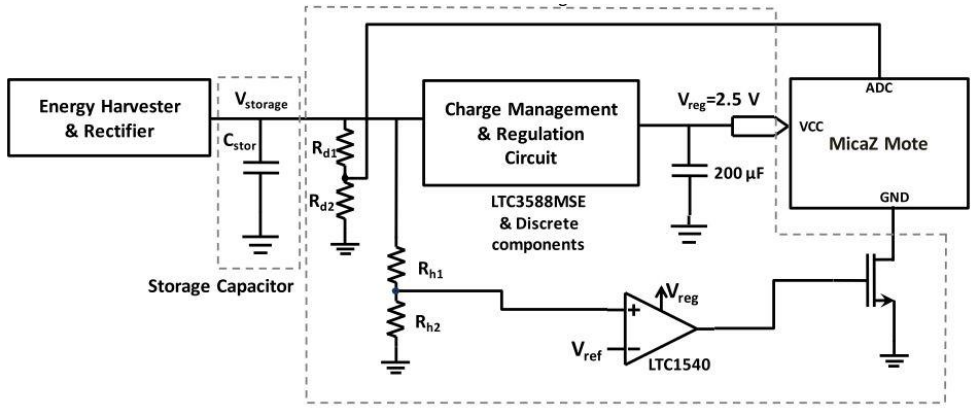

Figure 2.11: Schematic of the EH powered WSM in [96]

Among the different proposed energy-aware approaches for EH powered WSS, the hardware EAI between the WSS and energy harvesters or PMM circuit in the EH powered WSS is particularly important since it enables the generated energy to be stored in the energy storage device and has a low sleep energy consumption through turning off the connection between the WSS and energy harvesters or PMM circuit when there is not enough energy for the WSS during the active time. The system without the hardware EAI will never attain the required voltage supply that makes the WSS work properly in most cases. However, they can only turn on and turn off the WSS based on a single pre-fixed threshold voltage with very limited hysteresis. Apart from some straightforward algorithms for the microcontrollers to enter different modes based on the energy level as discussed earlier, there is a lack of energy-aware software that works in synergy with the hardware EAI to achieve energy saving or maximise the energy utilisation for meaningful tasks. There are three main drawbacks of the currently available energy-aware approaches. Firstly, if the WSS finishes the tasks early before the capacitor voltage drops to the pre-set threshold voltage, energy could be wasted as the WSS is still on in its idle state without doing anything meaningful. Secondly, if the WSM is still in the process of executing an operation

as the turn-off voltage threshold is reached, this would cause the WSS to be unable to finish the required tasks and waste the energy as well. Finally, the single threshold voltage of the EAIs limits the operation of the WSS to a short duration as the WSS will be turned off very soon after it has been turned on, which might not suit some tasks that require the WSS to be turned on for as long as possible. Given that energy-aware approaches have been proven to be widely applicable to different types of EH powered WSS, this thesis will research more sophisticated energy-aware approaches that would be practical for a wide range of real-world applications. Therefore, there is a lack of a comprehensive energy-aware method that considers energy-saving or maximum energy utilisation during the active phase of the WSS.

2.5 Summary

This chapter has discussed the following: (1) EH techniques, (2) wireless communication technologies and protocols, (3) energy-saving mechanisms for WSS, and (4) energy-aware approaches. Through these studies, the key research question of EH powered WSS has been obviously emerged, that is, there is a mismatch between the energy generated by the harvesters and the energy demanded by the WSS, as the limited energy is harvested and the WSS is power hungry.

Based on the literature review, the main research gaps that the thesis is addressing:

- Lack of available information focusing on energy consumption of EH powered WSM and WSN, not focusing on WSM and WSN technologies themselves;

- Lack of an interface between EH and WSS able to be efficient energy management and energy storage in the context of track condition monitoring user cases;

- Lack of the energy-saving approaches that focus on enabling the EH powered WSS to sample, transmission, commutation, and joining the network with the limited energy, since most of the previous energy-saving approaches on the WSM and WSN are powered by batteries;

- Lack of a comprehensive energy-aware approach that considers energy-saving or maximum energy utilisation during the active phase of the EH powered WSS;

- Lack of energy efficient hardware and software approaches to decrease current consumption for sleeping and for transmission in computing, sensing and communication to achieve ultra-low-power consumptions for implementation of EH powered WSS.

Therefore, the thesis will develop a method to deal with this mismatch through the design, implementation, characterisation of the WSS, and WSN powered by batteries and EH to identify the key issues and then to propose a combined energy-aware approach for EH powered WSM and WSN.

Moreover, based on the literature review, the following conclusions can be drawn:

- Compare with the performance among typical wireless communication technologies and protocols, ZigBee that is compliant to the IEEE 802.15.4 protocol, is selected for the development of EH powered WSS in the thesis since it has a low energy consumption, suitable transmission data rate, suitable transmission distance, and flexible network structure.

- The Jennic JN5148-001-M00 wireless module is selected for the development of EH powered WSM here since it has the lowest energy consumption of transmission and receiver process if compared with other commercially available modules.

- In order to reduce the energy consumption of the WSS in the EH powered WSS, understanding of power consumption of the WSM is the first task since it is helpful for designers to design the suitable approaches based on the energy level of every process of the WSS.

- Among the different proposed energy-saving mechanisms for WSS, energy-aware approaches are the most appropriate method for EH powered WSS. The hardware EAI between the WSS and PMM circuit of energy harvesters in the EH powered WSS is particularly important since it enables the generated energy to be stored in the energy storage device and has a low sleep energy consumption through turning off the connection between the WSS and PMM circuit of energy harvesters when there is not enough energy for the WSS during the active time. The system without the hardware EAI will never attain the required voltage supply that makes the WSS work properly in most cases.

Chapter 3 Experimental Analyses of Battery Powered Wireless Sensor Mote

The design of EH powered WSMs requires the knowledge of the energy consumption of WSMs. However, there is little information available on the energy consumption of WSMs. Understanding of the power consumption of battery powered WSMs is the first task for designing the EH powered WSMs. Therefore, a battery powered WSM is used to study the power consumption in the operational cycle of the WSM in this chapter.

The rest of the chapter is organised as follows: Section 3.1 describes a typical battery powered WSM system; Sections 3.2 to 3.4 describe a battery powered system implementation, including the hardware, the communication method, and the software for the power consumption study, respectively. Section 3.5 and 3.6 describe the experimental setup and results, respectively. Section 3.7 concludes the chapter.

3.1 Typical Battery Powered Wireless Sensor Mote

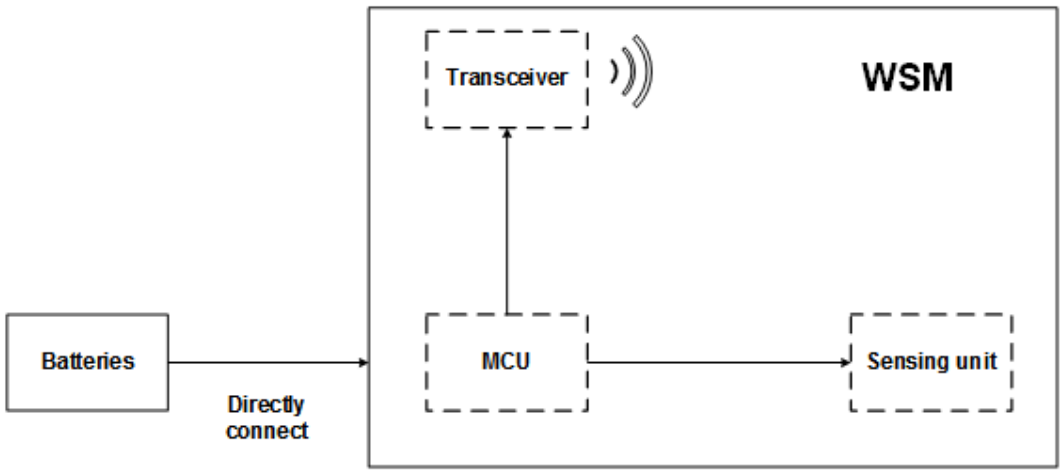

Figure 3.1: Block diagram of a battery powered WSM

The block diagram of a typical battery powered WSM [97] is presented in Fig. 3.1. The batteries are directly used to power the WSM. The WSM includes a Microcontroller Unit (MCU), a sensing unit, and a wireless transceiver. MCU is used to control the WSM operation, especially for the control of data reading from sensors and data transmission. The sensing unit may include at least one or several sensors with their peripheral circuits, which is used to measure the environmental and structural conditions. The transceiver transmits the measured data to the base station with a chosen wireless protocol.

3.2 Hardware Implementation of the Studied Wireless Sensor Mote

3.2.1 MCU, Transceiver and Sensors Choices

Based on the considerations described in the literature review, the wireless MCU of Jennic JN5148-001-M00 was chosen for the study. The sensors implemented in the mote were an ADXL335 3-axis accelerometer (Analog Devices,

Massachusetts, USA) [98] and an HIH-5030 low voltage humidity sensor (Honeywell, New Jersey, USA) [99]. The ADXL335 is a complete 3-axis accelerometer with signal conditioned voltage outputs and is able to measure accelerations with a range of ±3 g, including static acceleration of gravity in tilt-sensing applications and dynamic acceleration resulting from motion, shock, or vibration. The HIH-5030 humidity sensor is able to measure relative humidity (RH) from 0% to 100% RH. The output pin of all sensors can be directly connected to the Analog to Digital Converter (ADC) inputs of the MCU. Moreover, both of the sensors are chosen based on the low power consumption, and a small amount of signal processing required since the top consideration in the design of WSM is low energy consumption. The supply current of the selected accelerometer and humidity sensor are 350 μA and 200 μA, respectively.

3.2.2 Hardware Implementation

The simplified circuit diagram of the proposed WSM is shown in Fig. 3.2. The X-, Y- and Z-axis acceleration outputs of the accelerometer were connected with the ADC2, ADC3, and ADC4 pin of the MCU, respectively. It should be noted that there is a capacitor in parallel to each of the output pin, which is not shown in the figure since they are integrated with the accelerometer circuit. The capacitors are used to limit the output bandwidth, for example, to up to 50 Hz in the implemented circuit, acting as a low-pass filter for antialiasing and noise reduction. The output of the humidity sensor is connected with the ADC1 pin of the MCU. The software of the MCU controlled the integrated transceiver. The Joint Test Action Group (JTAG) debug is an IEEE1149.1 compliant JTAG port for the sole purpose of software code debug with the software development kit of Jennic. The JTAG

interface is disabled by default and is enabled under software control. Discrete Input / Output (DIO) 4 to DIO7 pins of the MCU are used for the JTAG interface.

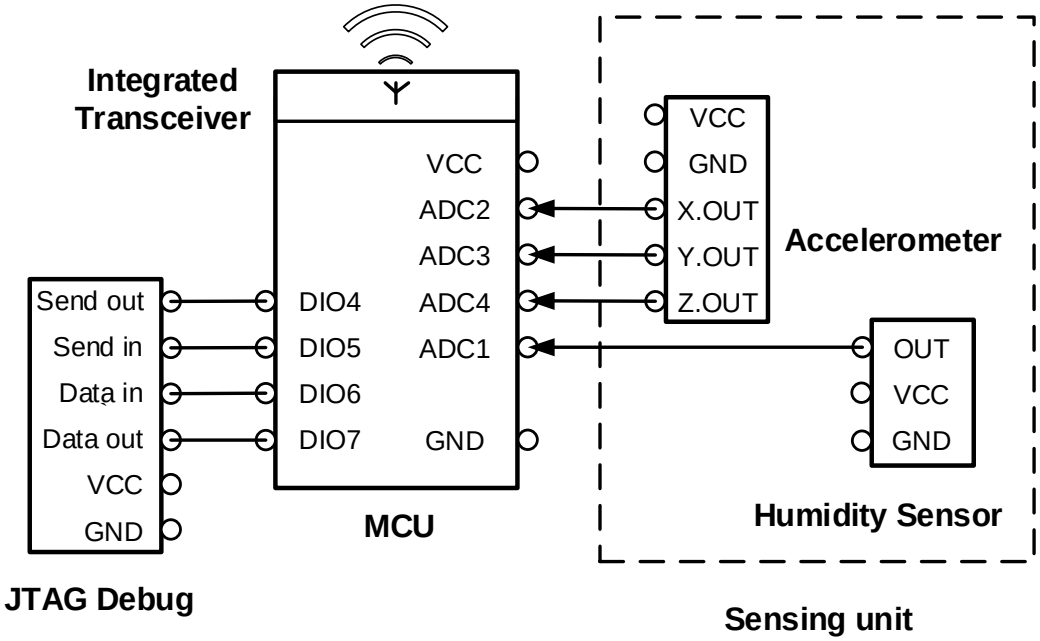

Figure 3.2: A simplified circuit diagram of the WSM used for the study of the battery powered WSM

Moreover, Fig. 3.3 shows the implemented hardware of the studied WSM on a breadboard. The humidity sensor circuit and the accelerometer circuit are placed on the left and right side of the MCU, respectively, since the ADC 1 pin and ADC2-4 pins are on those sides of the MCU, respectively. JTAG Debug is in the lower-left corner of the figure, and the green part at the top of the MCU is the integrated transceiver.

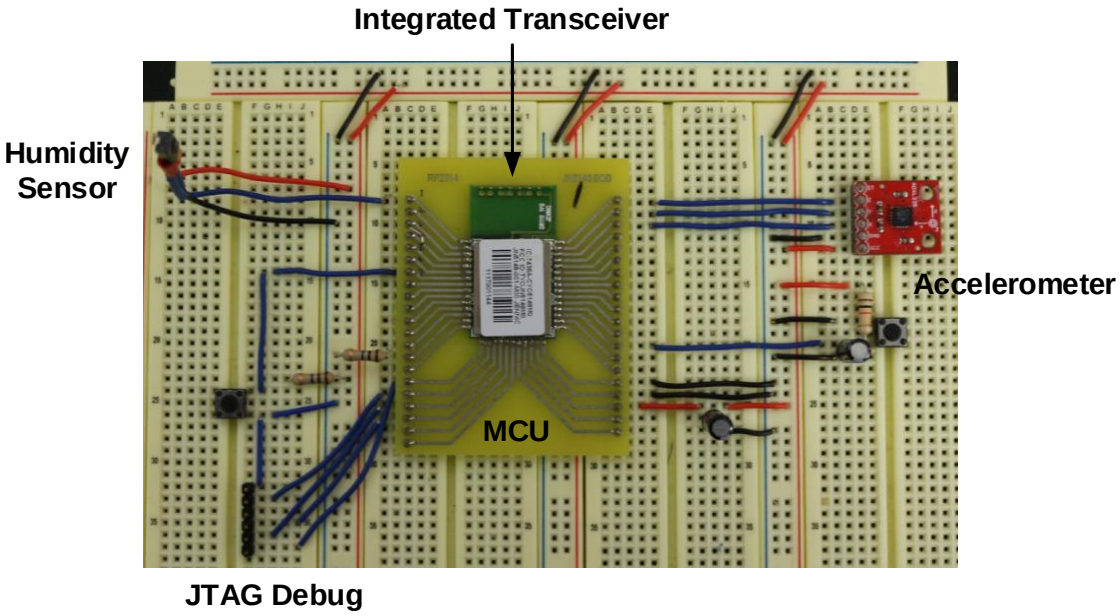

Figure 3.3: The WSM hardware implemented on the breadboard

3.3 Communication Technology of the Studied Wireless Sensor Mote

The integrated transceiver of MCU in the Jennic system uses the ZigBee protocol based on the 2.4GHz IEEE 802.15.4 standard. It is of low-cost and low-power. It is also targeted for low power consumption and low data rate applications. ZigBee Protocol transmission architecture specifies the physical layer, Media Access Control (MAC) layer, and network layer [47], as mentioned in the literature review. Furthermore, ZigBee-based networks, including mote to mote communication applications, have one base station device operating in either beacon-enabled or non-beacon enabled operating mode.

3.3.1 Network Layer

For the network layer and parts of the MAC layer, all ZigBee based communication operates in either beacon-enabled or non-beacon enabled operating mode. For the beacon mode, the base station sends out a periodic train of beacon signals containing information that allows the WSMs to synchronise their communications. A beacon also contains information on the data pending for the different nodes of the network. Fig. 3.4 shows the transmission of data from the WSM to the base station. When the WSM is required to send the data to the base station, it first listens to the beacon. On finding the beacon, it synchronises with the base station and then waits for the permission and the communication channel available for transmission. Once it gets permission, it will transmit the data to the base station. The base station may reply with an acknowledgment, which is optional, to confirm that the base station has received the data successfully [100].

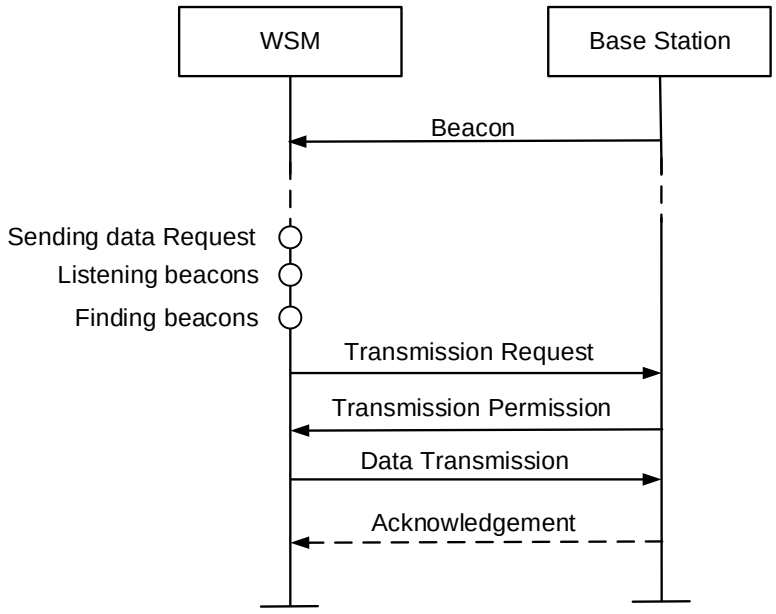

Figure 3.4: Communication between the WSM and the base station in a beacon enabled operating mode

However, the need to transmit and receive regular beacons puts certain power demands on both devices, especially the WSM, since it is necessary to keep listening to the beacon from the base station until it finds the beacon when it has the requests to send data. After that, it consumes the valuable energy on waiting for the base station response after transmitting the transmission request. Worse, it may cause data loss because of the uncertain active time due to the limited energy supply in most of the EH powered WSM applications. Therefore, the beacon-enabled operating mode is not suitable for EH powered WSM applications.

In the non-beacon enabled mode, beacons are not transmitted on a regular basis by the base station. Instead, communications are asynchronous, which means the WSM communicates with the base station only when it needs to, which may be relatively infrequent. Therefore, non-beacon enabled mode is useful in situations where the energy supply is limited, and light traffic is expected, especially for the mote to mote communication of EH powered WSM. The communication of the non-beacon enabled mode is also known as the one-way communication from the WSM to the base station.

3.3.2 MAC Layer

Fig. 3.5 shows a complete MAC frame format transmitted from the WSM to the base station. The frame format is a standard non-beacon enabled IEEE 802.15.4 packet, and it is composed of a MAC header (MHR), a MAC payload, and a MAC footer (MFR) [101].

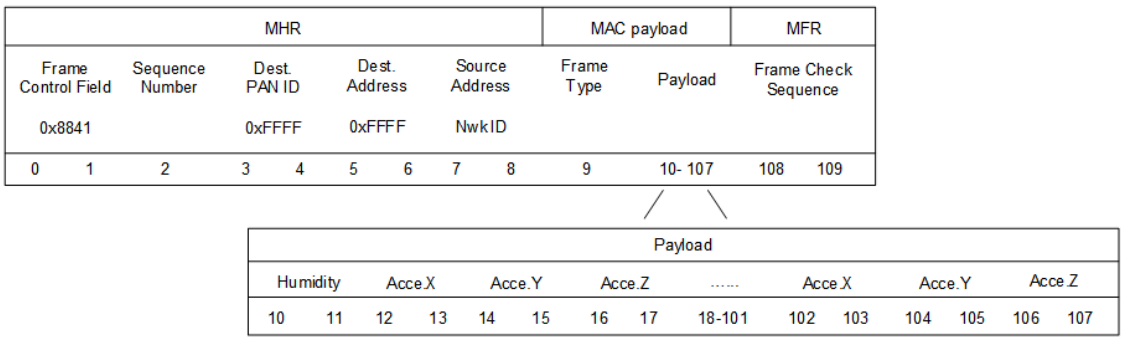

Figure 3.5: MAC frame format transmitted from the WSM to the base station

The fields of the MHR with the total length of 9 bytes appear in a fixed order. The frame control field is 2 bytes of the fixed 0x8841 in length, specifying a data frame. The sequence number field is 1 byte in length, specifying a unique sequence identifier for the frame. In the case that the frame control field and sequence number specify a data frame, it has no security and no acknowledgment involved, but it does include a destination Personal Area Network identifier (Dest. PAN ID), a destination address (Dest. Address) and a source address. The Dest. PAN ID and the Dest. The address field is both 2 bytes in length, specifying the unique PAN ID and the address of the intended recipient of the frame, respectively. They are set to a broadcast address of 0xFFFF, which is accepted as a valid PAN ID by all devices currently listening to the channel. The source address field is 2 byte in length, specifying the address of the WSM that sends out that frame.

For the MAC payload, the first field is a 1 byte frame type, which specifies whether the frame is the beacon, data, acknowledgment, or MAC command. Then, the rest of the payload contains the transmitted data, according to the application programmed in the WSM. In this chapter, the payload includes 2 bytes from the humidity sensor, and a pre-set number of reading, for example, 96 bytes from the accelerometer for a total of 98 bytes of data. The first two bytes are the humidity

data and the following data are the X-, Y-, and Z- axes of the accelerometer data in turn, which will be described in detail in the next section.

The MFR contains a 2 bytes frame check sequence (FCS), which is used to cyclic redundancy check based on the international telecommunications union-telecommunications standard.

3.3.3 Physical Layer

For the physical layer, the WSM is designed to use one fixed channel to transmit the data for saving the energy on searching and determining which channel is available before the WSM can transmit the data to the base station. For example, channel 26 (2405MHz) is chosen as the fixed channel to transmit the data from the WSM to the base station in the study.

3.4 Software Implementation of the Studied Wireless Sensor Mote

3.4.1 Implementation

The software is implemented based on the NXP's Jennic development platform, including Eclipse IDE (Integrated Development Environment) platform, JN51xx compiler for use by the Eclipse platform to build applications and produce binary files [102], and JN51xx flash programmer to load built applications into motes.
In detail, Eclipse IDE platform allows users to describe the application using a set of service calls and user functions written in the C/C++ language. It also allows users to edit and debug application codes. Moreover, it can be downloaded from

JN514x software developer's kit (SDK) libraries, including stack software and libraries of IEEE 802.15.4 protocols [103] for the software implementation of the studied WSM.

Programming application in the Eclipse IDE platform uses a function of the JN5148 integrated peripherals application programming interface (API) library to control the peripheral from the application, which runs on the WSM. API is a collection of C functions that can be incorporated in application codes that runs on a JN5148 microcontroller [104].

After the JN51xx compiler compiles the binary file which contains the programmed application from Eclipse IDE platform , the JN51xx flash programmer is used to load the binary file into the flash memory of the chip in the JN5148 microcontroller through a USB-to-serial cable [105].

3.4.2 Application Software Overview

The main operation of the WSM is described in Fig. 3.6. Upon being started, the first operation of the application is the initialisation of the hardware, stack, and application variables. Once this has been completed, the first sampling task begins, which is the MCU takes one reading from the humidity sensor [99]. After that, the accelerometer data reading loop is entered. The loop is executed based on pre-set iterative times and interval time, driven by events from a count function and a wake-up timer, respectively. The application sets the MCU to repeat each data reading process, for example, every 10 ms for 16 times. In each time, the MCU takes a total of three readings (6 bytes of data), each from x-, y-, and z-axis

of the accelerometer. Therefore, the MCU repeatedly takes 48 (16×3) readings, which make up 96 bytes of data during the duration of the loop.

Each reading is stored in the internal MCU RAM after each acceleration reading, and is transformed into the transmission frame data to will be transmitted after the loop ends. It should be noted that the maximum payload size in one transmission frame is about 100 bytes based on the 2.4 GHz IEEE 802.15.4 standard. This also explains the reason of iterating the loop for 16 times since this constitutes to a payload size that is within the limit and with sufficient data points. After that, the WSM transmits all the data stored in the RAM to the base station. Once the WSM finishes the transmission, it goes to the sleep with the RAM turned off since it is no longer required after the data has been transmitted, and a 32-kHz oscillator turned on to support timing function. The MCU wakes up through the time function to repeat the measurement.

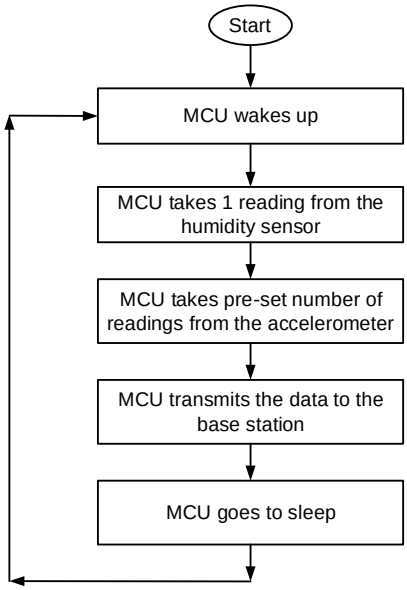

Figure 3.6 : The flowchart of the main operation of the studied WSM

3.4.3 Code and Function Description

This section provides details of codes and functions used in the software application. The flowchart of the main programme functions is shown in Fig. 3.7. It includes functions of the Initialisation, humidity sensor reading, acceleration reading loop, transmission function, and sleeping, which corresponds to the main operations shown in Fig. 3.6.

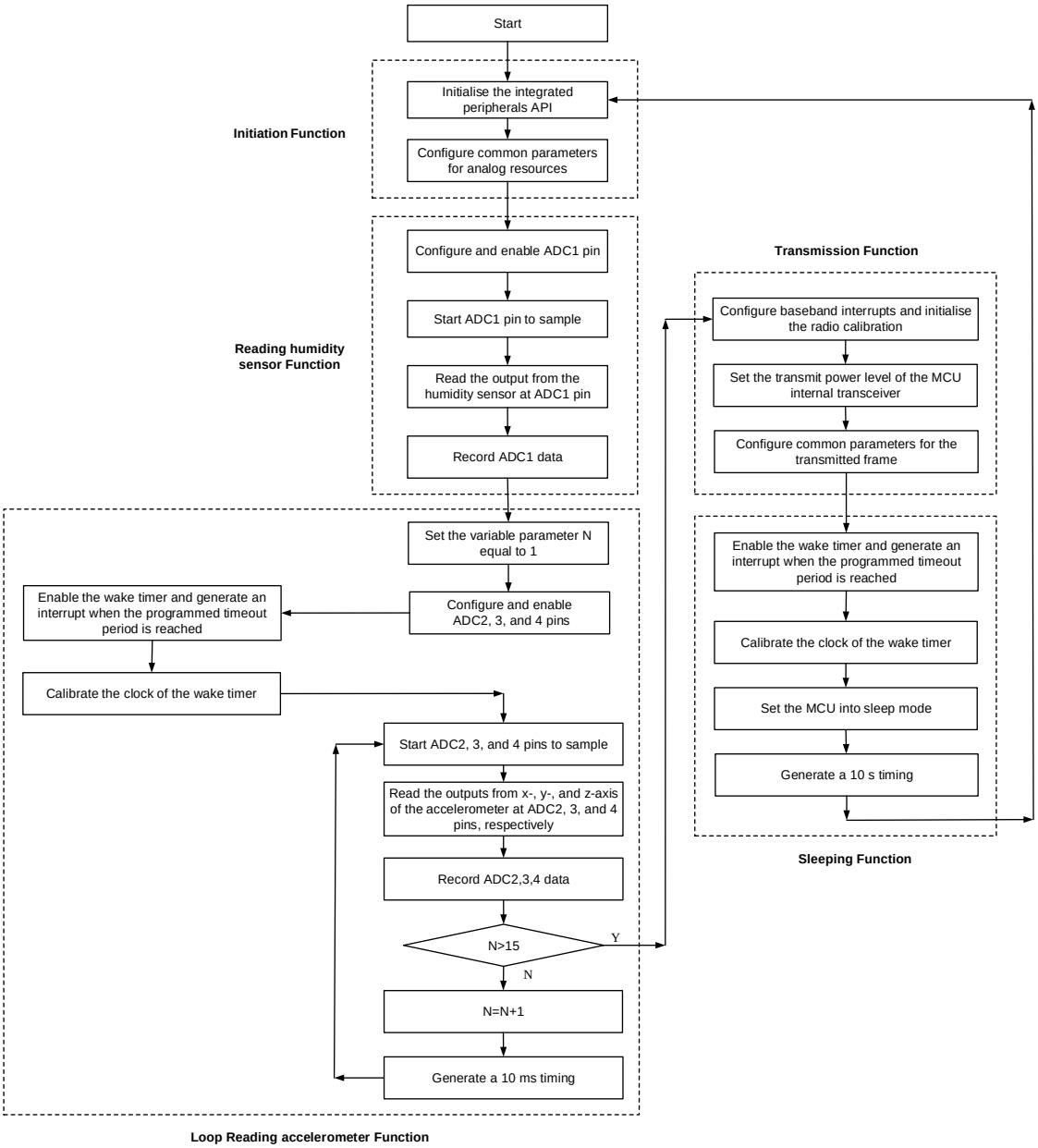

Figure 3.7: The flowchart of the main programme and its functions of the studied WSM

3.4.3.1 Realisation of Initialisation Function

The initialisation function is the main entry point of the application, called after the MCU gets the power to wake up. Upon being started, the function u32AHI_Init () is first called to initialise the integrated peripherals API. It is required to be called after every wake-up, and before any other, integrated peripherals API functions are called.

After that, the function vAHI_ApConfigure () is called to configure common parameters for analog resources. Through setting the function vAHI_ApConfigure (), in the implemented software, the MCU is programmed to enable the analog peripheral regulator, which uses a dedicated power source to minimise digital noise, and disable the interrupt after each ADC conversion. The frequency of ADC pin reading the input signal is able to up to 10 MHz. The reference voltage of ADC reading is set to use the internal voltage of the MCU.

3.4.3.2 Realisation of Reading Humidity Sensor Function

This function is used to control the MCU to take one reading from the humidity sensor, called after the Initialisation function is finished. Upon being started, the function vAHI_AdcEnable () is first called to configure and enable ADC1 pin to perform a single conversion with 2.4V reference voltage. It should be noted that, the function vAHI_AdcEnable () is able to set different input sources of the ADC, which can be selected from among ADC1 pin input, ADC2 pin input, ADC3 pin input, ADC4 pin input, on-chip temperature sensor and internal voltage monitor which is the voltage on the power supply pin. After that, the functions

vAHI_AdcStartSample () and vAHI_AdcRead () are called to start the ADC1 pin of the MCU to sample and read the output from the humidity sensor, and then store the data as an array of pointers in the MCU.

3.4.3.3 Realisation of the Loop for Reading Accelerometer Function

This function is a loop that controls the MCU to take 48 readings from the accelerometer, called after the reading humidity sensor function is finished. It iterates 16 times with an interval of 10 ms between each iteration, driven by three sub-functions: (1) judgment function, which is used to control the number of times that read from the accelerometer and judge when to stop the loop function, implemented by setting a variable parameter N to count the repetition times; (2) reading accelerometer function, which is used to control the MCU to read the accelerometer data and is implemented by setting a series of MCU reading ADC functions which are similar to the reading humidity sensor function; and (3) timing function, which is used to control the sampling rate of reading accelerometer and is implemented by setting the MCU wake timer.

Upon being started, the judgment function is programmed to set the variable parameter N equal to 1, and then the reading accelerometer function calls the function vAHI_AdcEnable () to configure and enable the ADC 2, 3, and 4 pins to perform a single conversion with 2.4V reference voltage. After that, the timing function calls the function vAHI_WakeTimerEnable () to enable the wake timer and generate an interrupt when the programmed timeout period is reached and u32AHI_WakeTimerCalibrate () to calibrate the clock of the wake timer to mitigate the effect from temperature, supply voltage, and manufacturing tolerance.

After the timing function completed, the reading accelerometer function calls the functions vAHI_AdcStartSample () and u16AHI_AdcRead () to sample the output from x-, y-, and z-axis of the accelerometer at the ADC 2, 3, and 4 pins, respectively. And then the data is stored as an array of pointers in the MCU. After that, the judgment function determines whether N is greater than 15. If so, the MCU goes to the next function. If not, N is increased by 1, and a 10 ms timing is generated as implemented by the function u8AHI_WakeTimerFiredStatus (), which is used to zero the selected wake timer and the function vAHI_WakeTimerStartLarge () which is used to start the wake timer countdown from the specified count value. After 10 ms timing, a new cycle of acceleration reading repeats, which starts at vAHI_AdcStartSample () and u16AHI_AdcRead () until N is greater than 15.

3.4.3.4 Realisation of Transmission Function

This function is used to control the MCU to transmit the data to the base station, called after the programme has judged N is greater than 15 and stopped the loop reading accelerometer function.

Upon being started, the function eLPTI_Init () is first called to configure baseband interrupts and initialise the radio calibration. Then, the function bAHI_PhyRadioSetPower () is called to set +2.5dBm transmit power level of the MCU internal transceiver to ensure a long transmitting distance of up to 10m.

After that, eLPTI_Transmit () is called to configure common parameters for the transmitted frame. The transmitted frame is configured by the communication channel, the long or short address of the transmitting device, the long or short address of the destination device, and whether the frame requires an acknowledgement from the receiver or not. In the implemented software, the MCU is programmed to set the communication channel as channel 26, since the communication is design as a fixed channel communication and the acknowledgement from the base station is not required in the communication because one-way communication is used.

3.4.3.5 Sleeping Function

This function is called after the transmission function is finished. It is used to control the MCU go to sleep, and then wake up to repeat the processes starting from the Initialisation function. It generates a 10 s sleeping timing, driven by two sub-functions from (1) timing function, which is used to control the sleeping time and is implemented by setting the MCU wake timer and (2) sleeping function, which is used to put the MCU into sleep mode.

Upon being started, the timing function is programmed by using the wake timer as the wake timer to generate a 10 s timing implemented by setting functions vAHI_WakeTimerEnable (), u32AHI_WakeTimerCalibrate (), u8AHI_WakeTimerFiredStatus () and vAHI_WakeTimerStartLarge () in sequence, which is similar to the timing function of the loop reading accelerometer function. After that, the sleeping function calls the function vAHI_Sleep () to set the MCU into sleep mode. During the sleeping time, the MCU is programmed to go to sleep

with the RAM off and the 32-kHz oscillator on, since all the data stored on the RAM would have been transmitted to the base station before the MCU goes to sleep and the 32-kHz oscillator is required for the timing function.

3.5 Experimental setup

In order to characterise the energy consumption of the implemented battery powered WSM, the experimental setup was shown in Fig. 3.8 and in Fig. 3.9. In the setup, the implemented WSM was powered by one direct current (DC) power source, representing the batteries. The source meter with two measured channels was used to measure the energy flow through the WSM. One channel was used to measure the current through the WSM at Points A and B, which was connected in series between the DC power source and the WSM. Another channel was used to measure the voltage across the WSM at Points C and D, which was connected in parallel to the WSM. A LabVIEW program running on the computer was used to control the source meter and display the measured results from the source meter. A base station was placed at a distance of 4 m to receive the data from the WSM.

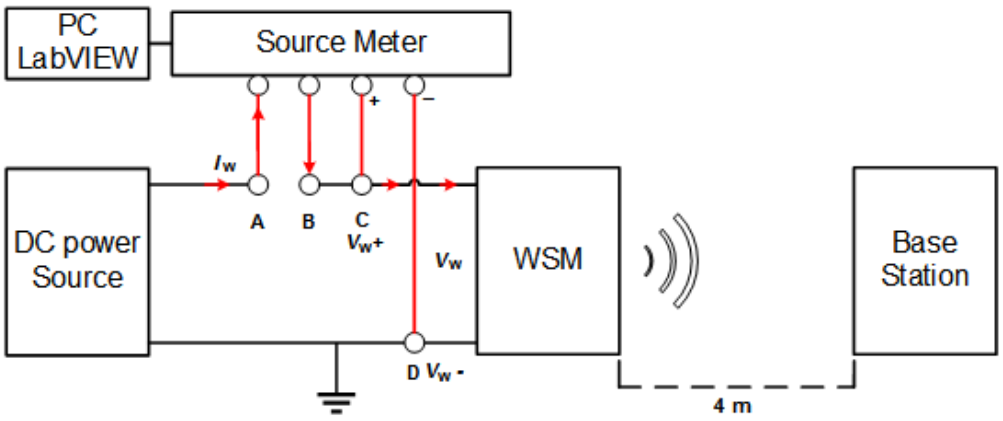

Figure 3.8: The block diagram of the experimental setup for characterising the DC power source powered the WSM

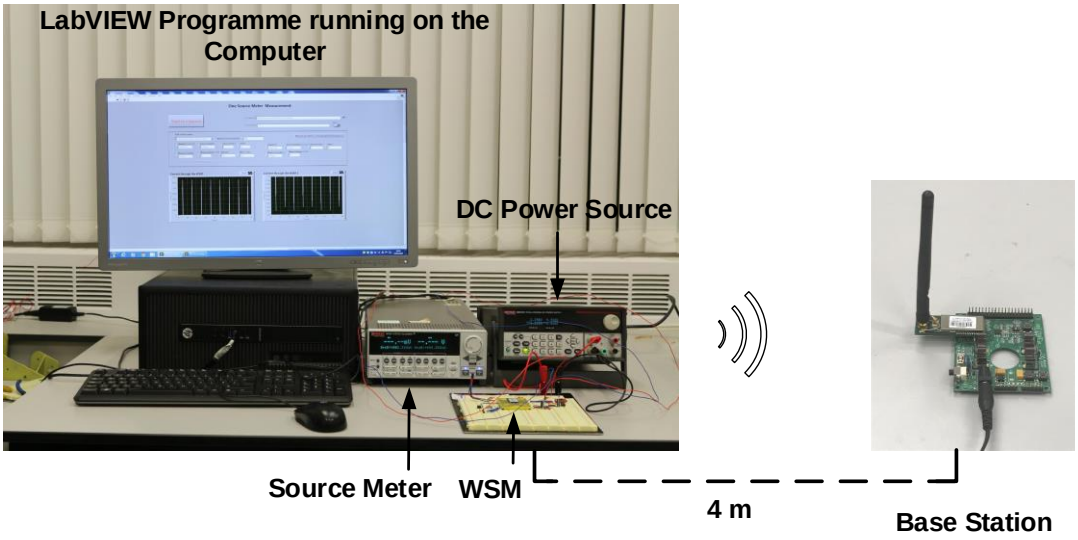

Figure 3.9: Photograph of experimental setup for characterising the DC power source powered WSM

3.5.1 DC Power Source

In order to properly represent the batteries to power the WSM, Keithley 2220-30-1 was used as the DC power source [106]. It has 2 channels having outputting 0 –30 V of voltage with 0.03% basic voltage output accuracy and 0–1.5A of current output with 0.1% current output accuracy, which are good enough to be used to power the implemented system. For the power setup, one outputting channel of the DC power source was connected to the WSM in series via the source meter, as shown in Fig. 3.8. The maximum output voltage was set to be 3.2 V, which is a standard supply voltage for the MCU of the WSM, and the output current was set to be 8 mA, which is the minimum current that has been found to enable the implemented system to operate.

3.5.2 Source Meter

Keithley 2612B source meter was used to measure the voltage and current of the WSM [107]. For the setup, there are four main parameters that need to be set for tests: (1) the number of power line cycles (NPLC), (2) the sampling time

interval, (3) the measurement range and (4) the number of data points which is related to the measurement time.

NPLC is used to reject the power line-induced Alternating Current (AC) noise during the measurement time. It sets the integration time in several power line cycles, which is the period that the analog-to-digital (A/D) converter of the source meter measures the input signal. The higher the NPLC, the more accurate the signal value will be, which means a more significant noise rejection and better resolution. 1 PLC specifies an integration time of 20 ms. The fastest integration time is 20 µs when PLC is set to be its minimum value of 0.001. Therefore, the maximum sampling rate of the source meter is 50 kHz. For the implemented circuit, the sampling time interval is the time between two readings of the source meter. To achieve a desired and constant sampling rate, this value needs to be specified. The relationship between maximum NPLC and sampling time interval or sampling rate is shown by the following equation 3.1.

$$\text{Maximum NPLC} = \frac{\text{Sampling time interval}}{0.02} = \frac{50}{\text{Sampling rate}} \tag{3.1}$$

The measurement range is also affected by the sampling of the source meter. When the auto range is turned on, the source meter will adjust the measurement range automatically according to the level of the signal. If the signal level is relatively stable, the source meter will not change its measurement range. In such a case, the auto range does not affect the sampling rate, and the source meter will sample the data at a constant sampling rate, determined by NPLC and time interval. However, when the measured signal level varies significantly, there is a varied sampling rate [107]. For example, the current consumed by the

microcontroller is expected to change dynamically since the microcontroller will stay at different states such as sleep and activity. Therefore, to keep a constant sampling rate, the auto-range function was turned off in the experiments.

3.5.3 LabVIEW Interface

A snapshot of the user interface created using LabVIEW is shown in Fig 3.10. It was used to set the channel function, the sampling interval, the measurement range, the number of data points, the NPLC, and the measurement time of the source meter. The graph on the left of Fig. 3.10 shows the current through the WSM, and the graph on the right shows the voltage across the WSM.

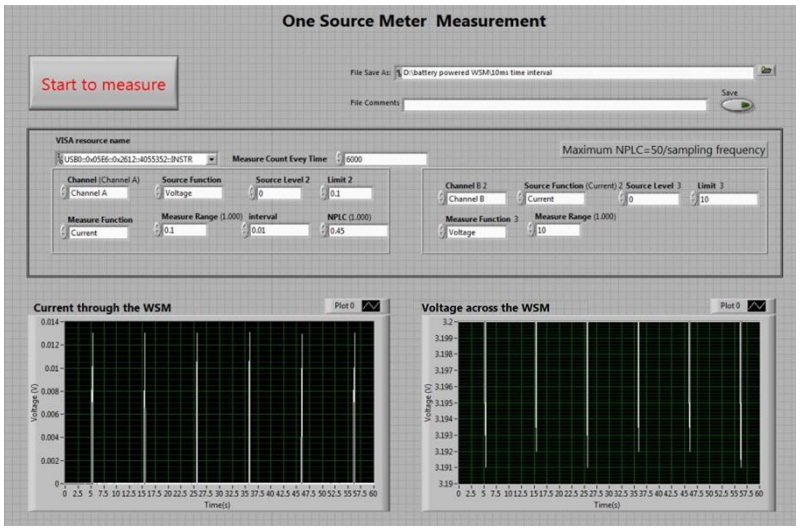

Figure 3.10: A snapshot of the LabVIEW program for displaying and recording the measured current and voltage

Two series of experiments were carried out to analyse the energy consumption of the WSM. Since the source meter has a limited number of data points, which directly affects the measurement time, as mentioned before, different settings are required for different experiments. The first experiment takes the measurements of multiple cycles of the WSM operation to verify the programmed application. The sampling interval was set to 1 ms, and NPLC was set to 0.05, which means

the sampling rate of the source meter was set to be 100 Hz. The number of data points was set to be 60000, which means the measurement time is 60 s. The second experiment focuses on only one cycle of the operation to further analyse the process of the WSM during the active time and sleep time. The sampling interval was set to be 0.1 ms, and NPLC was set to be 0.005, which means the sampling rate of the source meter was 1000 Hz. The number of data points was set to 120000, which means the measurement time is 12s.

3.5.4 Calculations of Power and Energy

As mentioned before, experiments measure the voltage across the WSM, V_{w}, and the current through the WSM , I_{w} . With V_{w} and I_{w} recorded, the instantaneous power consumption of the WSM, P_{w} at time (t_k) can be calculated by equation 3.2.

$$P_w(t_k) = V_w(t_k) \times I_w(t_k) \tag{3.2}$$

Where $P_w(t_k)$ is the instantaneous power consumption of the WSM at t_k , and $V_w(t_k)$ and $I_w(t_k)$ is the instantaneous voltage and current at t_k.

Therefore, the whole energy consumption of the WSM during a period can be calculated by equation 3.3.

$$E_w(t_n) = \sum_{k=i}^{n} V_w(t_k) \times I_w(t_k) \times \Delta t \tag{3.3}$$

Where $E_w(t_n)$ is the whole energy consumption of the WSM from the beginning at the time of t_i to the end at the time of t_n, Δt is the sampling time interval set by the source meter, and n is the number of data points.

3.5.5 Calculations of Average Current, Voltage and Power

In order to analyse the energy consumption of the WSM, the average current, the average voltage and the average power also need to be considered.

The average current I_{ave} of the WSM measured within a fixed timeframe of T can be calculated by equation 3.4.

$$I_{ave} = \frac{\sum_{k=1}^{n} I_w(t_k) \times \Delta t}{T} \tag{3.4}$$

Similarly, the average voltage V_{ave} of the WSM measured within a fixed timeframe of T can be calculated by equation 3.5.

$$V_{ave} = \frac{\sum_{k=1}^{n} V_w(t_k) \times \Delta t}{T} \tag{3.5}$$

Based on equation 3.3, the average power P_{ave} over the time period T can be calculated by equation 3.6 using V_{ave} and I_{ave}.

$$P_{ave} = \frac{\sum_{k=i}^{n} V_w(t_k) \times I_w(t_k) \times \Delta t}{T} \tag{3.6}$$

3.6 Experimental results and discussions

The measurements of the power consumption of the WSM for multiple and one cycle operations were performed using the implemented WSM, and the experimental setup described earlier. Table 3.1 shows the same points, different points, and significance of the experiments between one and multiple cycles of the WSM operations. It should be noted that the same implemented WSM, the same programme, and the same experimental method were used to characterise the power consumption in the experiments. The differences in both experiments are the sampling rate used, the measurement time, and the measured number of cycles of the WSM operation. 100 Hz of sampling rate used in the first experimental measurement, the longer measurement time is allowed for analyses of multiple cycles of the WSM operation. 1000 Hz of sampling rate for one cycle measurement time in the second measurement is allowed for a more detailed measurement on one active and sleep cycle to analyse the energy consumption of every process.

Table 3.1: Description of the same points, different points and significance of the experiments between one and multiple cycles of the WSM operations

WSM operation	Multiple Cycles of the WSM Operation	One Cycle of the WSM Operation
Measured WSM	Same	Same
Programme of the measured WSM	Same	Same
Measured the energy flow through the WSM	Same	Same
Sampling rate of the source meter	100 Hz	1000 Hz
Measurement time	Long	Short
Significance of measurement results	Long measurement time is able to analyse the average energy consumption of one active and sleep cycle among multiple active and sleep cycles	High sampling rate is able to analyse the detailed energy consumption of each specific process in one active and sleep cycle

3.6.1 Multiple Cycles of the Wireless Sensor Mote Operation

Figs. 3.11 (a) and (b) show the measured current of I_W and voltage of V_W with a 100 Hz sampling rate of the source meter. The figures show the multiple cycles of the WSM operation. Figs. 3.11 (c) and (d) show the calculated instantaneous power P_W and instantaneous energy E_W based on I_W and V_W from Figs. 3.11 (a) and (b). Figs. 3.11 (e) and (f) further show the measured currents of I_W during a complete active time and sleep time of the system, respectively.

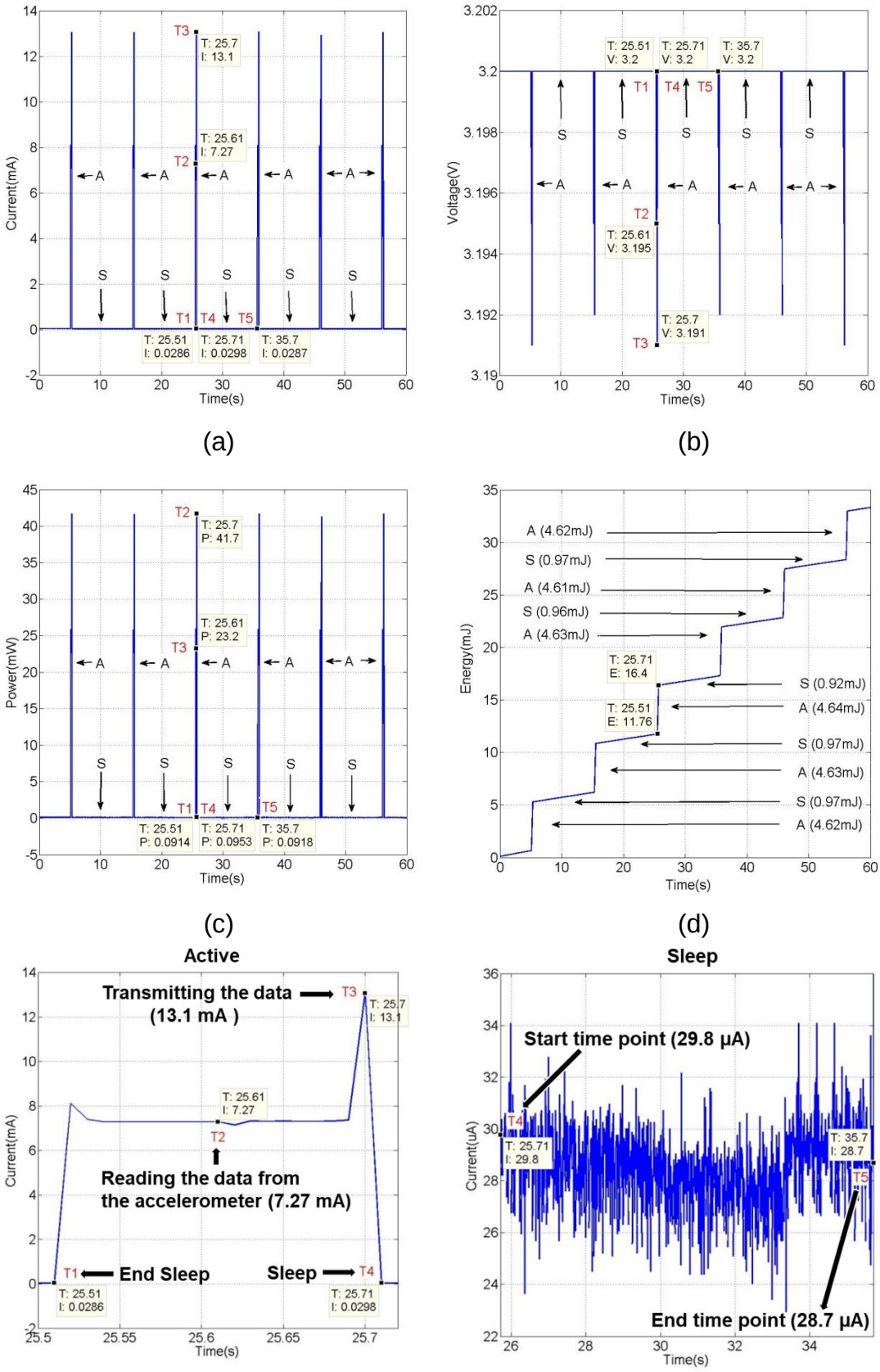

Figure 3.11: Measured results of (a) I_W and (b) V_W of the system using a sampling rate of 100 Hz. The calculated results of (c) P_W and (d) E_W are calculated based on the measured I_W in (a) and V_W in (b). The measured (e) I_W and (f) I_W are the enlarged plots of the measured I_W in (a) for a complete active time and sleep time of the system, respectively.

It can be seen that the WSM wakes up to execute the pre-set programmed tasks during the active time, which is noted as A in the figure after it has been powered up for about 5 s. After the WSM finishes the tasks, it goes to sleep for 10 s, which is the sleeping time programmed in the WSM as denoted by S in the figure. After the sleeping time, the WSM wakes up again and then repeat the same active and sleep operation mentioned previously until the DC power source is switched off.

Moreover, there are five typical time points, which are denoted as T1, T2, T3, T4, and T5 in the Figs. 3.11 (a), (b), (c), (e), and (f), respectively. They are used to illustrate the changes in the WSM current and voltage in different operational processes and are described below:

T1: The WSM starts to wake up at 25.51 s for the implemented WSM, with about 28.6 μA of current consumption at 3.2 V and, therefore, 0.0914 mW of instantaneous power.

T2: The WSM is reading the data from the accelerometer during the active time. The current consumption increases to about 7.27 mA, and the voltage drops to about 3.195 V. The corresponding instantaneous power increases to 23.2 mW.

T3: The WSM is transmitting the data to the base station during the active time with the maximum current consumption of 13.1 mA and minimum voltage 3.191 V. The corresponding instantaneous power increases to 41.7mW.

T4: The WSM starts to go to sleep after finishing the transmission, with about 29.8 μA of current consumption at 3.2 V and, therefore, 0.0953 mW of

instantaneous power. T4 also shows that the WSM experiences about 190 ms of active time between T1 and T4.

T5: The WSM starts to wake up again with about 28.7 µA of current consumption and, therefore, 0.0918 mW of instantaneous power. T5 also shows that the WSM experiences a 10 s sleeping time between T4 and T5.

Moreover, Fig. 3.11 (d) shows the energy consumption during one cycle of active and sleep times. The WSM consumed about 4.62 mJ, 4.63 mJ, 4.64 mJ, 4.63 mJ, 4.61 mJ, and 4.62 mJ of energy from the first to sixth active times, respectively. This yields an average energy consumption of about 4.63 mJ for the active time. The WSM consumed about 0.97 mJ, 0.97 mJ, 0.92 mJ, 0.96 mJ, and 0.97 mJ of energy for the first to fifth sleep times, respectively, which gives an average energy consumption of about 0.96 mJ for the sleep time.

It should be noted that, when the current consumption increases significantly, the corresponding voltage will drop. It is because a limit was set on the electrical output capacity of the DC power supply. However, this does not affect the energy consumption analyses of the system, since the energy consumption is calculated based on both current and voltage.

3.6.2 One Cycle of the Wireless Sensor Mote Operation

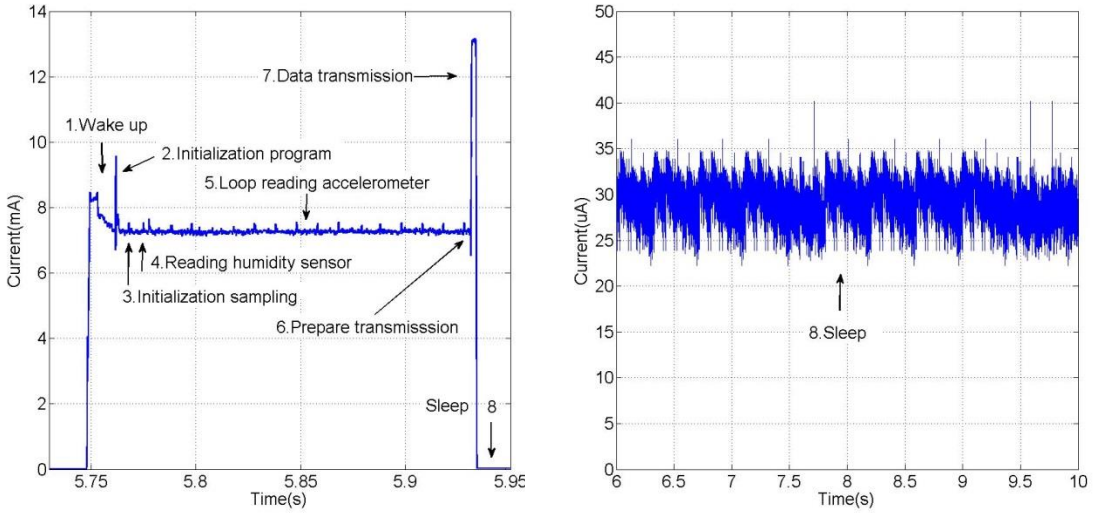

(a) (b)

Figure 3.12: The enlarged plots of the measured results of I_W, where (a) for a complete active time and (b) for the sleep time of the system using a sampling rate of 1000Hz

Fig. 3.12(a) shows the measured current of I_W in one active time and Fig. 3.12 (b) shows the measured current of I_W in sleep time. From the figures, it can be observed that the current consumption can be broken down into the following 8 operational processes:

Process 1: as the WSM wakes up, all the peripheral circuits and components are powered up, consuming an average current consumption of 7.42 mA in 13.5 ms.

Process 2: after waking up, the WSM starts to initialise the programme, performing the u32AHI_Init () function as described in Section 3.4, consuming an average current consumption of 7.35 mA in 6.3 ms.

Process 3: the WSM initialises the sampling process, performing the vAHI_ApConfigure() function as described in Section 3.4, consuming an average current consumption of 7.27 mA in 7.1 ms.

Process 4: the WSM reads the humidity sensor, which consumes an average current consumption of 7.29 mA in 2.8 ms.

Process 5: the WSM reads from the accelerometer 16 times with the interval time of 10 ms between successive readings, consuming an average current consumption of 7.27 mA in 150 ms.

Process 6: the WSM prepares the transmission, such as turns on the radio, and puts the sampling data into the transmission frame, consuming an average current consumption of 7.30 mA in 3.1 ms.

Process 7: the WSM transmits the data to the base station, consuming an average current consumption of 11.25 mA in 3 ms.

Process 8: the WSM executes the sleeping function and remains in the sleep state, consuming an average current consumption of 30.4 μA in 10 s.

3.6.3 Analysis of the Energy Consumption of the Process

Table 3.2 shows the average current, average voltage, average power, and energy consumption as calculated using equations 3.2 to 3.6 of every process of the experimental measurement in Section 3.6.2.

The total energy consumption is 5.57 mJ, which can be calculated as the sum of the “energy” column in Table 3.2. The energy consumption for one active cycle

is 4.60 mJ during 185.8 ms of active time, which means the average power for one active cycle is 24.8 mW. For the energy consumption during sleeping, the WSM consumed 97.28 μW for 10s, which means the average power for sleeping is 97.28 μW.

For the energy consumption of the data processing, it can be seen that WSM consumed 3.79 mJ (0.07+3.72) for reading 98 bytes (6×16+2) of data in 152.8 ms, which means the average energy consumption of the WSM for reading 1 byte is about 38.67 μJ. For transmitting 98 bytes of data, the WSM consumed 0.18 mJ (0.07+0.11) in 6.1 ms, which means the average energy consumption of transmitting 1 byte is about 1.84 μJ. In summary, the collective process of the WSM for processing 98 bytes (6×16+2) of data from waking up to the data transmission in 185.8 ms requires 4.60 mJ, which means the average energy consumption of processing 1 byte of data is about 46.94 μJ.

Table 3.2: Energy consumption of every process in the JN5148 and accelerometer

No.	Process	Average Current	Average Voltage	Average Power	Energy	Time
1	Wake up	7.42 mA	3.198 V	23.73 mW	0.32 mJ	13.5 ms
2	Initialisation program	7.35 mA	3.197 V	23.50 mW	0.15 mJ	6.3 ms
3	Initialisation sampling	7.27 mA	3.196 V	23.23 mW	0.16 mJ	7.1 ms
4	Reading humidity sensor	7.29 mA	3.195 V	23.29 mW	0.07 mJ	2.8 ms
5	Loop Reading accelerometer	7.27 mA	3.195 V	23.23 mW	3.72 mJ	150.0 ms
6	Prepare transmission	7.30 mA	3.195 V	23.32 mW	0.07 mJ	3.1 ms
7	Data transmission	11.25 mA	3.191 V	35.89 mW	0.11 mJ	3.0 ms
8	Sleep	30.4 µA	3.200 V	97.28 µW	0.97 mJ	10.0 s

3.7 Summary

This chapter has presented a customer developed batteries powered WSM system of hardware, software, and communication methods and analysed the energy consumption of the WSM in its operational cycles. The WSM was built with a JN5148 microcontroller and two sensors: accelerometer and humidity sensor. The integrated transceiver uses the ZigBee protocol based on the 2.4 GHz IEEE 802.15.4 standard. The main software function includes the initialisation function, reading humidity sensor function, reading accelerometer loop function, transmission function and sleeping function. The experimental results show that the WSM consumes about 4.60 mJ for carrying out the programmed tasks during one active cycle of 185.8 ms and 97.28 µW for one sleep cycle of 10 s. The average energy consumption of the WSM in processing 1 byte is 46.94 µJ /byte, including wake up, sampling, and transmission during active time.

Chapter 4 Energy-aware Approaches for Energy Harvesting Powered Wireless Sensor Mote

Chapter 3 has studied the energy consumption of the developed battery powered WSM. Chapter 4 will use the developed WSM in Chapter 3 to directly connect an energy harvester, discuss key issues of such an EH powered WSM, and address these issues by proposing and developing energy-aware approaches.

The rest of the chapter is organised as follows: Section 4.1 describes a typically existing EH powered WSM system. Section 4.2 identifies the cause of the risen issues in the EH directly powered WSM through experimental measurements. Section 4.3 discusses how to address the issues by proposing and developing energy-aware approaches, including hardware EAI, software EAI and sensing EAI, to manage the energy flow through the system to solve the identified issues. Section 4.4 shows the experimental setup and results of a custom-developed EH powered WSM system by use of the proposed energy-aware approaches. Section 4.5 concludes the chapter with a summary of the key findings.

4.1 Typically Existing Energy Harvesting Powered Wireless Sensor Mote

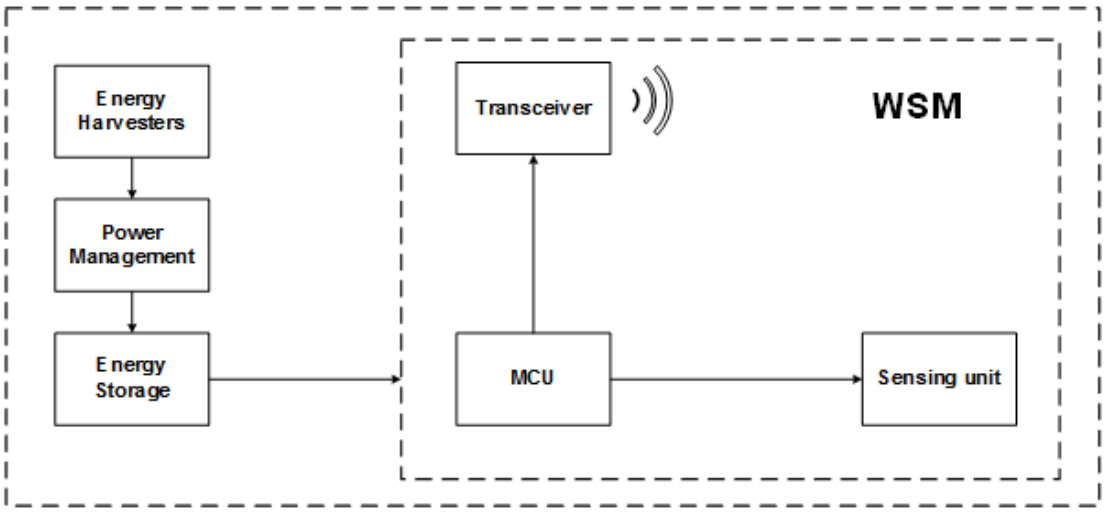

Figure 4.1: Block diagram of a typical existing EH powered WSM

A typically existing EH powered WSM block diagram is presented in Fig. 4.1 [14] and [108], which is composed of four main blocks: energy harvesters, a power management module (PMM), an energy storage, and a WSM. Compared with the battery powered WSM system shown in Fig.3.1, the energy harvesters, the PMM, and the energy storage replace the batteries to power the same WSM. Energy harvesters are used to harvest energy from the ambient environment. The harvested energy is regulated by the PMM and then stored in the energy storage. When the voltage across energy storage reaches the minimum operating voltage of MCU, the WSM starts to consume the stored energy to carry out pre-set tasks.

4.2 Analysing the Key Issues of Existing Energy Harvesting Powered Wireless Sensor Mote

In order to identify and understand the key issues of a typical EH powered WSM system, a custom developed WSM powered by a vibration energy harvester was used in the study. The energy flow through the system was analysed to determine the cause of the key issues.

4.2.1 Energy Harvester

A macro-fibre composite (MFC) was used as an energy harvester to convert strain energy induced by structural vibration into electrical energy. The MFC is a patch type of piezoelectric transducer that was developed by NASA Langley Research Centre [109]. It has been widely used as strain energy harvesters due to its extreme flexibility and durability together with high piezoelectric performance compared with traditional piezoceramic materials [110] and [111].

Fig.4.2. shows the photograph of energy harvester by adhesive bonding an M8528-P2 MFC (Smart Material GmbH, Dresden, Germany) onto one side of a carbon fire composite plate, which was implemented by the Energy Harvesting Research Group at the University of Exeter. The MFC has an overall length, width, and thickness of 103 mm, 31 mm, and 0.3 mm, respectively, but the dimensions of the EH area are 85 mm × 28 mm. The carbon fibre composite plate has a length, width, and thickness of 300 mm, 50 mm, and 5 mm, respectively. Both ends of the plate were sandwiched by two aluminium plates, which serve as the gripping platform that will be held by a testing machine in subsequent

experiments. Two electric wires connected to two electric electrodes of the MFC, which was used to generate the output energy from the MFC.

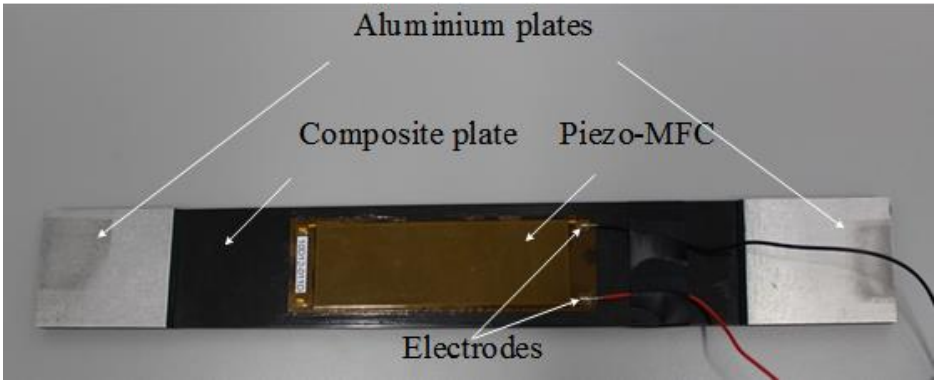

Figure 4.2: The implemented energy harvester by the Energy Harvesting Research Group

4.2.2 PMM, Energy Storage and the Studied WSM

The PMM used in this research and developed by the Energy Harvesting Research Group at the University of Exeter as well is shown in Fig. 4.3. It consists of (1) a full-wave diode bridge rectifier to convert the AC voltage produced by the energy harvester into DC voltage, (2) a maximum power point tracking (PMMT) circuit that allows as much power as possible to be transferred from the energy harvester to the energy storage, and (3) DC-DC converter to regulate the rectified DC voltage and produce a usable DC voltage for charging the energy storage and powering the WSM [112]. It should be noted that the rectifier is only needed for energy harvesters with AC output, such as the MFC. A 10 mF super-capacitor was used as the energy storage in the study. The studied WSM was the same WSM described in Sections 3.2 to 3.4, including its hardware and software.

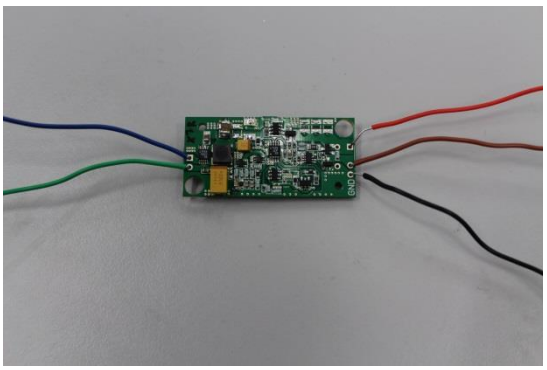

Figure 4.3: The PMM used in this research [112]

4.2.3 Experimental setup

A peak-to-peak strain loading of 600 με at 10 Hz was applied onto the strain energy harvester using an Instron E10000 ElectroPuls dynamic testing machine (Instron, High Wycombe, UK) as shown in Fig. 4.4.

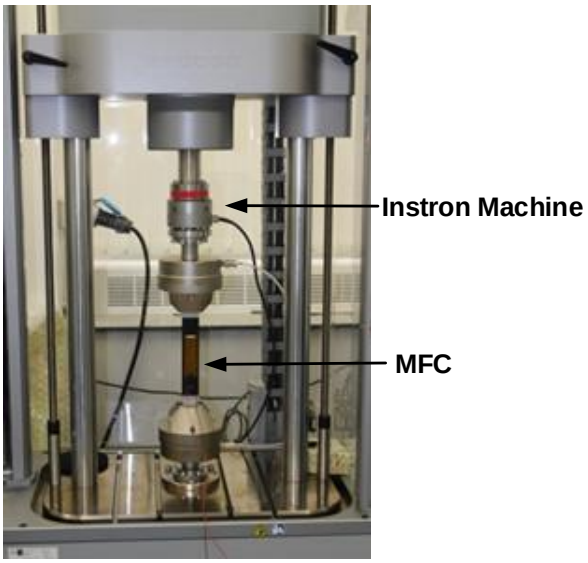

Figure 4.4: Instron machine with the MFC energy harvester

The experimental setup for measuring the energy flow throughout the implemented EH powered WSM system is schematically shown in Fig. 4.5. In the setup, all the measurements were made using two source meters with 1000 Hz sampling frequency. One was used to measure the voltage across the super-capacitor, V_{CS} at the points of A and B, and measure the input current to the

super-capacitor , I_{CS} at the points of C and D. Another source meter was used to measure the voltage across the WSM, V_W at the points of E and F and measure the current output to the WSM from the super-capacitor , I_W at the points of G and H. A LabVIEW program was used to control the measurements of the two source meters and display the measured results on the computer.

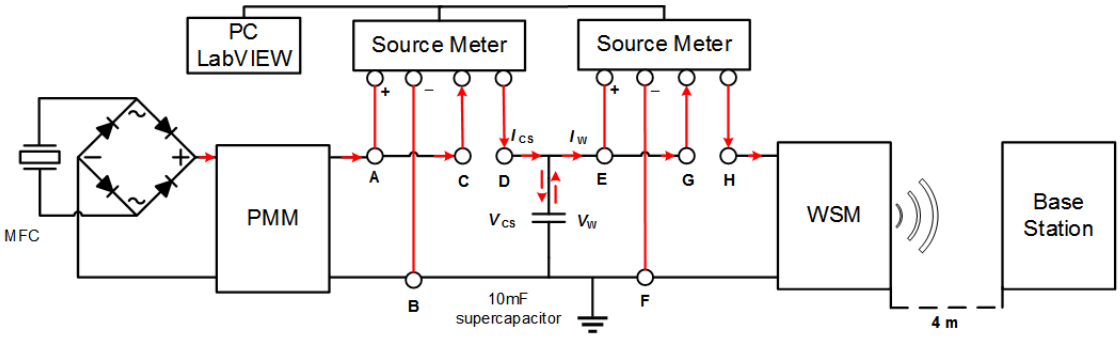

Figure 4.5: The schematic of the experimental setup for characterising the MFC powered WSM

The energy generated by the MFC that has been conditioned and outputted by the PMM, E_{CS}, within a timeframe can be calculated by equation 4.1. The energy consumed by the WSM, E_w, within a timeframe, can be calculated by equation 3.3.

$$E_{cs}(t_n) = \sum_{k=i}^{n} V_{cs}(t_k) \times I_{cs}(t_k) \times \Delta t \qquad (4.1)$$

where $E_{cs}(t_n)$ is the total energy that has been outputted by the PMM from the time beginning at t_i to the end at t_n, Δt is the sampling time interval of the source meter, which is set to be 1 ms and n is the number of sample/data count.

The accumulated energy stored in the super-capacitor, E_s, at a given time can be calculated by equation 4.2.

$$E_s(t_n) = E_{cs}(t_n) - E_w(t_n) \quad (4.2)$$

4.2.4 Results and discussions

Figs. 4.6(a) and (b) show the measured voltage of V_{CS} and current of I_{CS} across the super-capacitor, and Figs. 4.6 (c) and (d) show the measured voltage of V_w and the current of I_w, at the input to the WSM, respectively. It can be observed that V_{CS} is equal to V_w since they were connected in parallel in the system, and both of them are able to initially increase to about 2 V and then fluctuated around it. The DC-DC converter is enabled momentarily by the MPPT circuit to transfer the harvested energy from the MFC to the super-capacitor [112]. Therefore, the current profile of I_{CS} exhibits a non-continuous burst of spikes with a peak of around 100 mA. However, the maximum output current from the PMM is about 3.1 mA at V_{CS} of about 2 V, but I_w is steady at around 0.3 mA in most of the sleep time. This voltage and current are much lower than the minimum operating voltage of around 2.4 V and current of around 7 mA as required by the WSM to start the operation properly, as discussed earlier in the section.

Figs. 4.6 (c) and (e) show the energy flow of E_{CS}, E_w, and E_S. It can be observed that, when V_w increases to about 2.01 V at about 14.48 s, it cannot increases to the minimum operational voltage. This is because the energy consumption of the WSM begins to increase, causing the accumulated energy stored in the super-capacitor to decrease. Also, E_w increases significantly at the same time, and energy harvested is not high enough for MCU required. Therefore, V_w cannot increases to the minimum operational voltage shows that there is a gap between the energy generated by the energy harvester and the energy required by the

WSM. The system is not capable of storing enough energy effectively for the MCU to start up and so there is a start-up issue for the MCU since the accumulated energy is consumed by the MCU instantly.

The drastic increase in the energy consumption of the WSM when V_w reaches about 2 V at 14.48 s is because that the voltage level can only support part of peripherals of the MCU such as the ADCs, Digital Converter to Analog (DAC)s, comparators and the internal temperature sensor to start working. However, it is still lower than the minimum operating voltage of the MCU (2.4 V) to support all the peripherals of the MCU. Those parts, as mentioned above, are always powered on until there is a minimum operating voltage available to the core processor of the MCU for it to operate properly and control all the peripherals with proper initialisation. Therefore, with the MCU and some of its peripheral circuits continuously draw energy when the voltage supply is below the minimum operating voltage of 2.4 V while there is limited energy harvested by the MFC, the harvested energy cannot be accumulated in the energy storage.

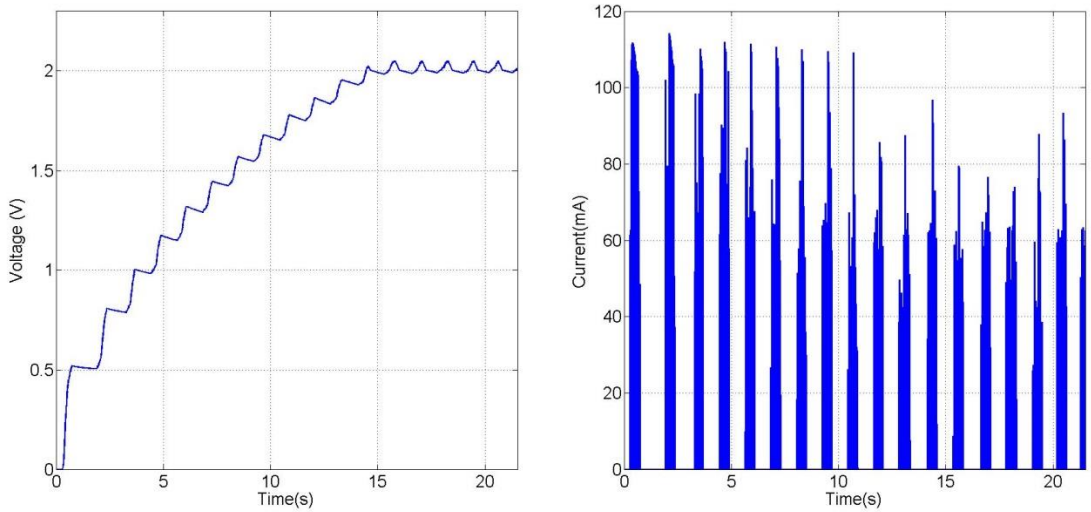

(a) (b)

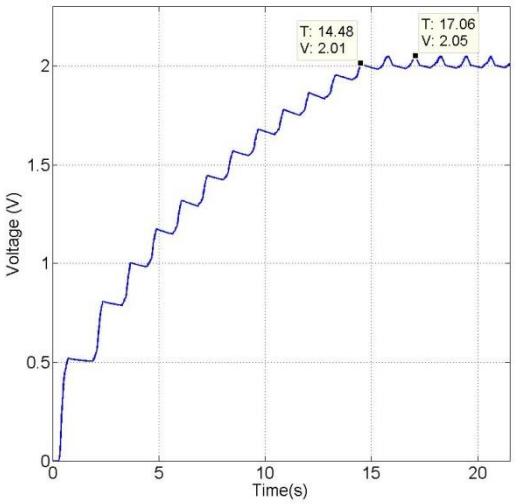

(c)

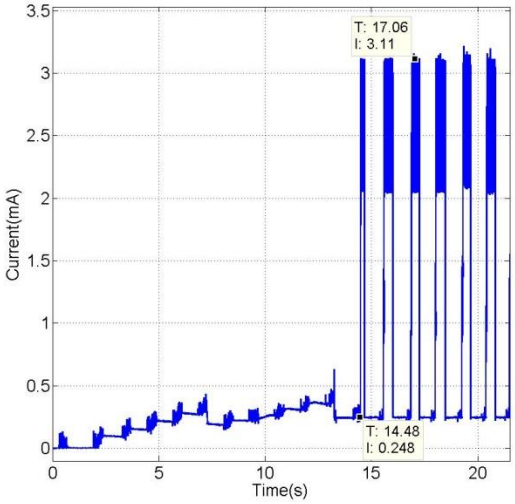

(d)

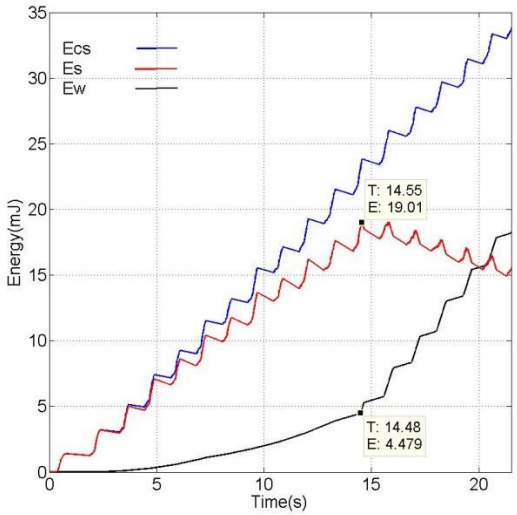

(e)

Figure 4.6 : Measured profiles of the (a) V_{CS}, (b) I_{CS}, (c) V_w, (d) I_w, and the calculated (e) E_{CS}, E_w, E_s of the system

4.2.5 Identified Causes of Issues

Through the above experimental discussions of the energy flow, it can be observed that the first key issue of the EH powered WSM systems are the energy gap where there is a mismatch between the energy generated by the energy harvesters and the energy demanded by the WSM, in which the former is usually lower than the latter. This means the energy supply from EH is usually insufficient to meet the energy requirements of WSMs instantly. The second key issue is

start-up where the WSM is not able to start where the harvested energy could not be accumulated in the capacitor since the WSM immediately consumes the energy, and therefore the supply voltage is not able to reach the required operating voltage of the WSM.

4.3 Proposed Energy-aware Approaches

In order to solve the issues of a typical EH powered WSM system as described in Section 4.2, the energy-aware approaches are proposed, designed, and implemented to deal with the start-up and the energy mismatch issues through reducing the power consumption during the active time and the sleeping time, including the cold sleeping time and the warm sleeping time. It should be noted that the active time is defined as the period where the WSM is activated to perform the pre-programmed tasks, which includes the operation starting from the WSM woken up until it finishes the transmission and then starts to go to sleep. The cold sleeping time is defined as the period where the energy storage is charged from zero to sufficient energy for the WSM to be firstly active to perform the pre-programmed tasks. The warm sleeping time is defined as the period of time where the WSM goes to sleep until it is activated again. The warm sleeping time is shorter than the cold sleeping time since the energy storage is not charged up from zero as there is some energy that remains in the energy storage but is not enough to support the operation of the WSM.

Fig. 4.7 illustrates the developed EH powered WSM with the energy-aware approaches. Compared with the typical existing EH powered WSM system shown

in Fig.4.1, the proposed system has added three main blocks: (1) hardware EAI, (2) sensing EAI, and (3) software EAI.

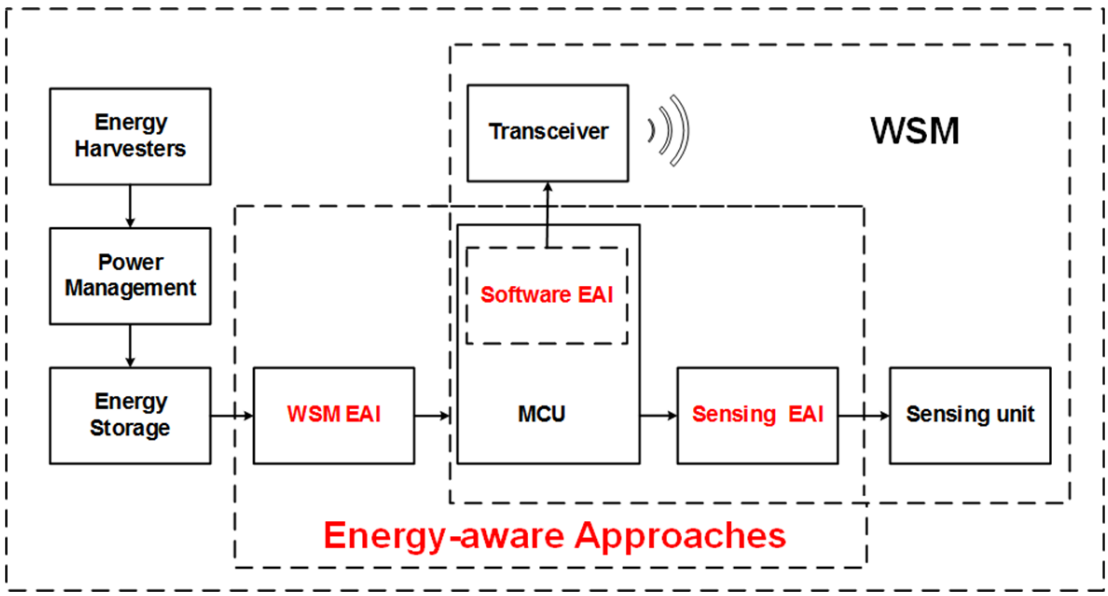

Figure 4.7: Block diagram of the developed EH powered WSM with energy-aware approaches

4.3.1 Hardware Energy-aware Interface

4.3.1.1 Concept

The hardware EAI is an interface between the energy storage and the WSMs, which is designed to solve the start-up problem and reduce the power consumption of the WSMs during sleeping time. It is used to monitor the voltage across the energy storage to judge if there is enough energy in the energy storage for the WSMs to perform the pre-programmed tasks and determine when to wake the WSM up.

4.3.1.2 Implementation

Fig. 4.8 shows the schematic of the developed hardware EAI. The circuit consists of: (1) an ultra-low power voltage supervisor (LTC2935-1, Linear Technology, United States) which is used for monitoring the voltage across the energy storage V_{CS} and controlling the on or off state of an N- Metal Oxide Semiconductor Field-

Effect Transistors (N-MOSFET), and (2) the N-MOSFET which is used as a switch to turn on or off the WSM as controlled by the voltage supervisor circuit.

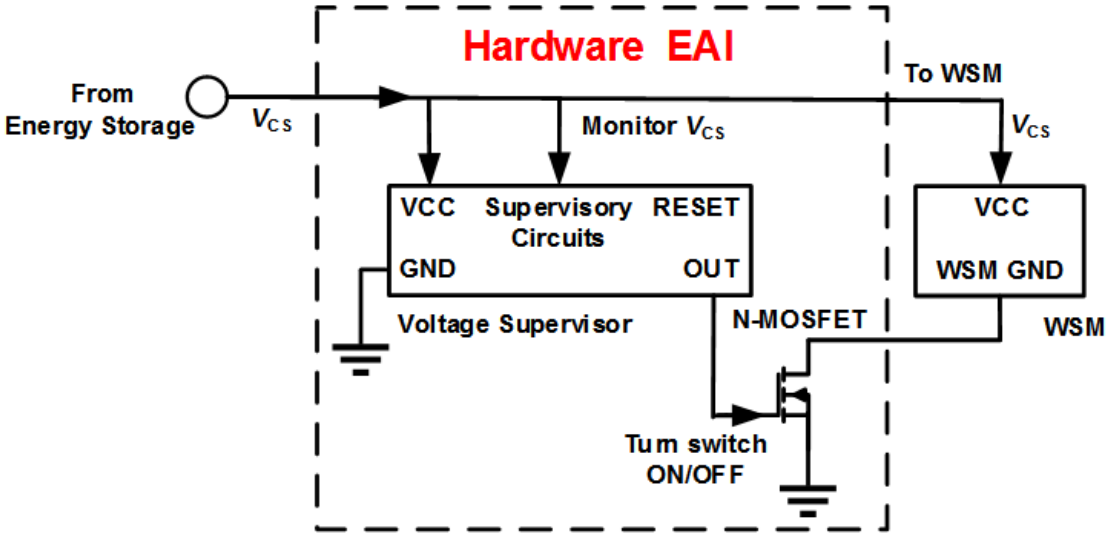

Figure 4.8: Schematic of the hardware EAI

The working principle of the hardware EAI is by using the low or high state of the OUT pin of the voltage supervisor to control the N-MOSFET switch to break or make the connection between the system ground and the negative terminal of the WSM to achieve the sleeping or active state of the WSM. In detail, the voltage supervisor monitor V_{CS} and pull the OUT pin low when V_{CS} is below a defined turn-on threshold voltage, V_{H-on}. Whenever V_{CS} rises above V_{H-on}, the OUT pin output changes from a low state to a high state, enabling the WSM to achieve the active state. When V_{CS} drops below a defined turn-off threshold voltage, V_{H-off}, the output of the OUT pin changes from a high state to a low state, enabling the WSM to achieve the sleep state. It should be noted that both V_{H-on} and V_{H-off} can be set to a fixed value with eight possible choices ranging from 1.6 V to 3.45 V in pre-determined increments [113].

4.3.1.3 Operation

Fig. 4.9 shows the illustration of the voltage V_{CS} changes under the control of hardware EAI and the operation is explained as follows: The energy storage device defined as C_S in the figure is initially charged from 0 V. The OUT pin of the voltage supervisor stays low when V_{CS} is lower than V_{H-on}. Since the power consumption of the hardware EAI is much lower than the energy generated by the energy harvesters, the harvested energy can be accumulated in the energy storage. Therefore, V_{CS} is able to increase during the cold sleeping time.

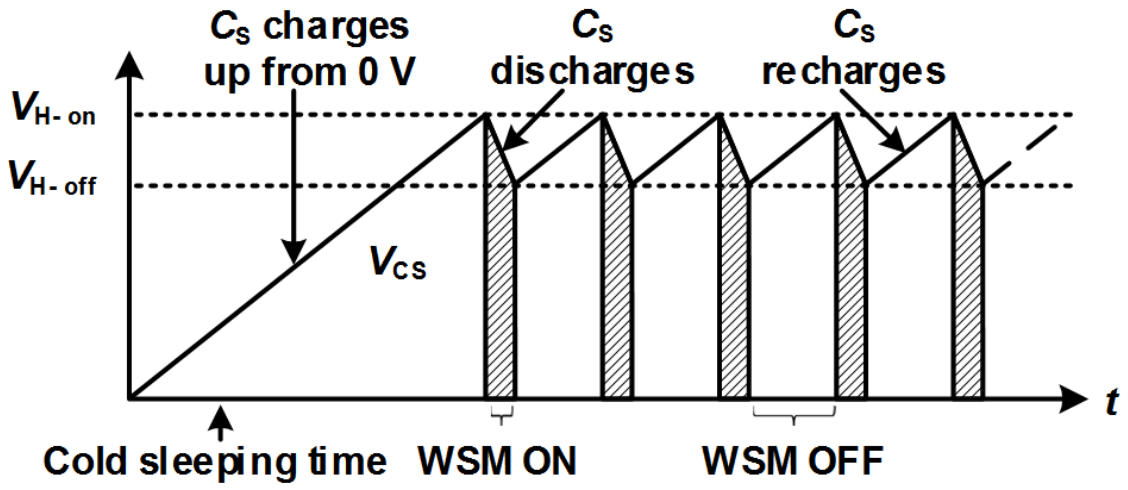

Figure 4.9: An illustration of V_{CS} changes under the control of hardware EAI where V_{H-on} is defined turn-on threshold voltage and V_{H-off} is defined turn-off threshold voltage

Once V_{CS} exceeds V_{H-on}, the output pin is set to be in a high state, which turns the N-MOSFET into a low impedance state, connecting the system ground and the negative terminal of the WSM. The WSM and the energy storage then form a closed circuit, where the WSM can draw the current, and consequently, the WSM becomes active to perform the pre-programmed tasks.

V_{CS} subsequently decreases during the active time, since the energy generated by the energy harvester is lower than the energy demanded by the WSM during

active time. When V_{CS} is lower than V_{H-off} , the voltage supervisor changes the out pin state from high to low, which turns the N-MOSFET off into a high impedance state, disconnecting the system ground and the negative terminal of the WSM. As a result, the WSM is disconnected from the energy storage and is switched off immediately. The WSM now turns into the non-active phase so that the energy storage can be charged up again if there is input energy from the harvester. The system remains in the sleep phase until V_{CS} reaches V_{H-on} again, and then the cycles repeat.

With the two different threshold voltages used in the EAI, the WSM certainly has sufficient energy to begin its pre-programmed task immediately once the capacitor voltage has reached the turn-on threshold voltage. Moreover, the proposed hardware EAI allows flexible control of the WSM as the actual operational state of the WSM is known to occur at the turn-on threshold of the EAI. The operational window of the WSM can be easily controlled by adjusting the difference between the two threshold voltages.

4.3.2 Software Energy-aware Interface

4.3.2.1 Concept

The software EAI is designed to increase the energy use efficiency to extend the active time so that the WSM is able to monitor more data from the surrounding environment. It is a virtual interface between the MCU and the transceiver, which is used to judge whether the energy stored in the energy storage device is enough for the WSM to carry out the next operation and ensure all the measured data is transmitted before the energy becomes too low for the operation of the WSM.

As mentioned before, the hardware EAI is used to turn on and turn off the WSM based on the pre-fixed threshold voltages V_{H-on} and V_{H-off} , respectively. Therefore, the WSM would be turned off when V_{CS} reached the pre-fixed threshold V_{H-off} regardless of the WSM operation states, which causes energy wastage if the WSM is in a period of active operation.

In order to solve these problems, the software energy-aware programme is introduced to monitor the voltage across the energy storage V_{CS} and to judge if there is enough energy in the energy storage for the WSM to carry out the next operation and ensure all the measured data is transmitted before the energy becomes too low for such an operation. Therefore, it enables the WSM to stay active for as long as possible to allow as many data as possible to be sampled and transmitted without being limited by a fixed duty-cycle.

4.3.2.2 Operation and Implementation

Fig. 4.10 shows the illustration of V_{CS} changes under both the control of software EAI and hardware EAI. Compared with the system under the control of the hardware EAI, the system adds three defined voltages: V_{END}, V_{S-off}, and V_{MIN}.

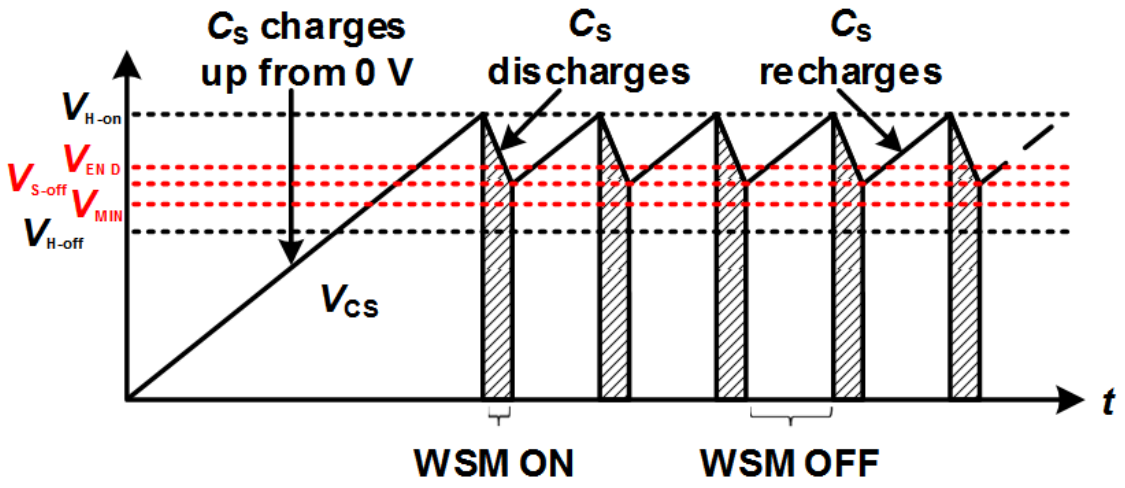

Figure 4.10: An illustration of the voltage V_{CS} changes under the control of hardware EAI and software EAI where V_{END} is the voltage that is used to judge whether the capacitor has enough effective energy to supply the WSM to perform the next tasks, V_{s-off} is the voltage that is used to judge whether the capacitor has enough effective energy to supply the WSM to perform the next tasks and V_{MIN} is the minimum operating voltage of the WSM

V_{MIN} is the minimum operating voltage of the WSM, which means the WSM is no longer able to operate properly below V_{MIN}. It should be noted that V_{MIN} is not the same as V_{H-off} since V_{H-off} is one of the eight fixed values provided by the voltage supervisor while V_{MIN} is based on the electrical characteristics of the chosen MCU. If V_{H-off} is set to be higher than V_{MIN}, the system will not be able to perform the measurements for as long as possible since the WSM will be turned off when it still has the energy and sufficiently high voltage level to support the WSM operations. Therefore, V_{H-off} should be set below V_{MIN}, which does not affect the maximum utilisation of energy by the WSM and also acts as a fail-safe mechanism that makes sure the WSM is able to change to the non-active state in case the software EAI loses its function.

V_{END} is the voltage that is used to judge whether the capacitor has enough energy to supply the WSM to perform the next tasks. Furthermore, the judged energy is defined as the energy that will be consumed by the WSM to complete the next tasks just before V_{CS} falls below V_{MIN}. Therefore, V_{END} is required to be higher than V_{MIN} by at least a level that is equivalent to the consumed energy of the next tasks.

V_{S-off} is the voltage when the WSM has been turned off through the software EAI after the WSM has judged that there is not enough energy for the WSM to perform the next tasks, which means the current voltage is lower than V_{END}. Therefore, V_{S-off} is lower than V_{END}.

It should be noted that the software EAI still rely on the hardware EAI to make the WSM sleep by switching the N-MOSFET off, but with more flexibility at an appropriate voltage level based on the energy level and tasks.

To sum up, the relationships among the voltages are $V_{H-on} > V_{END} > V_{S-off} > V_{MIN} > V_{H-off}$, shown in Fig. 4.10.

Fig. 4.11 shows the schematic of how the software EAI controls the hardware EAI. The programme begins with the WSM in the non-active phase until V_{CS} reaches V_{H-on}, where the hardware EAI turns on the WSM. After that, the MCU takes the pre-set number of readings from the sensors. Each reading is stored in the internal MCU RAM after each measurement. It should be noted that the pre-set number is for the sensor measurements to be made in one operational cycle,

for example, the pre-set number is set to be 16, which means the MCU is programmed to read a sensor for 16 times in one cycle, not the total number of readings in one active time, since the MCU will repeat the cycle several times. The energy consumed in that one cycle of measurement is calculated by the software EAI to judge whether the WSM is able to complete another cycle of measurement with the energy available.

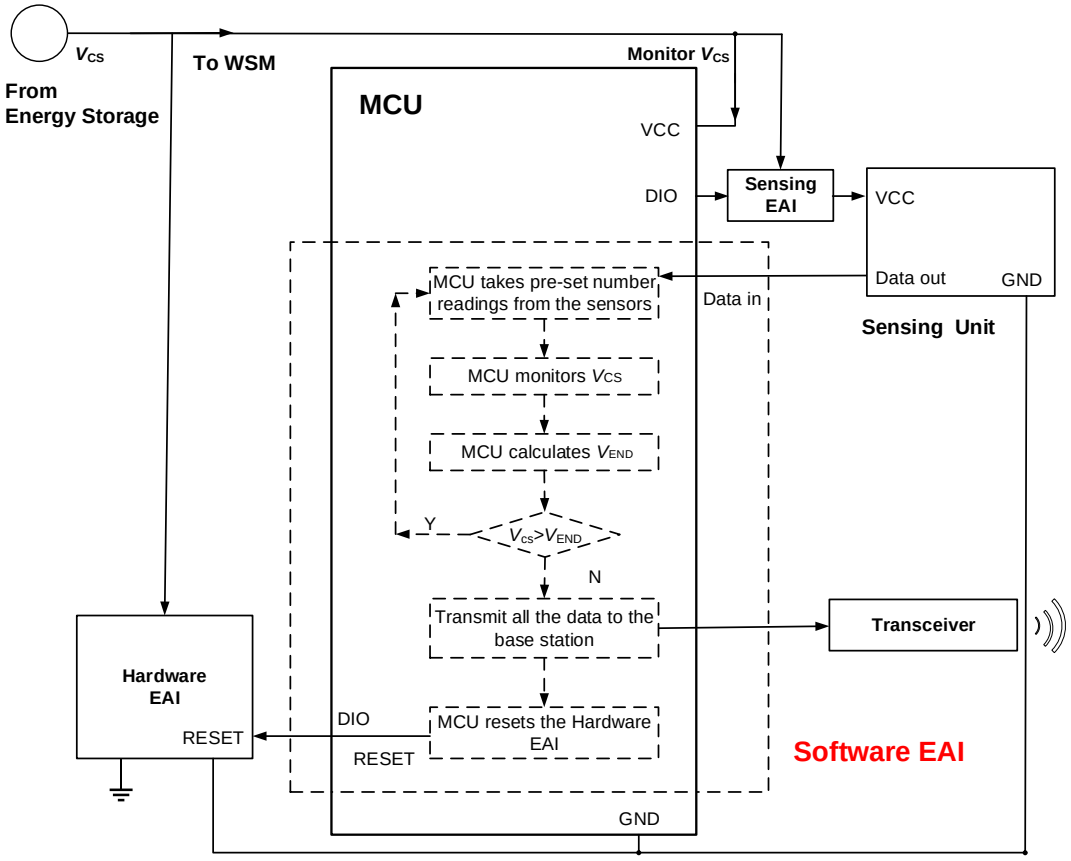

Figure 4. 11: The schematic showing how the software EAI controls the hardware EAI

After that, the MCU measures V_{CS} and then calculates V_{END}, which will be described in the next section. When the MCU has got the values of the current V_{CS} and V_{END}, it judges whether V_{CS} is larger than V_{END}. If so, this means the energy storage has enough energy for the WSM to perform the next measurement and transmission tasks. Therefore, the MCU will take another pre-defined number of readings from sensors and measure V_{CS} again. If not, this means the energy storage will not have enough energy for the WSM to perform

the next measurement and transmission tasks, and the MCU will not take any more measurement. Instead, it will transmit all the data stored in the RAM to the base station and then send a LOW signal to the RESET pin of the voltage supervisor. After that, the voltage supervisor turns off the N-MOSFET so that the WSM goes into the non-active phase, and the cycle repeats, alternating between active phase and non-active phase as long as there is enough energy stored in the capacitor for the next active operation.

4.3.2.3 Determination of V_{END}

As mentioned before, V_{END} serves as an indicator that the MCU should end its active phase, which is based on the effective energy stored in the energy storage and the energy required for the WSM to perform the tasks of taking one cycle of readings from the sensors and transmitting all the data stored in the RAM to the base station. It is determined by equations 4.3 to 4.6, and as a result, it is calculated by equation 4.7:

$$E_{\text{effective}} \geq E_{required} = E_{tx-samp} + E_{reset} \tag{4.3}$$

$$E_{\text{effective}} = \frac{1}{2} \times C \times {V_{CS}}^2 - \frac{1}{2} \times C \times {V_{MIN}}^2 \tag{4.4}$$

$$E_{tx-samp} = a \times E_{tx-1} + (M+1) \times b \times E_{tx-1} + b \times E_{samp-1} \tag{4.5}$$

$$E_{required} = \frac{1}{2} \times C \times {V_{END}}^2 - \frac{1}{2} \times C \times {V_{MIN}}^2 \tag{4.6}$$

$$V_{END} = \sqrt{\frac{2 \times E_{required} + C \times {V_{MIN}}^2}{C}} \tag{4.7}$$

where $E_{\text{effective}}$ is the effective energy stored in the capacitor; $E_{required}$ is the energy required for the next operation of the WSM, including the energy required

for taking one pre-set cycle sensor reading and transmitting all the data, $E_{tx-samp}$ and the energy required for resetting the voltage supervisor, E_{reset}; C is the capacitance of the energy storage capacitor; E_{tx-1} is the energy required for transmitting one byte of data; E_{samp-1} is the energy required for sampling one byte of data; a is the number of bytes of the WSM transmission data which is able to be expressed as one reading from a sensor such as humidity sensor; b is the pre-set number of bytes of the WSM transmitting data for sensors having one reading such as humidity sensor; b is the pre-set number of bytes of the WSM transmitting data for sensors having a set of reading data such as accelerometer in one sampling cycle; M is the number of the WSM sampling cycles. Therefore, as the WSM has made more cycles of measurements, more energy will be required for transmitting the increasing number of sampled data. Thus V_{END} moves further away from V_{MIN}.

In addition, E_{tx-1} +, E_{samp-1} and E_{reset} can be determined through programming the WSM to perform the individual tasks and then measure the energy consumption of the respective tasks. One source meter is used to measure the voltage V_S and current I_S supplied to the WSM, and then the energy consumption for performing the task can be calculated by using equation 4.2 where V_S and I_S correspond to V_w and I_w, respectively.

4.3.3 Sensing Energy-aware Interface

4.3.3.1 Concept

Sensing EAI is an interface between the MCU and the sensing unit, which is designed to reduce the power consumption of the sensors in the WSM during the active time. It is used to turn off the sensors when they are not required.

The sensors are unable to draw the energy during the sleep time since they are turned off by the hardware EAI. However, they waste some energy whey they are not required to read the sensor during the active time if the system is without the sensing EAI. This is because when the hardware EAI turns on the WSM, the sensors become active and stay in the active state during the whole active time. Therefore, it is not necessary to make all the sensors on all the time. For example, sensors such as temperature and humidity sensors only need to read the environmental data intermittently. Therefore, keeping those sensors on during the whole active time as controlled by the hardware EAI when they are not required is a waste of energy. The sensing EAI is introduced to further control the on and off states of the sensors when the WSM is turned on in the developed system since the sensors are not able to turn on and off by themselves to reduce the power consumption of the WSM during the active time.

4.3.3.2 Implementation

The single sensing EAI operation for one sensor is explained as follows. When the WSM does not require to read the sensor data after it is turned on, the output of DIO pin is set to be in a high state programmed by the MCU software

programme, which places the P-MOSFET in a high impedance state, disconnecting the system voltage supply and sensor voltage supply. Therefore, the sensor is in the non-active state and does not consume energy during the period. Whenever the MCU requires the sensor to sample data, it changes the output of the DIO state from high to low, which turns the P-MOSFET into a low impedance state, connecting the system voltage supply and sensor voltage supply. The sensor and the system voltage supply then form a closed circuit, where the sensor can draw current, and consequently, the sensor becomes active to sample data.

In the case of two sensors, as shown in Fig. 4.12, the MCU needs to set the output of the DIO pins accordingly. For example, if reading data from sensor 1 is required, the MCU needs to set the output DIO 1 in a low state and the output DIO 2 in a high state. Conversely, if the MCU wants to read the data from sensor 2, it needs to set the output DIO2 in a high state and the output DIO 1 in a low state. For more sensors, a similar control method can be used, that is, the MCU needs to set the output of the DIO pin that controls the sensor to be read from in a high state and others to the low state. It should be noted that the sensing EAI also allows one ADC pin to be shared with multiple sensors. However, it can only read data from one of the sensors at a time, which is useful when the MCU has limited ADC pins for sensing applications that do not require very frequent measurements.

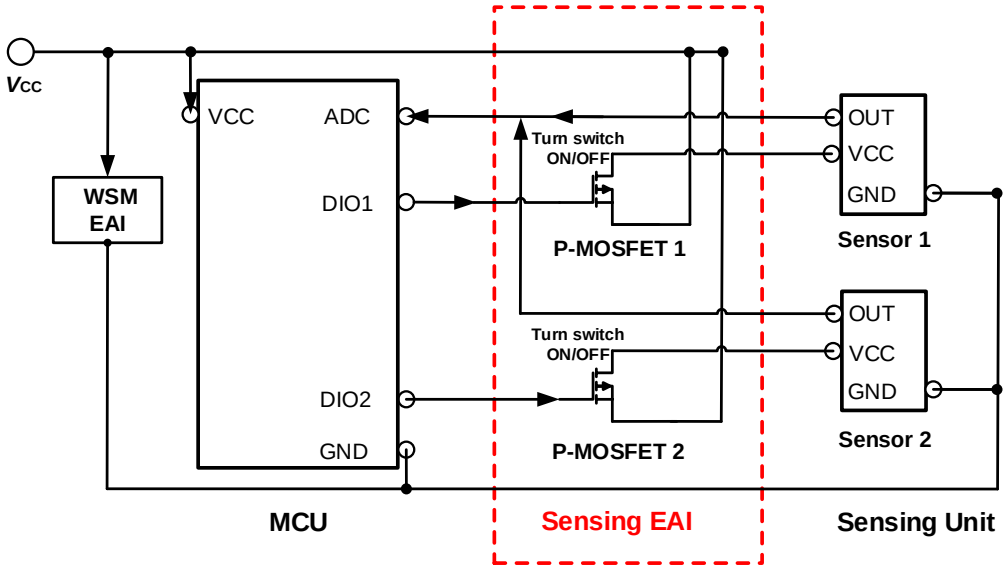

Figure 4.12: Hardware schematic of the Sensing EAI

4.3.4 Summary

In conclusion, Table 4.1 shows the comparison of hardware EAI, software EAI and sensing EAI. Furthermore, sensing EAI is independent, which means is able to achieve the function without hardware EAI and software EAI. However, hardware EAI and software EAI are combined together to achieve the function. Furthermore, software EAI is to improve the function of hardware EAI.

Compared with the EH powered WSM without hardware EAI, the system with hardware EAI is able to enable the harvested energy to be accumulated in the capacitor to deal with the start-up issue and allow the WSM to have a low sleep current. Furthermore, in the term of the supply voltage, the WSM is able to be turned on and turned off based on the pre-fixed threshold voltages V_{H-on} and V_{H-off} , respectively.

However, there is a drawback of hardware EAI that the WSM would stay active until the pre-fixed turn-off voltage threshold reached regardless of the WSN operation states. For example, if the WSM finish the tasks early, this could cause wastage energy as the WSM is still on; if the WSN is in the period of operation, this would cause the WSNs to be unable to finish the required tasks as the turn-off voltage threshold is reached. This is not ideal for real applications to use such a pre-fixed voltage threshold hardware switching approach.

Therefore, software EAI is introduced to utilize the energy stored in the capacitor more effectively, by monitoring the voltage in the capacitor to judge if there is enough energy in the capacitor for the WSM to carry out the next operation and ensure all the measured data is transmitted before the energy becomes too low for operation of the WSM. Compared with the EH powered WSM with hardware EAI, the system combined with the hardware EAI and software EAI is able to be turned on the pre-fixed threshold voltages V_{H-on}, and turned off on the flexible voltage V_{S-off} based on the stored energy level and the required energy of tasks, not the limited pre-fixed V_{H-off}.

It should be noted that software EAI does not change hardware EAI and it use the judgement programme and DIO function of the MCU to reset the hardware EAI through connecting DIO pin of the MCU and the reset pin of hardware EAI to turn off the WSM when needed.

Table 4.1: Comparison of hardware EAI, software EAI and sensing EAI

EAI	Function	Aim	Time	Main hardware circuit	Main software programme	Control function in the implemented WSM
Hardware EAI	Monitor the voltage across the energy storage to judge if there is enough energy in the energy storage for the WSMs to perform the pre-programmed tasks and determine when to wake the WSM up	Solve the start-up problem and reduce the power consumption of the WSMs during sleeping time	Sleep	N-MOSFET circuit; Voltage supervisor circuit	None	Turn on the WSM
Software EAI	Judge whether the energy stored in the energy storage device is enough for the WSM to carry out the next operation and ensure all the measured data is transmitted before the energy becomes too low for the operation of the WSM	Increase the energy use efficiency to extend the active time	Active	Hardware EAI	Judgement programme; DIO pin on and off function	Turn off the WSM through resetting hardware EAI
Sensing EAI	Turn off the sensors when they are not required	Reduce the energy consumption of the sensors	Active	P-MOSFET Circuit	DIO pin on and off function	Independently control the sensors on and off

4.4 Developed Energy Harvesting Powered Wireless Sensor Mote Using Energy-aware Approaches

4.4.1 Implementation

In order to understand the enhancement on the performance of the EH powered WSM due to the proposed energy-aware approaches, an EH powered WSM was implemented for study of this.

The schematic of the developed WSM hardware is shown in Fig. 4.13. It is composed of four main blocks: (1) the PMM in [112] (not shown in the figure), (2) a 10 mF super-capacitor, (3) energy-aware approaches including hardware EAI, software EAI and sensing EAI, and (4) WSM including a MCU and three different sensors. For a fair comparison, it was built using the same wireless MCU of JN5148 and the same sensors of ADXL335 3-axis accelerometer, HIH-5030 humidity sensor, and MCP9700 temperature sensor described in Chapter 3 and Section 4.2 in this chapter. The temperature and humidity sensors are designed to share the ADC4 pin, realised by the sensing EAI function mentioned in Section 4.3.3 since the MCU only has 4 ADC pins, which is not enough for 5 ADC readings from the three sensors, in which the accelerometer has three outputs. The X-axis, Y-axis, and Z-axis acceleration outputs of the accelerometer were connected with the ADC1 ADC2 and ADC3 pin of the MCU, respectively. Each axis has its own dedicated ADC because the acceleration measurements require a much higher sampling rate and as long as possible sampling time for real-world measurements. Therefore, the turn on and off as well as the ADC pin sharing introduced by the sensing EAI, is not ideal for such applications. A voltage reference (ISL21080CIH325, Intersil, California, USA) is used to provide a fixed

supply voltage of 2.5 V to the accelerometer during the active time of the WSM. This is because the electrical output signal from the accelerometer is the ratio to the supply voltage applied to the accelerometer. Therefore, a fixed and known supply voltage is essential in processing the sampled data later. It should be noted that the implementation of the hardware EAI is the same as described in Section 4.3.1, and the sensing EAI is the same as described in Section 4.3.3 with the two P-MOSFETs.

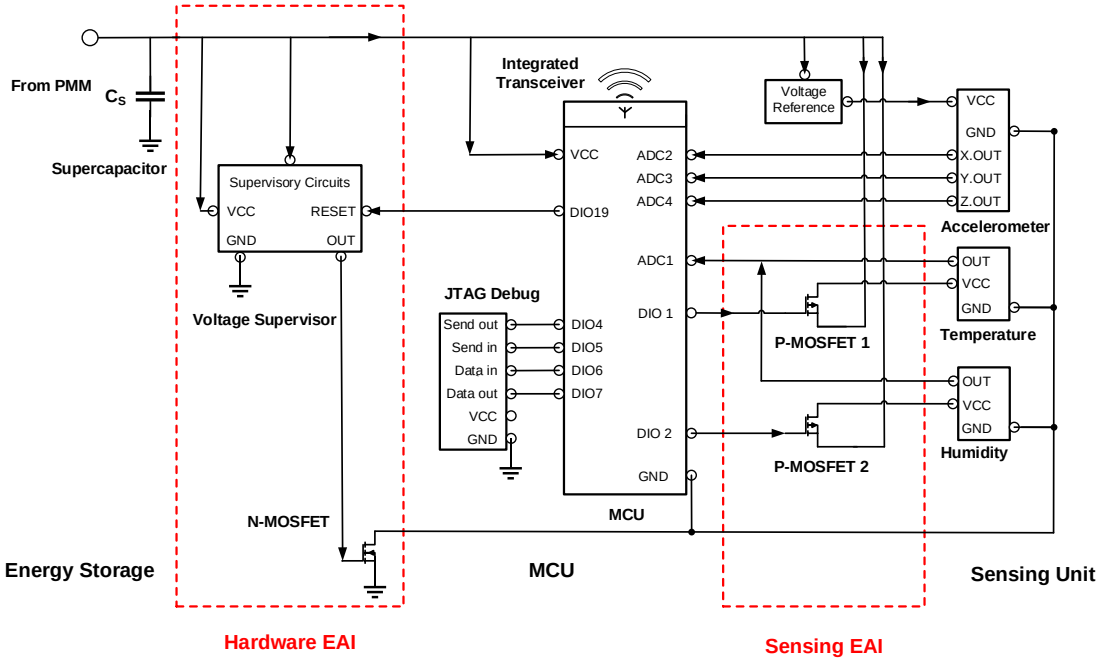

Figure 4.13: Hardware schematic of the custom-developed WSM connected with the EAI

4.4.2 Operation

The operation flowchart of the WSM is shown in Fig. 4.14. The operation begins with the WSM in the non-active phase until there is enough energy in the super-capacitor to turn on the MCU as determined by the hardware EAI. Once there is sufficient energy in the capacitor, the hardware EAI turns on the WSM, and then the WSM becomes active. After that, the sensing EAI sets the output DIO1 pin to a low state to turn on the temperature sensor and sets the output DIO2 pin to a high state to turn off the humidity sensor. Then, the MCU takes one reading from

the temperature sensor. After that, sensing EAI changes the output DIO1 pin from low to high state to turn off the temperature sensor and changes the output DIO2 pin to a low state to turn on the humidity sensor. Then, the MCU takes one reading from the humidity sensor before the sensor is turned off by sensing EAI.

After that, the MCU takes a total of three readings (one each from x-, y-, and z-axes) for each sampling from the accelerometer at every 10 ms. Each reading is 2 bytes of data and is stored in the internal MCU RAM after each measurement. The MCU repeatedly takes reading from the accelerometer until a pre-defined number of readings are made, for example, a total of 48 readings for 16 times of sampling the accelerometer, which corresponds to 96 bytes of data to ensure there are enough readings.

Then, the software EAI measures V_{CS} and calculates V_{END}, which is determined by equations 4.3 to 4.7. It should be noted that, in the equation 4.5, a is 4, which means there is 4 bytes of data that need to be transmitted, including 2 bytes from the temperature sensor and 2 bytes from the humidity sensor. b is 96, which means there is 96 bytes of data from the accelerometer in one sampling cycle that needs to be transmitted. E_{tx-1} +, E_{samp-1}, and E_{reset} have been found to be 4.38 µJ, 34.79 µJ, and 0.17 mJ, respectively, through the experimental method in Section 4.3.2, which is set the fixed values in the programme to calculate V_{END} . In equations 4.6 and 4.7, C is set as 0.01, which means the capacitance of the super-capacitor is 10 mF, a is 4, b is 96, and V_{MIN} is set to be 2.4 V.

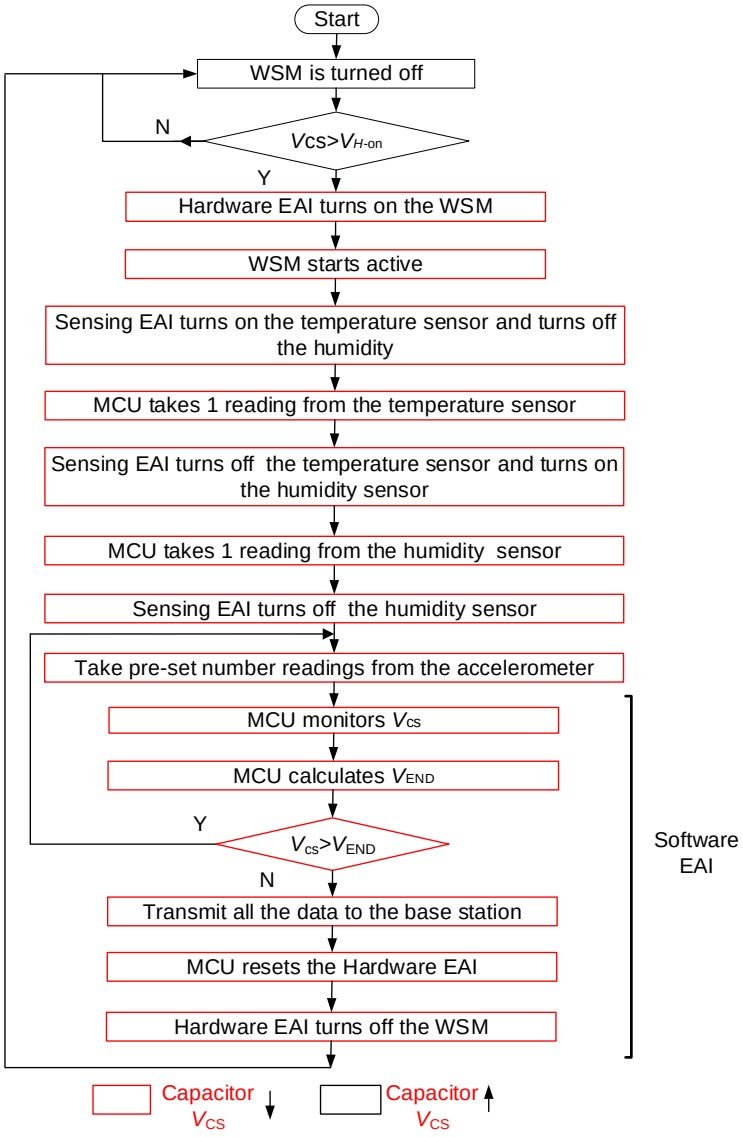

Figure 4.14 : Flowchart of the operation cycle of the developed WSM with energy-aware approaches

After that, the software EAI judge whether V_{CS} is larger than V_{END}. If so, the MCU will take another 48 readings from the accelerometer, store it in the RAM, and measure V_{CS} and calculate a new V_{END} again. If not, the MCU transmits all the data stored in the RAM and resets the hardware EAI to turn off the WSM so that the WSM goes into the non-active phase, and the cycle repeats, alternating between active phase and non-active phase as long as there is energy from the energy harvester. The data size to be transmitted in the first packet is 100 bytes, which consists of 4 bytes from the temperature sensor and humidity sensor, and

96 bytes from the accelerometer. The remaining packets only have 96 bytes from the 48 accelerometer readings. It should be noted that there is only one transmission process to transmit all the packets one by one at the end of the active time just before the WSM is switched off.

4.4.3 Experimental setup

Fig. 4.15 shows the experimental setup to measure the voltage across the super-capacitor, V_{CS}, and the current consumed by the WSM with the energy-aware approaches, I_W. In the setup, one source meter was used to measure V_{CS} at the points of A and B, which was connected in parallel to super-capacitor and I_W at the points of C and D, which was connected in series between the super-capacitor and the hardware EAI. It should be noted that V_{CS} is the same as the voltage across the hardware EAI and the WSM since they are all connected in parallel in the circuit. Other parts were similar to the experimental setup described in Section 4.2.3.

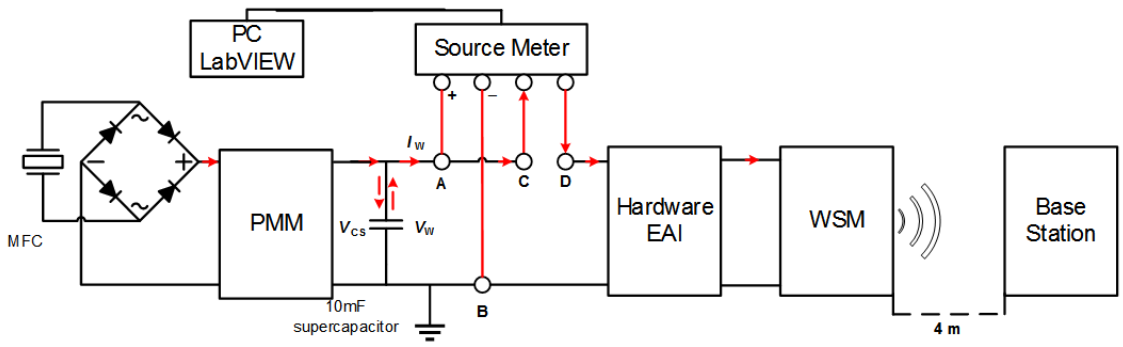

Figure 4.15: The schematic of the experiment setup for characterising the MFC powered WSM

4.4.4 Results and discussions

The measured voltage of V_{CS} and current of I_W are shown in Fig. 4.16. It is shown that, from the beginning at 0 s to 22.56 s, the capacitor was charged by the PMM with the harvested energy from the energy harvester and its voltage V_{CS} increases from zero to 3.16 V. During this period, the voltage V_{CS} is below the pre-set threshold V_{H-on} of 3.16 V, and so the WSM is off. As soon as V_{CS} reaches 3.16 V, the hardware EAI turns on the N-MOSFET switch, enabling the capacitor to release its energy to the WSM. It is also shown that, after initial charging of the capacitor for about 22.56 s, the energy harvester was able to power the WSM for a period of 1.15 s (active time) every 7.79 s (sleeping time) with a limited energy harvested of 3.2 mW by the energy harvester which is subjected to a peak-to-peak strain loading of 600 με at 10 Hz vibration. Consequently, a drop in V_{CS} and a surge in I_W is observed in Fig. 4.16(a) and (b) respectively as the WSM is switched into its active phase for about 1.15 s, including 0.17 s for waking up, 0.06 s for taking 1 reading each from the temperature and humidity sensors, 0.64 s for reading from the accelerometer for 4 cycles, 0.12 s for determining the effective energy for 4 cycles), 0.14 s for transmitting 388 bytes of measured data and 0.02 s for resetting the WSM, shown in Fig. 4.16 (c).

During the active phase, the software EAI calculates V_{END} and resets the hardware EAI once V_{CS} drops below V_{END} of about 2.58 V, calculated from equation 4.8 in the studied case. Therefore, the WSM was switched off at around 2.47 V of V_{S-off}, as shown in Fig. 4.16(a), which is slightly higher than 2.4 V. This shows that V_{END} and V_{S-off} are not the same as V_{MIN}, which verifies the operation of the software EAI. With the introduction of V_{END}, the implemented

WSM is able to complete all the measurement tasks and transmit all the data in the end of active time before the energy is below the requested level.

During the sleeping time, the WSM is turned off by the hardware EAI, consuming an average current of 0.95 µA, calculated using the measured current shown in Fig. 4.16 (d) and based on equation 3.4. The main reason for the WSM to have such a low sleep current is that the EAI is able to completely switch off the WSM, including the MCU and other sub-circuits during the sleeping time. This means the power consumption of the WSM is almost zero. This average sleep current is mainly consumed by the voltage supervisor and N-MOSFET of the hardware EAI.

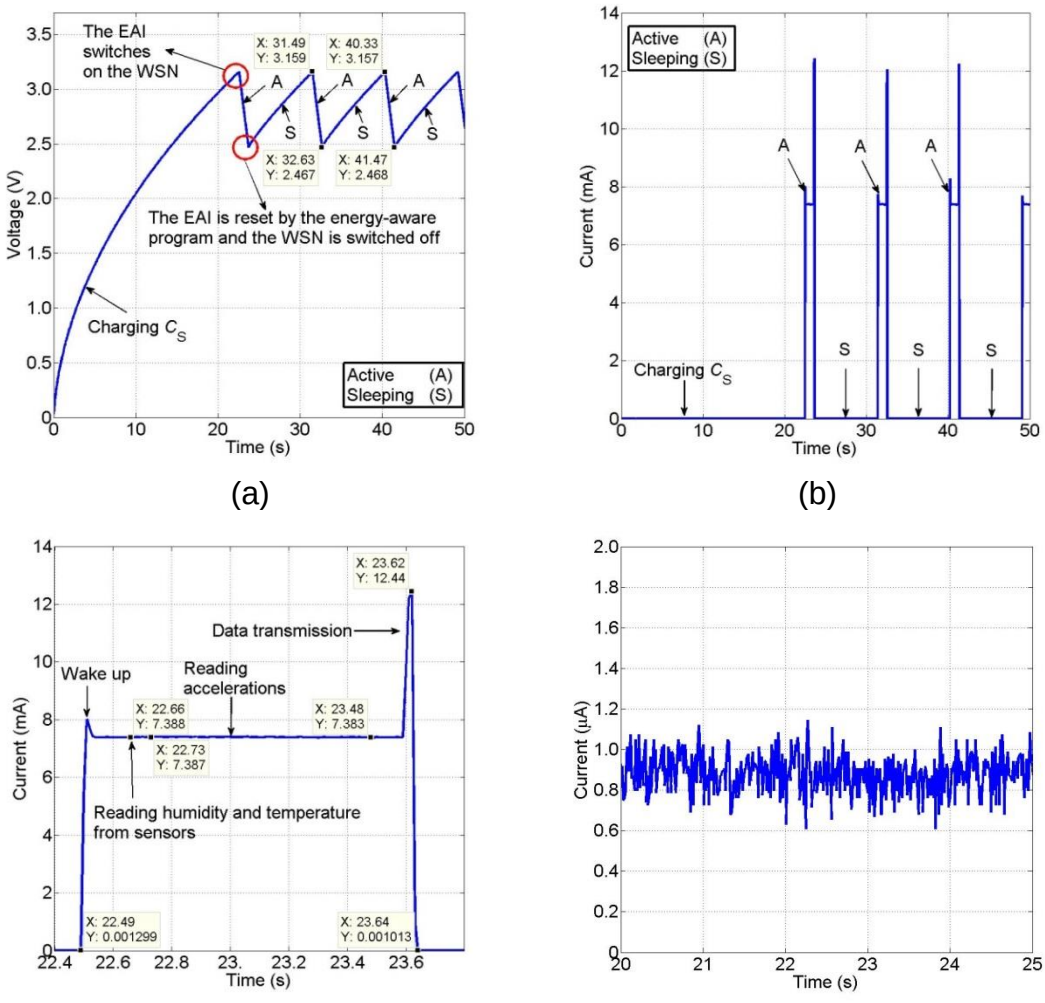

Figure 4. 16: Time dependence of (a) the voltage V_{CS}, (b) the current I_W with enlarged plots (c) during a complete active time, and (d) during the sleeping time.

4.4.5 Comparisons of the three configurations

In order to further understand the advantages of the energy-aware approaches for the EH powered WSM, characterizations, and comparisons of 3 different configurations were performed. Configuration 1 is defined as the system in Section 4.4: EH powered WSM with energy-aware approaches, and the non-active phase current is shown in Fig. 4.16 (d); Configuration 2 is defined as the system in Section 4.2: EH powered WSM without energy-aware approaches, and the non-active phase current is shown in Fig. 4.6 (d); and Configuration 3 is defined as the system in Section 3.6: DC power Source powered WSM without energy-aware approaches, and the non-active phase current is shown in Fig. 3.12 (b).

The performances and the non-active phase currents of these three configurations are summarized in Table 4.2. Compared with configurations 1 and 2, it can be seen that the energy-aware approaches play an important role in dealing with the mismatch between the energy generated by the harvesters and the energy demanded by the WSMs to perform the required tasks. The energy-aware approaches enable the WSM to be powered by EH technology when there is limited energy harvested. For example, using the same 3.2 mW of power from the energy harvester, the WSM without the energy-aware approaches is not able to operate, but the EH powered WSM with the energy-aware approaches is able to operate. This is because the energy-aware approaches enable the energy generated during the non-active phase to be accumulated effectively in the capacitor without being consumed immediately by the WSM. Compared with configurations 1 and 3, it can be seen that the energy-aware approaches can

reduce the power consumption of the WSM during the sleeping time from 30.4 µA of a normal sleep mode to 0.95 µA. This is because with the EAI in Configuration 1, the internal wake-up timer and other associated circuits are all switched off with minimum energy consumption. Configuration 2, which does not have the EAI, could not accumulate the energy effectively at all and consume energy by the internal wake-up timer and other associated circuits. Therefore, it can never start up in the studied case.

Table 4.2: Comparison of the performance and average non-active currents of the WSM with three configurations

No	Configuration	Addition feature	Performance	Non-active phase current (µA)
1	EH powered WSM with energy-aware approaches	Software EAI	WSM able to work	0.95
2	EH powered WSM without energy-aware approaches	MCU running in a normal sleep mode	V_{CS} increases to about 2 V, but WSM is not able to start	310
3	DC power Source powered WSM without energy-aware approaches	MCU running in a normal sleep mode	WSM is able to start and operate	30.4

4.5 Summary

This chapter has shown the energy-aware approaches to manage the energy flow from the energy storage capacitor to the WSMs and to deal with the start-up issue and the mismatch between the energy generated by the harvesters and the energy demanded by the WSMs to carry out required tasks. It has been shown that a typical EH powered WSM without the proposed energy-aware approaches is not able to start and, therefore, cannot operate when there is limited energy harvested, which demonstrates the importance of the energy-aware approaches proposed and developed in this chapter. The combined hardware, software, and sensing energy-aware approaches were implemented and experimentally studied in a custom developed piezoelectric vibration EH powered WSM. The experimental results show that, with a limited energy harvested, the energy-aware approaches enable (1) the harvested energy to be accumulated in the capacitor to deal with the mismatch for enabling the WSM operation, (2) solve the start-up issue, and (3) allow the WSM to have a low sleep current reducing from 30.4 µA of a commercial WSM to 0.95 µA.

Chapter 5 Energy Analyses of Energy Harvesting Powered Wireless Sensor Network

From Chapter 4, it can be seen the energy-aware approaches have been successfully applied in the custom-developed WSM to address issues of the start-up and the mismatch between the energy generated by the harvesters and the energy demanded by the WSMs to carry out the required tasks. Chapter 5 will move on from EH powered WSM to EH powered WSN, that is, from a mote to a network. The energy analyses of EH powered WSM joining the network and effects of the duty cycle of WSM operation, and the capacitor size of energy storage on EH powered WSN joining processes are analysed through the experimental measurements using the implemented EH powered WSN. Following this, the problem of the EH powered WSN joining process is identified and will form the research work by developing an energy-aware approach for EH powered WSN in Chapter 6.

The rest of the chapter is organised as follows: Section 5.1 describes the proposed EH powered WSN topology. Section 5.2 describes the implementation of the system. Section 5.3 gives an overview of the studied EH powered WSN. Section 5.4 presents the energy analyses, and associated processes of EH powered WSM joining the network. Section 5.5 describes the EH powered WSM operation. The experimental setup and results are shown in Sections 5.6 and 5.7, respectively. Following this, Section 5.8 discusses the problem of the network joining process, and finally, Section 5.9 concludes the chapter.

5.1 Description of the Studied Network Topology

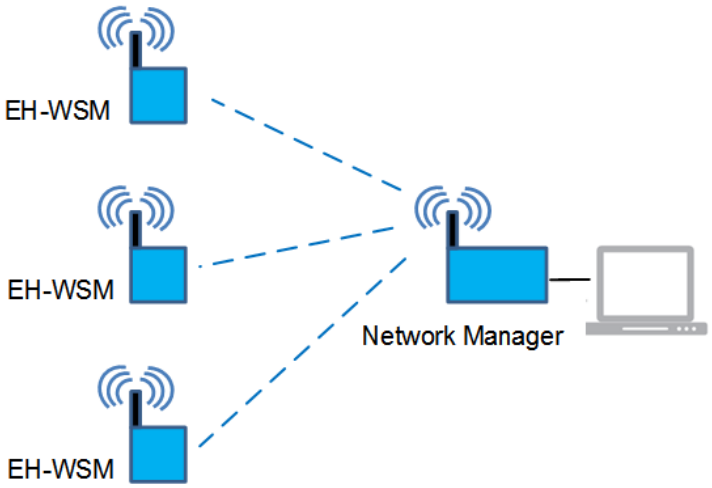

Figure 5.1: Schematic of the studied EH powered WSN topology

The schematic of the implemented EH powered WSN is presented in Fig. 5.1. The network topology is a star network, which consists of a network manager and three EH powered WSMs. The network manager is used to manage and control all functions of the network, such as the communication time and the frequency slot of the WSMs in the network and the WSMs are used to collect data from the environments and then transmit them to the network manager when they have enough energy. The implemented WSMs are different from previous implemented WSMs in that they are capable of two-way wireless communication with the network manager. The network manager aggregates all the collected data on the network and then passes to an assigned computer.

The advantage of star topology is that most of the network functions, such as the communication time and the frequency slot of each WSMs, are given to the network manager, which is helpful to reduce the energy consumption in the network behaviour of the WSMs. Moreover, it is able to reduce the impact of a transmission line failure by independently connecting each mote to the network manager. The failure of a transmission line linking any mote to the network

manager will result in the isolation of that mote from all others, but the rest of the motes in that network will be unaffected.

It should be noted that, mesh topology is also an option, which is a more complex and expensive network than the star network, where all motes cooperate to distribute data amongst each other. It consists of a self-forming multi-hop mesh of motes and an access point mote that connects the motes to the network manager. Motes are capable of two way communication and collect and relay data. The data is propagated along a path by hopping from mote to another mote until it reaches its destination. However, the mesh network needs to have several motes staying in the active state at the same time, which is difficult in the EH-WSN system, since the active time of the motes is very short due to energy limitation. In most cases, only a few motes are active and remain in the network for a short time. Moreover, for the mote itself in a mesh network, it has to undertake not only the tasks of sampling and communication with the network manager, but also need to communicate with other motes to achieve some network functions, which cost more energy than the motes in the star network where the network function is controlled by the network manager. Therefore, star topology is considered here as it is a more viable network that can be powered by using energy harvesting.

5.2 Implementation of the Studied Network

5.2.1 Hardware Implementation

The studied network is implemented by an IEEE 802.15 4 compliant platform of Linear Technology. The reason for using a Linear Technology is that the motes in the network are able to deliver a highly flexible network with proven reliability and ultra-low energy consumption performance [70]. The studied network manager is built with a Linear Technology DC9011A network manager, connected with a computer through a Linear Technology DC9006 Eterna™ interface, and powered by the computer through a USB connection or a CR2032 coin battery.

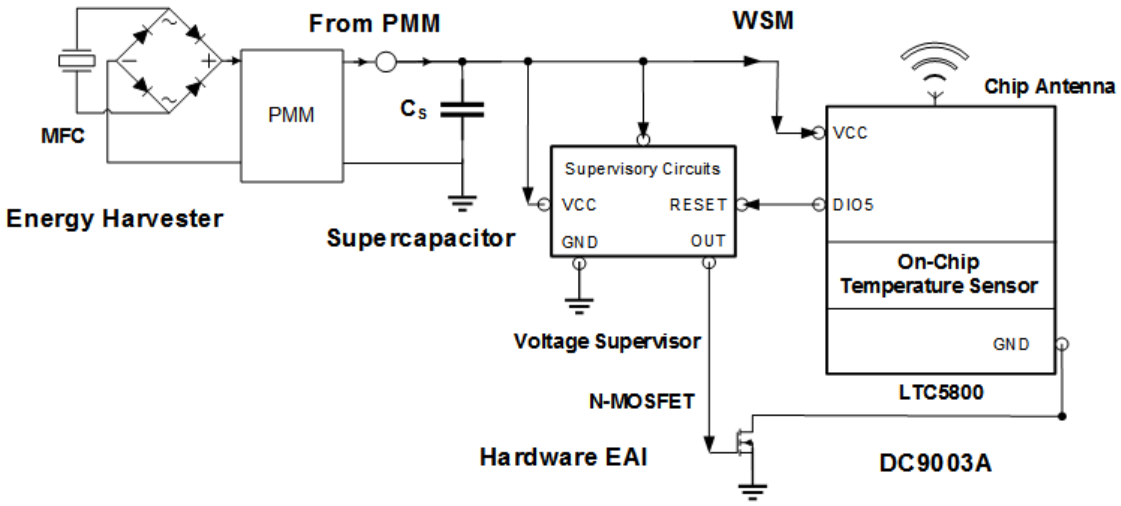

Figure 5.2: Schematic of the studied EH powered WSM with the hardware EAI developed in Chapter 4

The architecture of the studied EH powered WSM is shown in Fig. 5.2. It consists of an energy harvester, a PMM circuit, a super-capacitor, a hardware EAI circuit, and a WSM. The energy harvester, PMM circuit, super-capacitor and hardware EAI are the same as those described in Chapter 4.

The WSM is built with a Linear Technology DC9003 A-B Evaluation/Development Mote, which includes an integrated LTC5800 Mote-on-Chip microcontroller, a chip antenna, and a chip build-in temperature sensor [114]. The current consumption of LTC5800 chip transmitting at 8 dBm and receiving a packet is about 9.7 mA and 4.5 mA, respectively [70]. The chip build-in temperature sensor is used to read the local temperature data for wireless transmission.

5.2.2 Software Implementation

The network and the WSM operation is configured programmatically via an API, that is, an application programming interface. The network manager and the WSM are connected to the DC9006A interface board for programming and debugging them. The software of the network manager is implemented based on the Python platform to interact with the serial API of the network manager. The software of the WSM is implemented using IAR Embedded Workbench for Advanced RISC Machine (ARM) platform to develop C-code applications for executing and writing applications directly on the WSMs. Furthermore, "IAR" is an abbreviation of Ingenjörsfirman Anders Rundgren, which means Anders Rundgren Engineering Company.

It should be noted that the WSM can operate in the master and slave modes. Running in a master mode, the on-board ARM Cortex-M3 processor of the LTC5800 can access sensors and other input/output components directly, where it runs an application that commands and controls network joining. Alternatively, the mote can run as a slave mode, expecting the master device to control its operations via a serial API. Based on the case of EH powered WSN applications, the WSM is chosen as the master mode, since it is required to operate

autonomously by directly judging if the local energy level stored in the super-capacitor is enough for the next action after it wakes up, rather than being controlled by another connected device that also requires energy, which is impractical in real-world applications of EH powered WSNs.

5.3 The Studied Network Overview

5.3.1 Communication protocol

The communication protocol of the studied WSN is based on Time Slotted Channel Hopping (TSCH) of the IEEE 802.15.4e standard. The TSCH is a channel access method for shared medium networks. It can be seen as a combination of time division multiple access and frequency division multiple access mechanisms as it uses diversity in time and frequency to provide reliability to the upper network layers. In the TSCH network, the time is organised into time slots, and communication channels are separated by different frequency bands based on the IEEE 802.15.4e standard. The network shares a communication schedule controlled by the network manager. The schedule provides instructions to each mote on what to do in each time slot: transmit with which channel, receive with which channel, or sleep, which allows the WSM to know in advance when to turn on or off its radio to save energy. Typically, the network based on the TSCH has a reliability of over 99.999% while consuming less than 10 mA of current for its communication [115].

5.3.2 MAC Layer

The network communication uses the standard IEEE 802.15.4e packet in the beacon enabled mode. The network starts to form when the network manager begins sending advertisements. The advertisements are IEEE 802.15.4e beacon frames that contain information that enables a WSM to synchronise to and request to join the network. The advertisements also describe when the new WSM can send in a request to join the network, and when it should expect a reply. This results in temporary shared links being assigned to the joining WSM that it will use until the WSM gets its specific dedicated links from the network manager. This message exchange is part of the security handshake that establishes encrypted communications between the network manager and the WSM. Once the WSM has joined the network, it maintains precise synchronisation through time correction messages exchange with the network manager. Then, the WSM can request to have particular timeslots assigned to it.

5.3.3 Physical Layer

For the physical layer, the network operates in the IEEE 802.15.4e standards-compliant platforms with 16 channels from 2.4 GHz to 2.48 GHz. The 16 channels across the frequency bands are numbered 0 to 15 with increasing frequency, corresponding to IEEE 2.4 GHz channels 11 to 26. It should be noted that, in the studied network, the number of communication channels of the network manager is set to be down to 7 out of the 15 available channels to reduce the network communication time. Because the studied network includes one manager and up

to three WSMs, which does not use all the channels to commutation and the minimum setting channels of the chip manufacturer is 7.

5.4 Joining Processes of the Studied Mote Powered by Energy Harvesting

The processes of the WSM joining the network are shown in Fig. 5.3. The network starts to form when the network manager begins to send advertisements. The operation of one of WSMs joining the network can be broken up into four phases: high-voltage search process, low-voltage research process, negotiating process, and connected process.

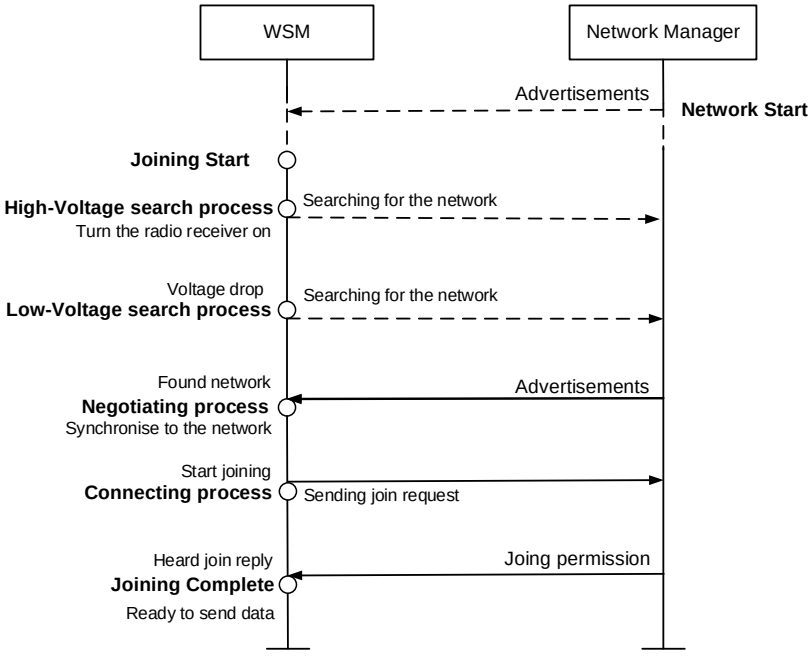

Figure 5.3: The processes of the WSM joining the network

When a WSM wants to join a network, the WSM starts searching for a network to join. Searching means it listens on a single channel for a while, and then sleeps for a while, and then resumes listening on a different channel. The join duty cycle

is the ratio of active listening time to doze times (a low-power radio state for sleep) during the period when the mote is searching for the network.

High-voltage Search Process: The WSM will get time-synchronised to the network to allow the network manager to manage the network. Therefore, the WSM starts to join the network by turning on its radio receiver to search for the network that matches its network ID by listening to the advertisements messages sent by the matched network manager. This first process of network joining is defined as the high-voltage search process in this chapter.

Low-voltage Search Process: Once the voltage drops to a threshold that the WSM is not able to keep the radio receiver working with the current power supply, the WSM will increase the current consumption to keep the radio signal strength stable at the configured decibel-milliwatts level of 16.2 mW [70]. The change is controlled by a hardware-based autonomous media access controller managing radio operation, which incorporates a co-processor for controlling all of the time-critical radio operations [70]. It should be noted that this does not happen in the case that the WSM is powered by a constant power source such as batteries because of the stable supply voltage. This process of network joining is defined as the low-voltage search process in this chapter.

The high-voltage search process and low-voltage search process can be collectively referred to as the search process, which can be 10's of seconds to 10's of minutes. It should be noted that the WSM join duty cycle is that how much time a searching WSM spends listening for a network versus sleeping, which has

a large impact on the search process since it controls the turn-on time of the radio receiver and will be discussed in the next sections.

Negotiating Process: The WSM has heard an advertisement and has synchronised to the network. After that, the WSM starts to communicate with the network by sending a join request to the network manager and then waits for a response. This process is defined as the negotiating process.

Connecting process: The WSM has heard the join reply from the network manager and is being configured by it, which is defined as the connecting process. As soon as the network joining process is completed, the WSM becomes operational and is ready to send data to the manager.

5.5 The Studied Mote Operation

The operation flowchart of the WSM is shown in Fig. 5.4. The operation begins with the WSM in the non-active phase until there is enough energy in the capacitor to turn on the WSM. Once there is sufficient energy in the capacitor, the hardware EAI turns on the WSM, and then the WSM becomes active. After that, the WSM sets the output DIO5 pin to a high state to ensure that the hardware EAI will keep the WSM on. Then, the WSM starts to join the network and then start to search process. Once the WSM has found the network, it starts to achieve the negotiating process and connecting process. After the WSM joined the network successfully, it takes one reading from the on-chip temperature sensor and then transmits the data to the network manager. After that, the WSM sets the DIO5 pin to a low state to reset the hardware EAI to turn off the WSM. Then, the

WSM goes into the non-active phase, and the cycle repeats, alternating between the active phase and the non-active phase as long as there is energy from the energy harvested form energy harvester and stored in energy storage. It should be noted that this chapter focuses on research on the energy consumption of the WSM joining network so that the sampling task implemented here was kept as simple as possible.

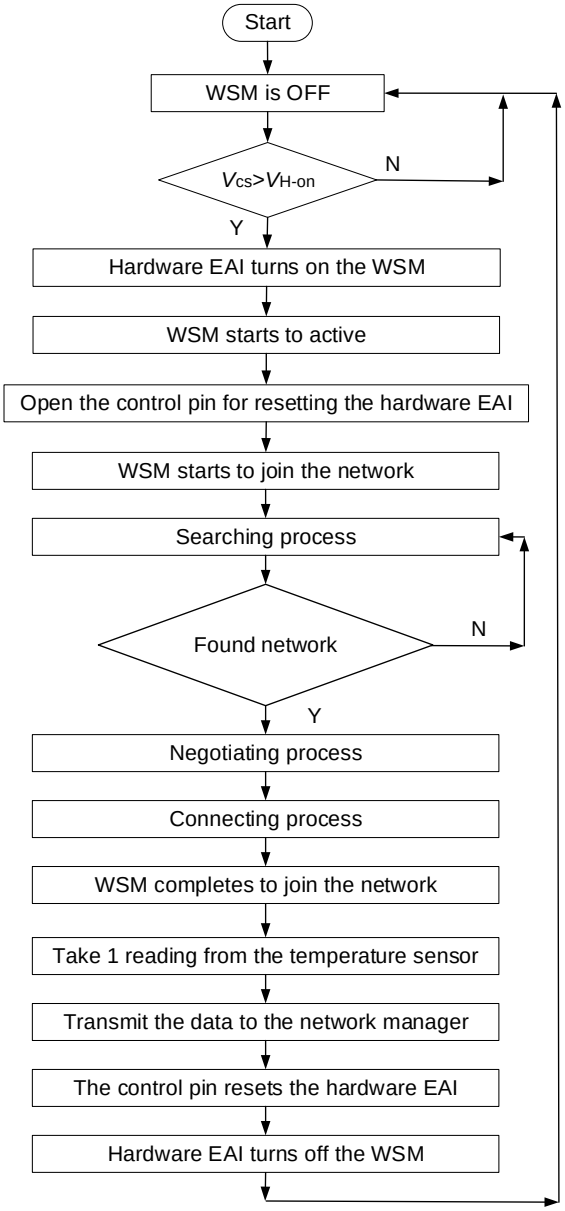

Figure 5.4: Flowchart of the operation cycle of the studied WSM with the hardware EAI

5.6 Experimental Setup

The same experimental set-up, including the MFC energy harvester and Instron E-10000 dynamic machine, was used as one described in Chapter 4, as shown in Fig.4.4. The machine was set to apply a 600 με peak-to-peak strain level at 10 Hz vibration frequency in the study. One source meter was used for simultaneous current and voltage measurements to determine energy consumption. Fig. 5.5 (a) shows the image of the measured WSM. It consists of: (1) the PMM circuit which is connected with the MFC (the MFC is not shown in the figure), (2) four different sizes of super-capacitors of 22 mF, 33 mF, 50 mF, and 100 mF prepared, (3) the hardware EAI, and (4) a DC9003 A-B Evaluation/Development Mote (Linear Technology/Analog Devices, Norwood, Massachusetts, USA) for the study. The red and black lines connected with DC9003 are the power and ground pins of the mote, respectively. The black line at the bottom of the figure connected with DC9003 is used to reset the hardware EAI. Fig. 5.5 (b) shows the network manager, which is a commercially available development kit of a DC9011A and DC9006 interface (Linear Technology/Analog Devices, Norwood, Massachusetts, USA).

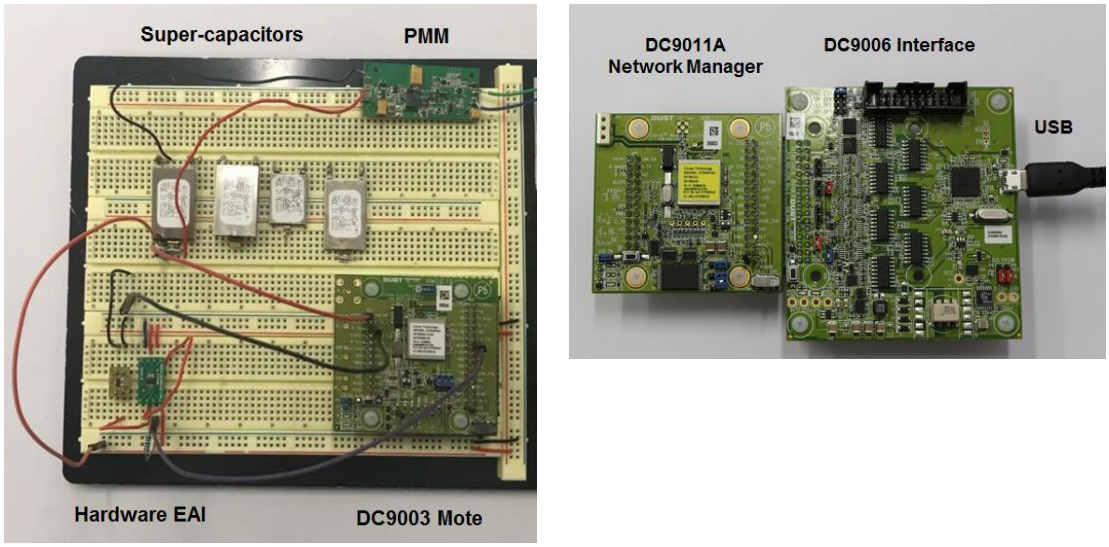

(a) (b)

Figure 5.5: Image of (a) the measured EH powered WSM and (b) the network manager

In order to understand the studied EH powered WSN system, three different measurements were performed, as shown in table 5.1:

The first one is used to analyse the energy consumption of the processes when the WSM is joining the network. The system used a 100 mF super-capacitor and 100% network joining duty cycle. The measurements used 2 kHz sampling frequency and focused on the operation of the WSM joining the network and sending the data after it has joined the network successfully.

The second is used to analyse the impact of the duty cycle on the network joining process. The system still uses the 100 mF super-capacitor. The measurements used 200 Hz sampling frequency to allow a longer measurement time and focused on the operation of the WSM searching for the network with different duty cycles.

The third is used to analyse the impact of storage capacitor sizing on the network joining process. The measurements used 200 Hz sampling frequency and focused on the enabling maximum searching time of the system with different capacitor sizes and the time required to charge up the super-capacitor from 0 V to the turn-on threshold voltage of the hardware EAI.

Table 5.1: Comparison of three experimental setups for the studied EH powered WSN system

No.	Aim	Super-capacitor	Network joining duty cycle	Sampling frequency of source meter	Used MCU	Used EAI	Kay Results
5.7.1	Analyse the energy consumption of the processes when the WSM is joining the network	100 mF	100%	2k Hz	DC9003	Hardware EAI	Energy Consumption of Network Joining Processes
5.7.2	Analyse the impact of the duty cycle on the network joining process	100 mF	100%, 50%, and 25%	200 Hz	DC9003	Hardware EAI	Searching time required to join the network successfully
5.7.3	Analyse the impact of storage capacitor sizing on the network joining process	22 mF, 33 mF, 50 mF, and 100 mF	100%	200 Hz	DC9003	Hardware EAI	Enabling maximum searching time with different capacitor sizes and the time required to charge up the super-capacitor from 0 V to the turn-on threshold voltage of the hardware EAI

5.7 Evaluation and Discussion

5.7.1 Energy Consumption of Network Joining Processes

It is well known that in the case of energy harvesting powered WSNs, energy is very limited. Therefore, it is crucial to identify which processes are power hungry so that appropriate measures can be taken to reduce energy consumption. The measured current profile I_W of the WSM joining network process, as well as the sensing and communication, is shown in Fig. 5.6. It begins with the hardware EAI turns on the WSM when there is sufficient energy in the super-capacitor and ends with the hardware EAI turns off the WSM. The processes can be divided into 7 processes, as shown in Fig. 5.6. It should be noted that this section focuses on

studying the network joining processes and their energy consumption, which is marked as 3 to 6 in Fig. 5.6.

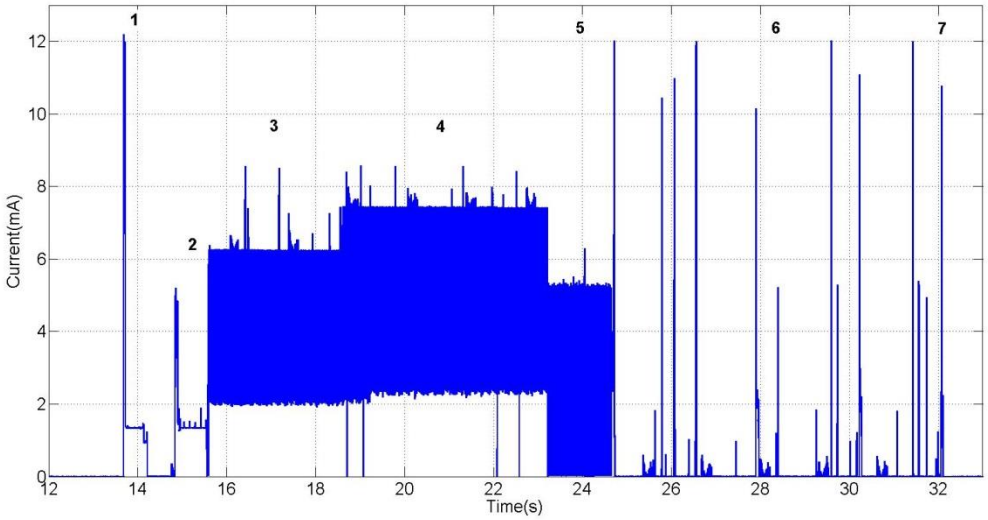

Figure 5.6: Measured results of I_W of the WSM during one cycle operation

5.7.1.1 The Operation of Before and After Network Joining

The processes 1 and 2 are the operation of the WSM before joining the network, and process 7 is the operation of the WSM after joining the network. The current profiles of these processes in Fig. 5.6 are enlarged and shown in Fig. 5.7.

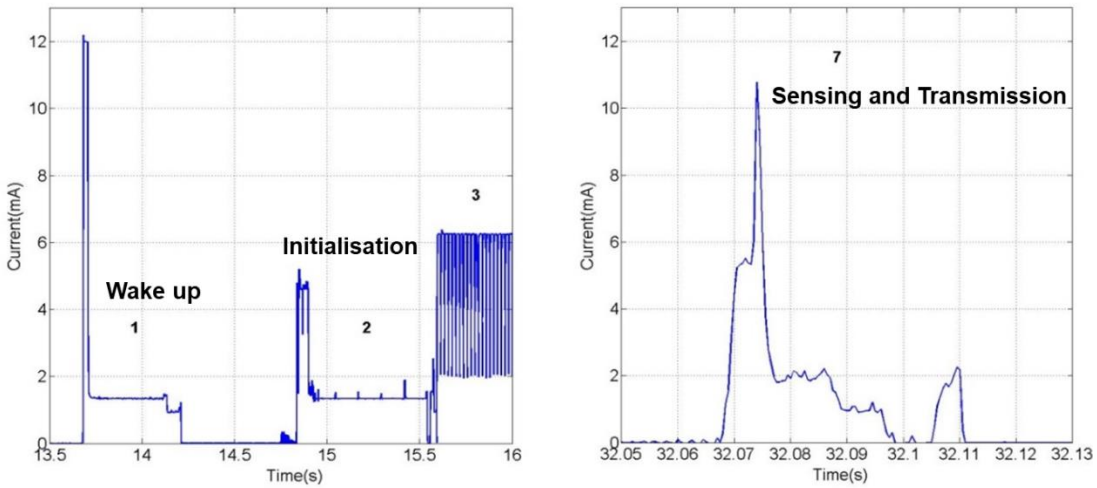

(a) (b)

Figure 5.7: I_W from Fig. 5.6 with the enlarged plots of the defined processes (a)1, 2 and (b) 7

Process 1: As soon as V_W reaches the pre-fixed turn-on threshold voltage, the WSM is turned on by the hardware EAI and then the super-capacitor powers up all the peripheral circuits and components of the WSM, which causes a current peak of about 12 mA at the beginning when the WSM starts to wake up.

Process 2: After waking up, the WSM begins to initialise the programme, such as importing the library files, which consumes a current of about 5 mA at the beginning. Then, it executes the first pre-programs task, which is to set the DIO5 pin high for controlling the hardware EAI. It consumes an average current of about 1.8 mA.

Process 7: After the WSM has joined the network successfully, it takes, for example, one reading from the on-chip temperature sensor, that is, the case studied here, and then transmits the data to the network manager with a current peak of about 11 mA. After that, it resets the hardware EAI to turn off the WSM.

5.7.1.2 The Operation and Processes of Network Joining

The operation of the WSM joining the network includes the processes from 3 to 6, as shown in Figs. 5.8 (a), (b), (c) and (d), respectively. The processes are the high-voltage search process, low-voltage search process, negotiating process, and connecting process, respectively. Moreover, Fig.5.8 (e) and Fig. 5.8 (f) show the measured voltage profile V_W of the WSM joining network process as well as the sensing and communication and the calculated energy E_W based on the measured V_W and I_W, respectively.

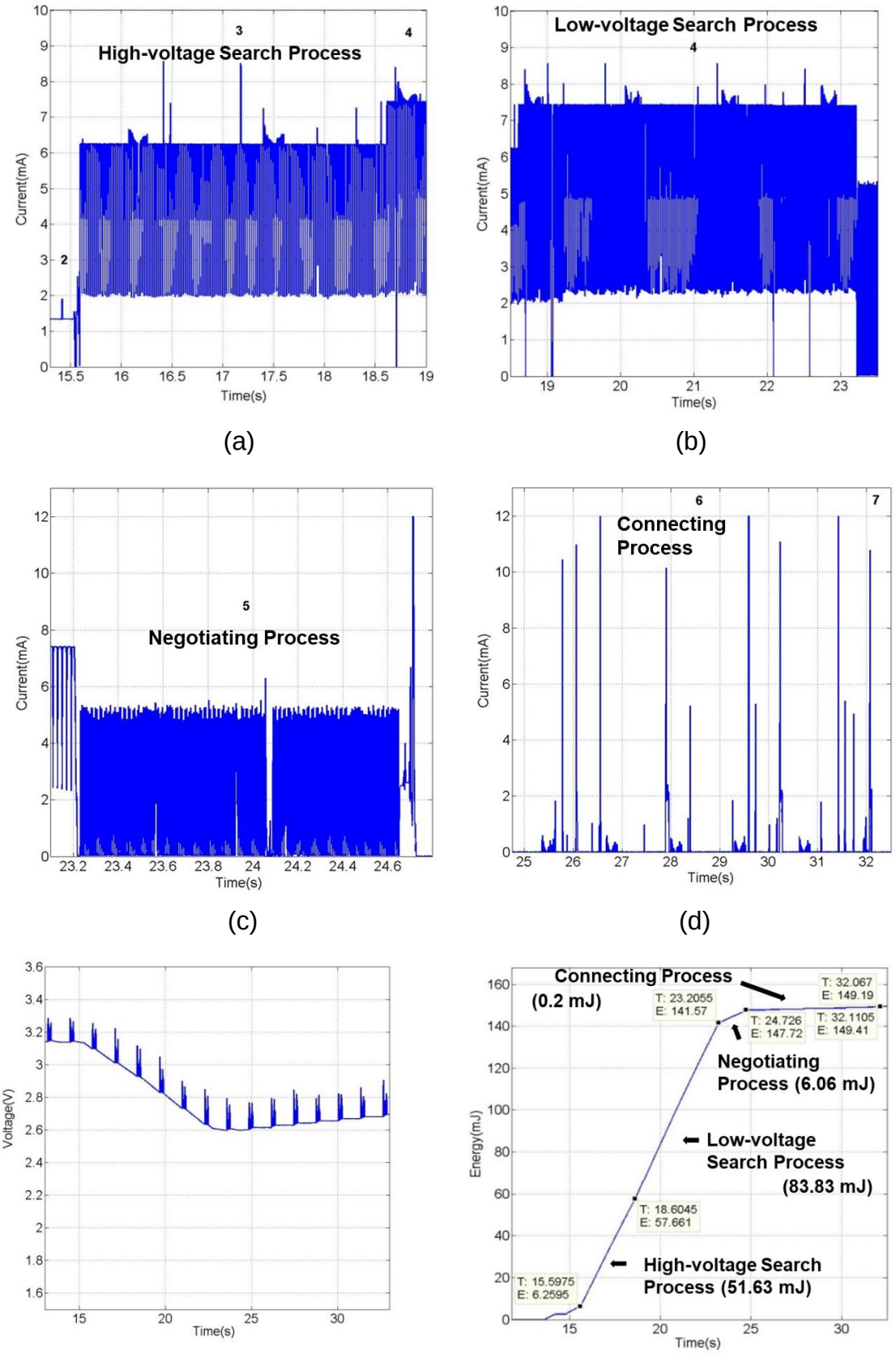

(a) (b)

(c) (d)

(e) (f)

Figure 5.8: The enlarged plots of I_W in Fig. 5.6 during processes (a) 3, (b) 4, (c) 5, and (d) 6. (e) Measured capacitor voltage V_W of the WSM during one cycle of operation. (f) The energy consumed E_W that is calculated based on the measured I_W in Fig. 5.6 and V_W in Fig. 5.8 (e)

Process 3 - high-voltage search process: the process is a repeating cycle with a current consumption range from about 2.1 mA to 6.2 mA. The average current consumption is about 5.71 mA, and the average voltage is about 2.990 V. The energy consumption for the process is about 51.63 mJ within 3021 ms, and as a result the average power is about 17.09 mW.

Process 4 - low-voltage search process: the process is a repeating cycle with higher current consumption than that of the low-voltage search process, which ranges from about 2.3 mA to 7.2 mA. The average current consumption is about 6.69 mA and the average voltage is about 2.721 V. The energy consumption for the process is about 83.83 mJ within 4603 ms. As a result, the average power is about 18.21 mW.

Process 5 - negotiating process: the process begins with the WSM synchronising to the network, which is a repeating cycle with the current consumption from about 0 mA to 5 mA. When the synchronisation is finished, the WSM starts to communicate with and send a join request to the network manager, which causes a current peak of about 12 mA at the end. The average current consumption is about 1.55 mA, and the average voltage is about 2.591 V. The energy consumption for the process is about 6.06 mJ within 1509 ms. As a result, the average power is about 4.01 mW.

Process 6 - connecting process: the WSM communicates with the network manager several times to being configured by the network manager, which causes several current peaks of about 12 mA. Although the peak current during the communication is higher than most of the other processes, it only lasts for a

very short time, which leads to a low average current consumption of about 0.08 mA. The average voltage is about 2.637 V. The energy consumption for the process is about 0.20 mJ within 7432 ms, and as a result, the average power is about 1.47 mW.

The average current, average voltage, average power, energy consumption, and time of every process are shown in Table 5.2. The high-voltage search process and low-voltage process consume much higher average power than the other processes. It should be noted that, although the high-voltage search process and the low-voltage process occur in the same operation of the WSM searching the network, the average power of the low-voltage search process is higher than that of the high-voltage search process.

Moreover, after several measurements, it was found that, the uncertain time ranges of the negotiating process and the connecting process are less than 50 ms in most cases, since both processes happened after the WSM has found the network manager, which means it is certain for the WSM to communicate with a known network manager. However, the high-voltage search process and low-voltage process have the longest uncertainty time during the joining network process, which can last from several milliseconds to several minutes or even more. Therefore, reducing the energy consumption of the high-voltage search process and the low-voltage process should be the priority, which will be studied in Chapter 6.

Table 5.2: Energy consumption of every process in the studied EH powered WSN system

No.	Process	Average Current (mA)	Average Voltage (V)	Average Power (mW)	Energy (mJ)	Time (ms)
1	Wake up	0.45	3.134	1.41	1.38	974
2	Initialisation	1.55	3.127	4.85	3.67	757
3	High-voltage Search Process	5.71	2.990	17.09	51.63	3021
4	Low- voltage Search Process	6.69	2.721	18.21	83.83	4603
5	Negotiating Process	1.55	2.591	4.01	6.06	1509
6	Connecting Process	0.08	2.637	0.20	1.47	7342
7	Sensing and Transmission	1.88	2.665	4.94	0.22	44

5.7.2 Effects of Duty Cycling on Network Joining Process

As mentioned in Section 5.4, the join duty cycle is the ratio of active listening time to doze times (a low-power radio state for sleep) during the period when the mote is searching for the network. It is a one-byte field by setting the ‘joindc’ parameter of the LTC5800 chip between 0 and 255, representing about 0.5% to 100%. For example, if the ‘joindc’ parameter was set to 255, the WSM will constantly listen, changing channels every few seconds. If the ‘joindc’ was set to 26, the WSM will spend about 10% of the time (26/255) listening and 90% of the time sleeping. The greater portion of the time the WSM listens, the higher the chance that the WSM will hear an advertisement and join the network faster, but at an increased average current consumption for a given timeframe. It should be noted that, join duty cycle only affects the average current consumption without excessively affecting the total energy of the whole network joining process based

on the same active listening time, since the energy consumption during the doze time is much lower than during the active listening time. Therefore, an appropriate join duty cycle is essential to the success of the network joining process in the EH powered WSN since it directly affects the time spent on searching.

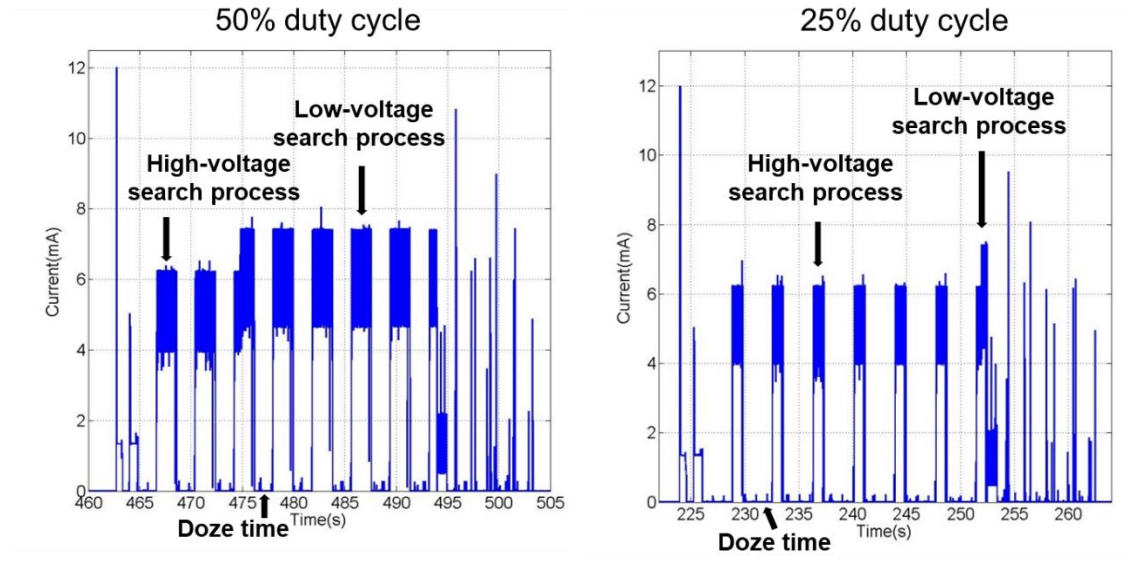

Figure 5.9: Current profiles of the WSM when the network joining process is (a) at 50% duty cycle and (b) at 25% duty cycle

Their current profiles will be compared here using network joining duty cycles of 100%, 50%, and 25%. Fig. 5.6, Fig. 5.9 (a) and Fig. 5.9 (b) show the current consumption of the WSM to analyse the effects of the duty cycle when it is joining the network at the duty cycle of 100%, 50%, and 25%, respectively. It can be seen that the duty cycle only affects the searching process, including the low-voltage and high-voltage search processes. The average current consumptions during doze time with different duty cycles are similar, which is about 3 µA with several 0.2 mA current peaks. The amplitude of the current during the active listening process with different duty cycles are also similar, including the high-voltage and low-voltage search processes which are 5.71 mA and 6.69 mA, respectively.

To further verify the effect of the duty cycle on the network joining process, 50 measurements of testing the joining time required to join the network successfully were taken to determine the distribution of the joining time for each duty cycle, respectively. Fig. 5.10 shows the search time in high-voltage, and low-voltage search processes, sorted from low to high in 50 measurements with the network join duty cycle of 100%, 50%, and 25%, respectively. It should be noted that the search time studied here is the time for the high-voltage and low-voltage search processes, not the whole network joining time, including the extra time of the negotiating and connecting processes since the duty cycle of the network joining process only affects the search time. The search time in Fig 5.10 includes the active listening time and doze time.

It can be seen that the search process time is inconsistent regardless of the duty cycle. For example, the WSM may join the network with 35 s when the join duty cycle is 100% in Fig 5.10 (a), and may join the network with 10 s when the join duty cycle is 50% in Fig 5.10 (b). However, when the join duty cycle is 100%, the search time is mostly within 15 s and when the network join duty cycle is reduced to 50% and 25%, the occurrences of the search time within 15 s slightly decrease. It means a high duty cycle can increase the probability that the search time is completed in a short time. For example, there are about 30 times that the WSM joins the network less than 10 s when the join duty cycle is 100% in Fig 5.10 (a), but there are about 20 times that the WSM joins the network less than 10 s when the join duty cycle is 25% in Fig 5.10 (c). In addition, the high duty cycle can effectively avoid long searching time. For example, the longest time spending on search time is about 35 s when the join duty cycle is 100% in Fig 5.10 (a), but the longest time spending on search time is about 90 s when the join duty cycle

is 50% in Fig 5.10 (b). It should be noted that all the discussions here are probabilities.

In the EH powered WSN, the WSM needs to communicate with the network manager as soon as possible in the most cases, because the energy harvested is limited and so the duration of active time is limited as well, or it takes a long time to wake up again with a limited energy supply. Therefore, in order to make the WSM join the network as soon as possible, 100% duty cycle is chosen, since the low duty cycle will increase the searching time because of the extra doze time. It should be noted that, although the system with a low duty cycle has a lower average current consumption than that with a high duty cycle, it does not mean that the system has lower energy consumption with low duty cycle, since the active listening process of the system is the same regardless of the duty cycle. Conversely, the energy consumption of the system with the low duty cycle is higher than that with the high duty cycle because of the extra energy consumption during the doze time and the leakage current of the system while the active listening time is still the same.

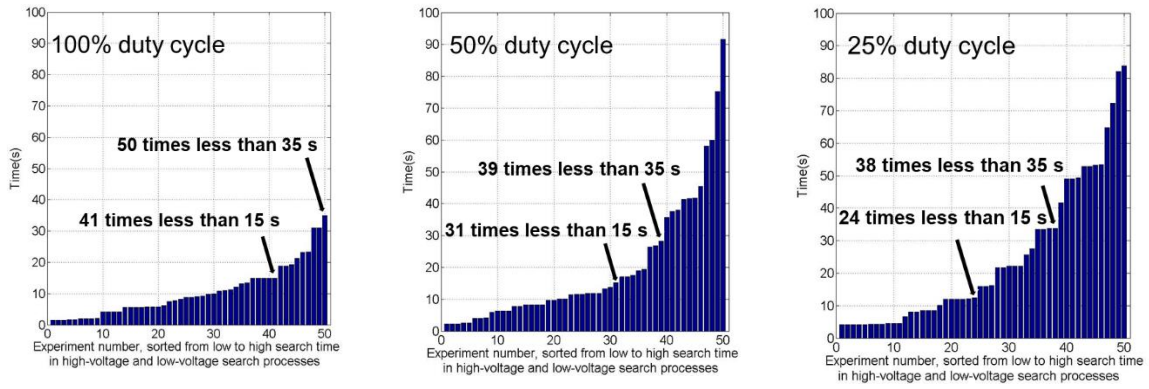

(a) (b) (c)

Figure 5.10: Search time in high-voltage and low-voltage search processes when the WSM successfully join the network, sorted from low to high in 50 measurements (a) at 100% duty cycle, (b) at 50% duty cycle and (c) at 25% duty cycle

5.7.3 Storage Capacitor Sizing

Choosing an appropriate storage capacitor size is important to the EH powered WSN since the capacitance requirement in the EH powered WSN is different from that in the EH powered WSM as the search time is random. The detailed analyses are given below. Comparing with the network joining process, the energy consumption of EH powered WSM during active time is relatively fixed or has a relatively low value when the WSM is pre-programed to perform a fixed task. Although the peak current of several processes, such as wireless transmission is high, it can know the energy consumption in advance because of the predictability in each process. Therefore, the capacitance requirement in the EH powered WSM is that the stored energy of the capacitor should be sufficient to support the WSM to carry out the tasks in the active time when the voltage across the capacitor is between the minimum operation voltage of the WSM and the turn-on threshold voltage of the hardware EAI. It should be noted that the stored energy discussed in the section is the consumable energy for the WSM, not the total stored energy in the capacitor calculated from 0 V.

However, the energy consumption of network joining process during the active time is random in the EH powered WSN, since the time of the high-voltage search process and the low-voltage search process are random because of the uncertainty of the WSM in searching for the network and waiting for the network manager to response as discussed in Section 5.7.2. Therefore, an appropriate storage capacitor size is essential to the success of the network joining process since the capacitor size directly affects the maximum allowed time for the network joining process. Careful consideration of it should be taken into account to ensure

a successful network joining of the WSM with the fewest attempts to avoid energy wastage.

Four different capacitor sizes of 22 mF, 33 mF, 50 mF, and 100 mF were used in this experiment. The system performance was assessed using these capacitors one by one. The capacitance of the energy storage chosen is in the milliFarads range since one of the fundamental requirements is that the energy stored in the energy storage must be enough for the WSM to complete its network join process. Based on the earlier study in Section 5.7.2, the network joining duty cycle of 100% was used in all the tests. The measured currents that were consumed by the WSM during the network searching process with the four super-capacitor sizes are shown in Fig. 5.11. It should be noted, in order to measure the maximum searching time that a capacitor can sustain, the measurements in Fig. 5.11 are all performed with the network manager turned off. Because the WSM will continue to search for the network when it cannot find the network manager. With the 22 mF, 33 mF, 50 mF, and 100 mF super-capacitors, the maximum searching time is about 2.98 s, 4.10 s, 6.87 s, and 13.91 s, respectively.

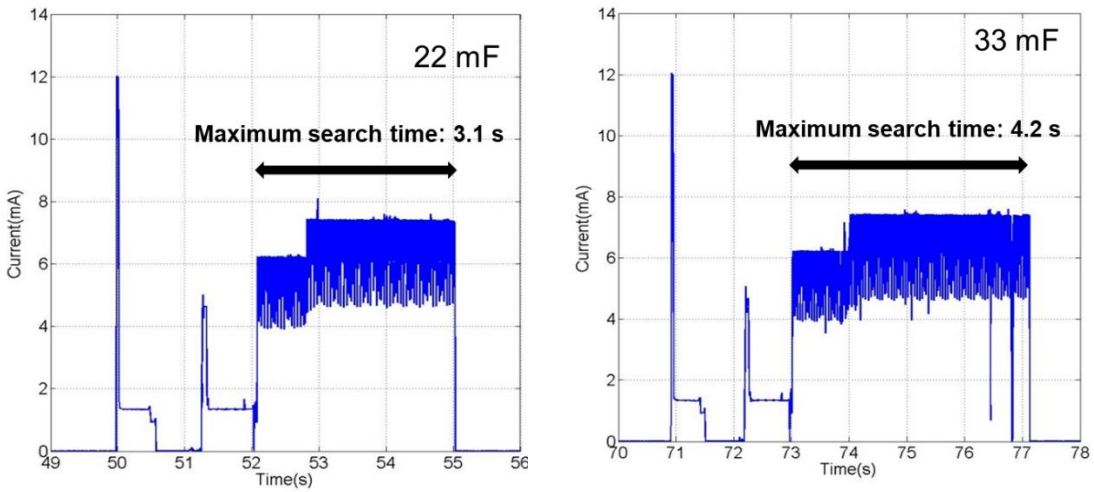

(a) (b)

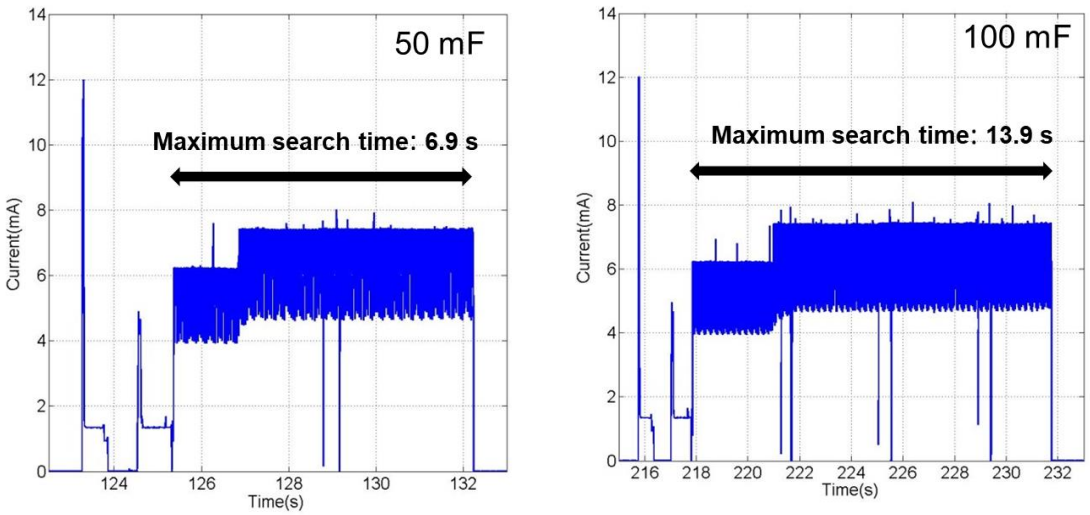

(c) (d)

Figure 5.11: Current consumed by the WSM when a peak-to-peak stain loading of 600 με at 10 Hz was applied onto the MFC using a super-capacitor size of (a) 22 mF, (b) 33 mF, (c) 50 mF, and (d) 100 mF

To further verify the effect of the storage capacitor size on the network joining process100 measurements of the above test were taken to record the proportion of the WSM successfully joining the network for the first joining attempt with the four different capacitor sizes, respectively. The performances of the system are shown in Table 5.3.

With the 22 mF, 33 mF, 50 mF, and 100 mF super-capacitors, the average time of the voltage charged from 0 V to turn-on voltage (3.15 V) are about 49.9 s, 70.9 s, 123.3 s, and 215.7 s, respectively. The average maximum search time is about 3.1 s, 4.2 s, 6.9 s, and 13.9 s, respectively. The energy consumption of the system in the searching time with them is 58.5 mJ, 78.6 mJ, 128.5 mJ, and 254.9 mJ, respectively. It should be noted that the energy consumption of the WSM here may a little higher than the stored energy calculated according to the capacitance itself since the MFC keeps charging the system during the active time.

The proportion of the WSM with 22 mF capacitor successfully joining the network for the first time is about 18% and increases to 26%, 42%, and 72% for the one hundred measurements when the capacitor increases to 33 mF, 50 mF, and 100 mF, respectively. This is because the larger the capacitor size, the longer the time window for searching the network. Similar to the network join duty cycle, the number of attempts in successfully joining the network using different capacitor sizes is relatively random. An energy storage that is sufficiently large is able to sustain the network joining process for a longer period and, therefore, has a higher successful network joining chance in one attempt. This agrees with the results in Table 5.2, where the rate of successfully joining the network increases with the amount of time given to join the network. However, a large capacitor also takes longer to charge up, which may result in a short active phase frequency of the WSM to meet the requirements of the EH powered WSN application for specific analyses or monitoring, since the WSM has to wait for a long while to be activated. Therefore, appropriate sizing of the capacitor based on the input power from the energy harvester is required to optimise the network joining process. Therefore, 100 mF is selected as the storage capacitor size in the EH powered WSN systems studied in Chapter 5 and 6, because it can support the WSM searching time of approximately 14 s, which enables the WSM to successfully join the network in most cases and do not have to wait for too long, such as one hour to be activated.

Table 5.3: Performances of the EH powered WSM joining the network with 22, 33, 50, and 100 mF super capacitors

Capacitor size (mF)	Average charging time (s)	Average allowed searching time (s)	Energy consumed during searching time (mJ)	The success rate in 100 times for network searching (%) for the first time
22	49.9	3.1	58.5	18
33	70.9	4.2	78.6	26
50	123.3	6.9	128.5	42
100	215.7	13.9	254.9	72

5.8 The Problem of the Network Joining Process in Energy Harvesting Powered Wireless Sensor Network

As can be seen from the above experiments, joining the network is a random process, especially in the searching process, which can spend several minutes or more. This uncertainty may cause the EH powered WSM to be turned off before joining the network or unable to complete the pre-programing tasks after successfully joining the network since joining the network consumes most of the energy. If these happen, a lot of the harvested energy will be wasted, and the energy storage requires extra time and energy to be recharged again. In the case of EH powered WSNs, where energy harvested is limited, the energy consumed by every unsuccessful network joining attempt or no follow-up sampling and communication after successfully joining the network is undesirable. Therefore, it is important for the WSM to deal with this problem.

5.9 Summary

This chapter studies a star topology EH powered WSN that comprises one network manager (Linear Technology DC9011A), and three EH powered WSMs that consist of a strain energy harvester, a PMM, a super-capacitor, hardware EAI and a Linear Technology DC9003 A-B Evaluation/Development Mote. In particular, the main focus was on the analyses of the energy consumption of the network joining process and the effects of the duty cycles and the energy storage size on the network joining process.

Detailed analyses revealed that the network joining process is very power hungry, especially for the low-voltage search and high-voltage search processes. Reducing the network joining duty cycle does not necessarily save the energy required for network joining. An appropriate size of the capacitor is crucial to ensure that the mote is able to join the network from the first attempt.

The main problem found is that the high-voltage search process and low-voltage process have very long uncertainty time. This uncertainty may cause much energy wasted by every unsuccessful network joining attempt or no follow-up sampling and communication after successfully joining the network.

Chapter 6 Network Energy-aware Approaches for Energy Harvesting Powered Wireless Sensor Networks

From Chapter 5, it can be seen that the network joining process of the EH powered WSM in the EH powered WSN is a random process and consumes more energy than the sampling and transmission tasks of a WSM. This uncertainty, especially the searching process may cause the WSM to waste a lot of energy as the WSM may be repeatedly turned off due to depleted energy before it can join the network or may be unable to complete the pre-programing tasks after successfully joining the network. Also, synchronisation of the network among the motes is important for the tasks management and scheduling of the motes. Therefore, Chapter 6 proposes and develops a network energy-aware approach to deal with the identified problem of the uncertainty. The network energy-aware approach studied in this chapter is a collective approach that includes the hardware EAI, the software EAI and the sensing EAI that have been described previously in Chapter 4 as well as some a new programme for the network joining and synchronisation that will be studied in this chapter.

The rest of the chapter is organised as follows: Section 6.1 describes the proposed network energy-aware approach for the network joining. Section 6.2 describes the programme for synchronised operation and Section 6.3 describes the implementation of the developed EH powered WSN with the proposed network energy-aware approach. Section 6.4 describes the experimental setup and Section 6.5 shows the results and discussions. Section 6.6 concludes the chapter with a summary of the key findings.

6.1 Network Joining Process with Energy Awareness

6.1.1 Concept

The uncertainty in the network joining process means that the WSM will not know whether it will be able to join the network successfully within the timeframe that it has been powered up based on the capacitor size. Even if the WSM successfully completes the network joining process after a lengthy search process, it is no longer able to operate properly or perform the subsequent tasks when the supply voltage is between the minimum operating voltage V_{MIN} that the WSM can work properly and the turn-off threshold of the hardware EAI. The energy available in the capacitor between these two voltages is generally insufficient for completion of a task. If the WSM continues to operate, the voltage level will quickly drop to the turn-off threshold, which resets the WSM even though the tasks are incomplete, and wastes all the energy used for previous processes. The WSM will then have to re-join the network once its capacitor has been recharged to the turn-on threshold. Therefore, on top of energy-aware approaches for WSMs that was previously studied in Chapter 4, the network energy-aware approach is studied here to reduce the energy consumption and prevent energy wastage when the EH powered WSM fails to join the network because of the limited energy supply. The network energy-aware approach is designed to trace the energy consumption of every EH powered WSM in the EH powered WSN during the targeted joining network processes, especially for those with a high power consumption and a long uncertain time. The network energy-aware approach determines whether the WSM has been staying in searching for network joining processes for too long, which results in insufficient energy to perform the next processes, including the other processes of network joining and the basic tasks

such as data sampling and transmission. By resetting the hardware EAI to put the WSM into an inactive phase in advance before the capacitor voltage drops to the turn-off threshold of the hardware EAI, the energy stored in the WSM will be higher than the case where the WSM continues to stay in the search process until the voltage of the energy storage drops to the turn-off threshold of the hardware EAI. Therefore, the energy storage can be recharged faster to the turn-on threshold to power up the WSM again sooner. Once the WSM has successfully joined the network, other network joining process programme together with the EAIs of WSMs will then be used, which will be explained in Section 6.2.

According to the different average powers of the high-voltage search process and the low-voltage search process, studied in Chapter 5, the WSM is able to judge whether it is in the high-voltage search process or the low-voltage search process by continuingly measuring the voltage across the capacitor, V_{CS}, and then calculating the average power between the measurement interval. However, this method consumes a lot of energy, since a continuous voltage monitoring operation with a few milliseconds of monitoring intervals is required to determine the voltage changes accurately and timely.

Moreover, since the time spent on each of the processes during the network joining is uncertain, even if it is able to determine which process the WSM is currently in, it is impossible to predict the time spent on next process when the WSM is joining the network. Therefore, a network energy-aware algorithm in the targeted processes of network joining for several uncertain processes is designed to deal with the aforementioned problems while tracing and managing the energy flow of the WSM to determine when it needs to be turned off. The targeted

process is set as the search process that includes the high-voltage search process and the low-voltage search process, since these two processes are the most power hungry processes and have the longest uncertainty time during the join network process, as mentioned in Chapter 5.

It should be noted that there is no changes were made to the hardware EAI when the network energy-aware approach were implemented. The sensing EAI and the software EAI will realize the function after the WSM join the network successfully, which means they are not related to the network energy-aware approach focusing on the WSM joining the network. In the term of the software EAI, the method has not changed, but the specific values used to judgement program have changed, since the MCU and sensor are different from those of Chapter 4.

6.1.2 Network Energy-aware Approach

In the network energy-aware programme, the completion of a process that the WSM is currently running is used to judge whether the current remaining energy is sufficient. Typically, the WSM is able to determine whether it has completed the network joining process through registering the call-back functions to handle a number of notifications that indicate three flowing processes:

(1) The WSM has heard the advertisement messages sent by the network manager, which means there is a joining notification that shows the WSM has completed the search process.

(2) The WSM has been synchronised to the network and started to join the network, which means that there is a connected notification that shows the WSM has completed the negotiating process.

(3) The WSM has got the joining permission to complete the network joining process and became operational to execute its pre-programmed tasks, which means there is an active notification that shows the WSM has completed the connecting process and joined the network successfully.

Therefore, the WSM is able to be programmed to judge whether the search process, negotiating process or connecting process has completed or not based on the receipt of the relevant notifications. However, it is impossible to tell when the high-voltage search process changes to the low-voltage search process during the search process by the call-back functions, since the change is controlled by a hardware-based autonomous media access controller managing radio operation, which incorporates a co-processor for controlling all of the time-critical radio operations [70]. Additionally, it is a software-independent timing control of the radio and radio-related functions, which handles precise sequencing of peripherals, including the transmitter, the receiver, and advanced encryption standard peripherals to minimise central processing unit (CPU) activity, thereby preventing variable software latency from affecting network timing and greatly reducing system power consumption by allowing the CPU to remain inactive during the majority of the radio activity [70]. Nevertheless, as shown in Chapter 5, the average power consumption of the low-voltage search process is higher than that of the high-voltage search process. Therefore, the average power consumption of the low-voltage search process is used as a reference in

the network energy-aware approach. This is because it is better to slightly overestimate the energy usage to ensure that the WSM will not be reset to be off by the hardware EAI during the period of asks.

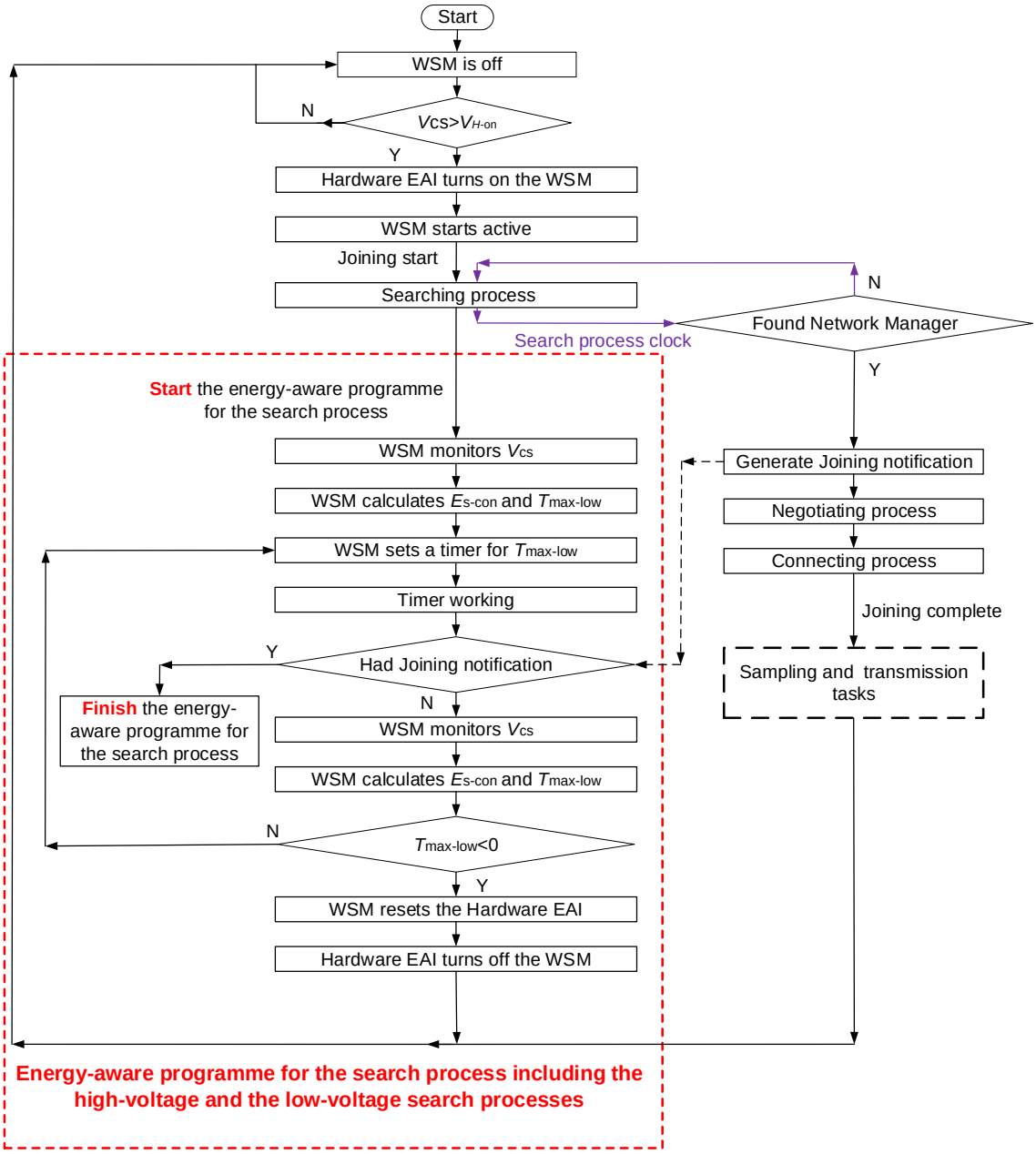

Figure 6.1: The flowchart of the energy-aware programme for the high-voltage search process and the low-voltage search process

Fig. 6.1 shows the flow chart of the energy-aware programme for the search process. The programme begins after the WSM starts to join the network. The WSM measures V_{CS} and then assumes the current available energy is only used for the low-voltage search process. Following this, the WSM calculates the

remaining energy in the capacitor, E_{con} and the maximum consumed energy of the WSM by staying in the low-voltage search process, $E_{\mathrm{max-low}}$ and then determines the maximum allowed time that the WSM is able to stay in the low-voltage search process, $T_{\mathrm{max-low}}$ based on the average power consumed by the WSM in the low-voltage search process, $P_{\mathrm{low-v}}$ by using equations 6.1, 6.2, and 6.3, respectively.

$$E_{con} = \frac{1}{2} C V_{CS}{}^{2} - \frac{1}{2} C V_{\min}{}^{2} \tag{6.1}$$

$$E_{max-low} = E_{con} - E_{nego} - E_{connected} - E_{b-samp} \tag{6.2}$$

$$T_{max-low} = \frac{E_{max-low}}{P_{low-v}} \tag{6.3}$$

where $V_{\min}$ is the pre-set minimum operating voltage of the WSM, which means that the WSM is no longer able to operate properly below it; E_{nego} and $E_{\mathrm{connected}}$ are the average energy required for the WSM to complete the negotiating process and connecting process, respectively; and $E_{\mathrm{b-samp}}$ is the energy required for the WSM to complete the basic tasks including sampling, transmitting and resetting the hardware EAI. E_{nego} , $E_{\mathrm{connected}}$, $E_{\mathrm{b-samp}}$ and $P_{\mathrm{low-v}}$ can be determined through programming the WSM to perform the individual tasks and then measuring the energy consumption of the tasks, which are similar to the determination of V_{END} described in Section 4.3.2.

It should be noted that $T_{\mathrm{max-low}}$ is also used to judge whether the WSM has enough energy to perform the next processes. If $T_{\mathrm{max-low}}$ is higher than 0, it means the WSM still have the energy and therefore, time to stay in the search process. If $T_{\mathrm{max-low}}$ is lower than 0, it means the WSM does not have the

sufficient energy and therefore, will stop the search process. As a result, the WSM will reset the hardware EAI to turn itself off so that the super-capacitor can be recharged for a new attempt of joining the network.

A timing function is called to create a timer to record $T_{\max-\text{low}}$. After the time that is equal to $T_{\max-\text{low}}$ has elapsed, the WSM determines the status of the search process by checking whether the joining notification has been obtained or not. If it has, this means the WSM has already completed the search process. Therefore, the network energy-aware programme for the search process ends here. The energy which has been consumed by the search process will not cause the WSM to have insufficient energy to perform the next processes since it has already been considered in the calculation of $T_{\max-\text{low}}$. Also, the calculation of $T_{\max-\text{low}}$ actually overestimates the energy usage using only the low-voltage search process as reference while the search process includes the high-voltage search process that consumes less power. This guarantees that there will always be some energy left after $T_{\max-\text{low}}$ has elapsed. If the WSM did not receive the notification, it will measure a new V_{CS} to calculate a new $T_{\max-\text{low}}$ to be compared with 0. If the new $T_{\max-\text{low}}$ is higher than 0, which means the WSM still have the energy to stay in the search process, the WSM will generate a timing function to record the new $T_{\max-\text{low}}$ and set a new timer. If the new $T_{\max-\text{low}}$ is lower than 0, which means the energy storage will not have enough energy for the WSM to perform the next processes even if the search process can be completed later. Therefore, the WSM will immediately implement the software EAI programme to reset the hardware EAI to put itself into an inactive phase. The whole cycle repeats when the WSM wakes up to join the network again.

Under most circumstances where there is no power or the power from the energy harvesters is lower than the power consumed by the WSM during the search process, it is expected that the loop of the approach shown in Fig. 6.2 will not repeat for more than three times. This can be explained using the following scenarios:

(1) The first case is that the WSM has already received the joining notification after $T_{\mathrm{max-low}}$ has elapsed. This means the search process is completed and the WSM finishes the energy-aware programme for the search process.

(2) The second case is that the WSM has already completed the high-voltage process and stays in the low-voltage search process after $T_{\mathrm{max-low}}$ has elapsed. This means the system still has the energy to support the WSM in the low-voltage search process for a while, since $T_{\mathrm{max-low}}$ is calculated based on the low-voltage search process which has the higher average power than that of the high-voltage search process. However, the WSM still has not obtained the joining notification. It then measures V_{CS} and calculates $T_{\mathrm{max-low}}$ for the second time, which should be higher than 0.

After the second $T_{\mathrm{max-low}}$ has elapsed, if the WSM has already completed the low-voltage search process, which is same as case 1, the WSM will finish the energy-aware programme. If not, the WSM will measure V_{CS} and then calculate $T_{\mathrm{max-low}}$ for the third time. This time, the thirdly calculated $T_{\mathrm{max-low}}$ is likely to be lower than 0, since the WSM is already in the low-voltage search process during the second calculated $T_{\mathrm{max-low}}$,

which is also the maximum time that the energy remained is able to sustain the low-voltage search process. Therefore, the WSM will reset the hardware EAI.

Occasionally when the power from the energy harvesters is very high, which recharges the super-capacitor and increases the capacitor voltage, the WSM could still be in the high-voltage search process after $T_{\mathrm{max-low}}$ has elapsed. The WSM will repeat the operation to get a newly measured V_{CS} and calculated $T_{\mathrm{max-low}}$ until it gets a join notification to finish the programme or until the calculated $T_{\mathrm{max-low}}$ is lower than 0 to reset the hardware EAI in the case that no join notification is received and the power from the energy harvesters suddenly becomes unavailable or too low.

Therefore, the network energy-aware approach is able to cover all the possible scenarios of the search process with minimal number of voltage monitoring times while tracing and judging whether the remaining energy of the WSM is sufficient to support the next processes instead of doing a constant monitoring with milliseconds interval. Since the judgment method is based on the current remaining energy of the WSM, any additional energy from the energy harvesters that replenishes the energy storage during the monitoring process will also be considered. For example, assume that the WSM is in the previously mentioned second scenario running the timer function for the second time. If there is additional energy that replenishes the super-capacitor and is high enough to support the WSM to remain in the search process for a period of time just before $T_{\mathrm{max-low}}$ elapsed, the following thirdly calculated $T_{\mathrm{max-low}}$ will be higher than 0.

As a result, the WSM will continue to stay in the search process if it still has not completed the search process.

6.2 Developed Energy Harvesting Powered Wireless Sensor Networks with the proposed Network Energy-aware Approaches

6.2.1 Network Communication

The communication between the EH powered WSM and the network manager in the EH powered WSN is two-way communication, which is different from the one-way communication between the EH powered WSM and the base station in Chapter 4. It should be noted that in the one-way communication, the EH powered WSM is able to communicate with the base station but will not get any response from it. For example, when the EH powered WSM transmits the data to the base station, it is not able to acquire a transmission response from it, which means that the EH powered WSM is not able to know whether the transmission is successful or not. In contrast, the two-way communication allows the EH powered WSM to get a response from the network manager. The EH powered WSM is able to ask for the transmission response from the network manager after it transmits the data to determine whether the transmission is successful or not. If the transmission response says some data is lost during the transmission, the EH powered WSM is able to resend the data. Moreover, since the EH powered WSM is able to communicate with the network manager, it also can retrieve the network time from the network manager and then synchronised with the network to achieve synchronised measurements and transmissions. This allows a network with many motes to be synchronised and managed by the network manager to ensure a reliable wireless network and achieve the operation in the

synchronous measurements application which will be described in detail in the next section.

6.2.2 Hardware Implementation

In order to understand the performance of the EH powered WSM in the network using the proposed network energy-aware approach, an EH powered WSN was implemented for the study. Similar to the network schematic of the EH powered WSN in Chapter 5, the studied network topology is a star network. The EH powered WSN in this chapter consists of three DC9003A-B motes and a DC9001B network manager that all have the LTC5800 chip. Since the network manager has a very important role in managing the network, it will be connected to a computer to get a steady power supply to ensure that it is always on, and to allow more control and processing from the computer. Moreover, two of the WSMs are powered by the vibration and airflow energy harvesting, respectively and one WSM is powered by battery.

It should be noted that, the proposed network energy-aware approaches focus on avoiding the wasted energy during the WSM joining the network, since joining the network is a random process, especially in the searching process, which can spend several minutes or more. Therefore, the complexity of the network structure will not affect the function of the network energy-aware approaches. For example, as there are more WSMs in the network, each WSM may take longer time to join the network, but this does not affect the energy-aware approaches to determine whether the current WSM has enough energy to continue to join the network. The energy-aware approaches does not focus on changing the length of time that each WSM joins the network, but rather whether the WSM wastes the

energy on meaningless waiting, which results in insufficient energy to perform the next processes. Because joining the network is only the first step in the case of EH powered WSNs, the more important step is that the WSM samples the data and sends it to the network manager after successfully joining the network. For example, the WSM may unable to complete the pre-programing tasks after successfully joining the network since joining the network consumes most of the energy. If these happen, a lot of the harvested energy will be wasted, and the energy storage requires extra time and energy to be recharged again.

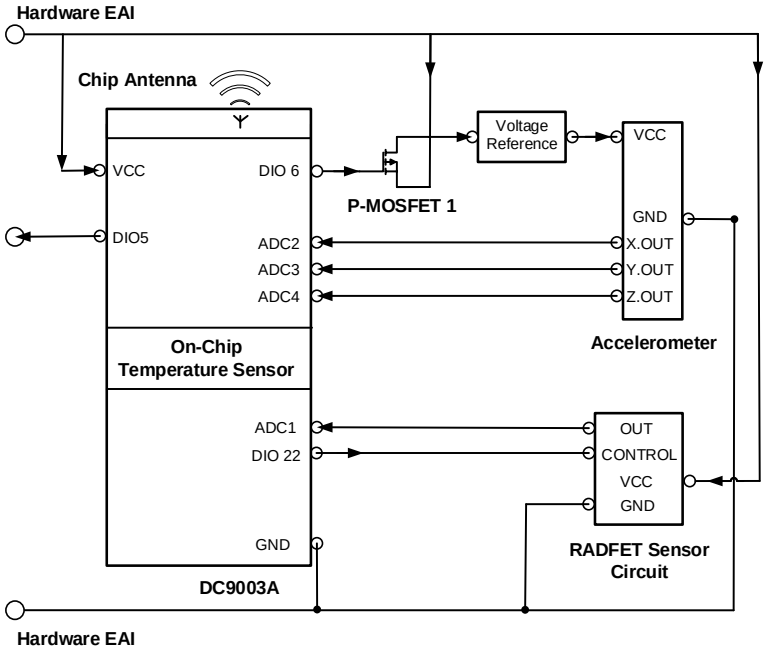

Figure 6.2: Schematic of the studied WSM in the EH powered WSM

The first EH powered WSM consists of an energy harvester, a PMM circuit, a super-capacitor, a hardware EAI circuit and a WSM. The energy harvester, PMM circuit, and hardware EAI are the same as those in Chapter 4. The system used a 100 mF super-capacitor and the architecture of the WSM is shown in Fig. 6.2. The first EH powered WSM includes three analogue sensors:

(1) The acceleration sensing circuit includes a ADXL335 3-axis accelerometer and a voltage reference (ISL21080CIH325, Intersil, California, USA), which is used to provide a fixed reference voltage of 2.5 V to the accelerometer during the active time of the WSM, since the accelerometer requires a fixed reference voltage to determine the accelerations from the sensor readings but the direct supply voltage from the capacitor is not constant throughout the active phase. Moreover, the acceleration sensing circuit includes the sensing EAI which is built with one P-MOSFET to turn on and off the connection between the system and the sensor power as controlled by the high and low signal generated by the DIO6 pin of the DC9003A, respectively. The ADC2, ADC3 and ADC4 pins of the DC9003A are individually connected to the three outputs (acceleration in x-, y- and z-axis) of the 3-axis accelerometer.

(2) The radiation sensing circuit [116] which is shown in Fig. 6.3 is built around Tyndall TY1003 RADFETS [117] for measuring ionising radiation dose for aerospace industry to assess environmental conditions in a high altitude. An analogue switching circuit is used to turn on and off the radiation sensor as controlled by the high and low signal generated by the DIO22 pin of the DC9003A, respectively. The ADC 1 pin of the DC9003A is connected to the output of the radiation sensor to read the output signal from the radiation sensing circuit.

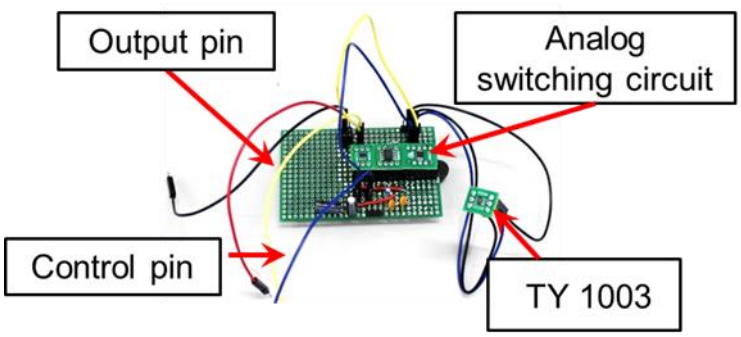

Figure 6.3: Schematic of the studied WSM in the EH powered WSM

(3) The temperature sensing circuit is the built-in temperature sensor on DC9003A, which is used to acquire the local temperature data for wireless transmission.

The second EH powered WSM consists of an energy harvester, a PMM circuit, a super-capacitor, a hardware EAI circuit and a WSM. An airflow energy harvester is used to generate electrical energy from airflow to the EH powered WSM. Fig. 6.4 shows the airflow energy harvester which consists of a modified helical Savonius turbine, which is connected to an electromagnetic generator to convert energy from airflow into electrical energy, developed by the Energy Harvesting Research Group at the University of Exeter. The turbine and the generator have the dimensions of Ø15 × 20mm and Ø7 × 16mm, respectively [118]. The generator and a power management circuit were put into a case with the dimensions of 35 × 16 × 66 mm for ease of holding the EH module. A portable wind generator was used to generate the airflow for this test. The portable wind generator is adjustable to generate different airflow speeds, where the airflow speed can be measured by an anemometer at the air outlet of generator. The, hardware EAI and the super-capacitor are the same as the first EH powered

WSM. The second EH powered WSM includes an ADXL335 3-axis accelerometer circuit and a built-in temperature sensor.

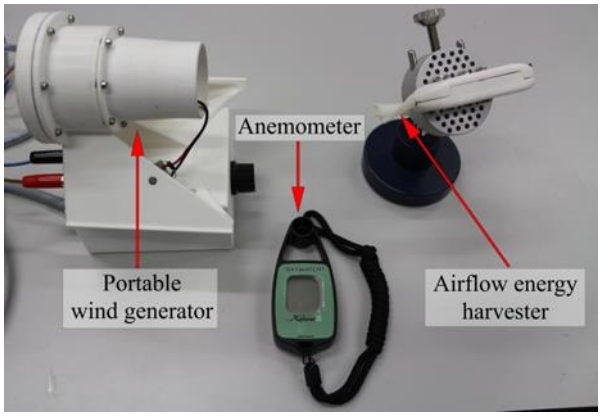

Figure 6.4: Airflow energy harvester

The third WSM is powered by batteries and the sensing platform includes the same ADXL335 3-axis accelerometer circuit and a built-in temperature sensor.

6.2.3 Implemented Software Overview

All the motes were programmed with the network energy-aware approach. After the WSM has successfully joined the network as controlled by the network energy-aware programme, it will run the programmes including basic sampling application, asynchronous acceleration measurements application (AAM) and synchronous acceleration measurements application (SAM), as shown in Fig. 6.5, which will be further explained later.

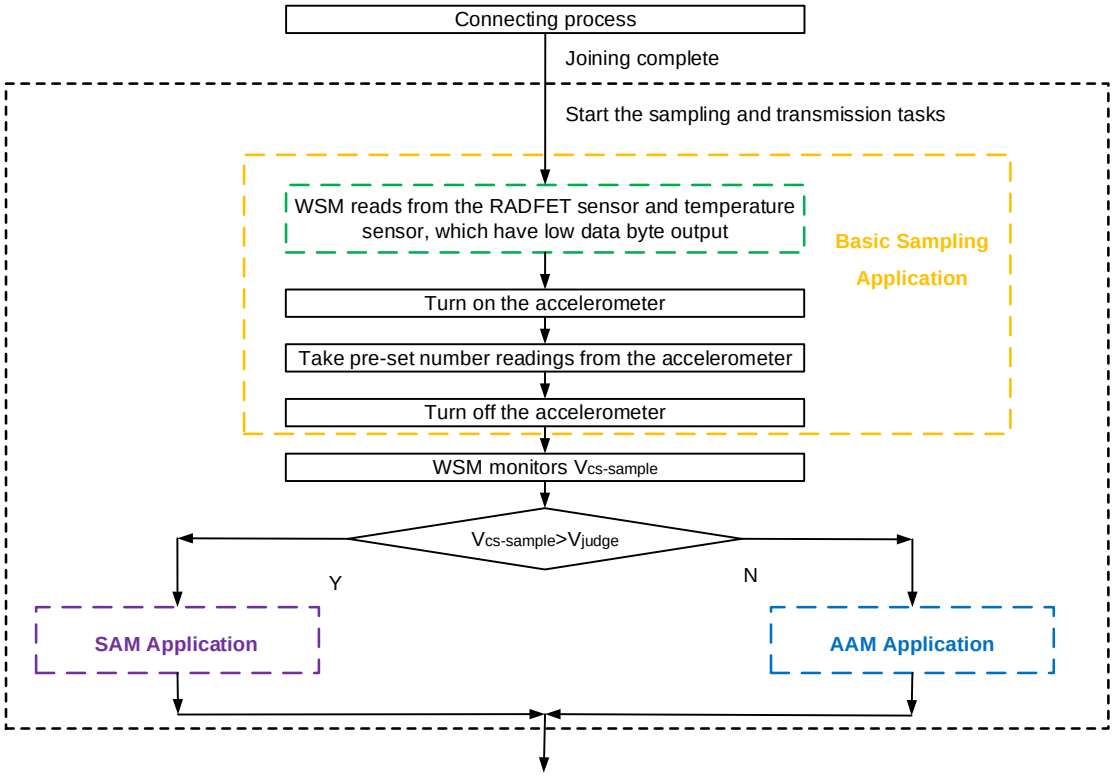

Figure 6.5: The flowchart of the sampling and transmission tasks programme after the WSM has joined the network

The flow chart of the network joining operation is the same as the mentioned in Fig. 5.4 between the WSM starts to join the network and completes to join the network, and therefore will not be repeated here.

6.2.3.1 Basic Sampling Application

This function is used to control the WSM to achieve the basic sampling function that reads from sensors with small amount of data bytes such as the temperature sensor, humidity sensor and radiation sensor first. It then proceeds to get one set of data from the accelerometer and determines the next sampling application of either AAM or SAM to be executed, depending on the remaining energy in the capacitor when the basic sampling application has completed. In the basic sampling application, the five sub-functions of dn_open (), dn_ioctl (), dn_close (), dn_read () and dn_wirte () are used to access the WSM to enable the relevant

pins of the WSM including sensors, actuators, ADC and digital interfaces, control a previously enabled pin, disabled a previously enabled pin, read from a previously enabled pin and write to a previously enabled pin, respectively. It should be noted that at the beginning of the programme, the sequences and the number of times that these sub-functions will be called might differ from one mote to another depending on the types and number of sensors used.

Fig. 6.6 shows the flowchart of the first EH powered WSM reading from the RADFET sensor and temperature sensor, which have low data byte output at the beginning of the basic sampling application.

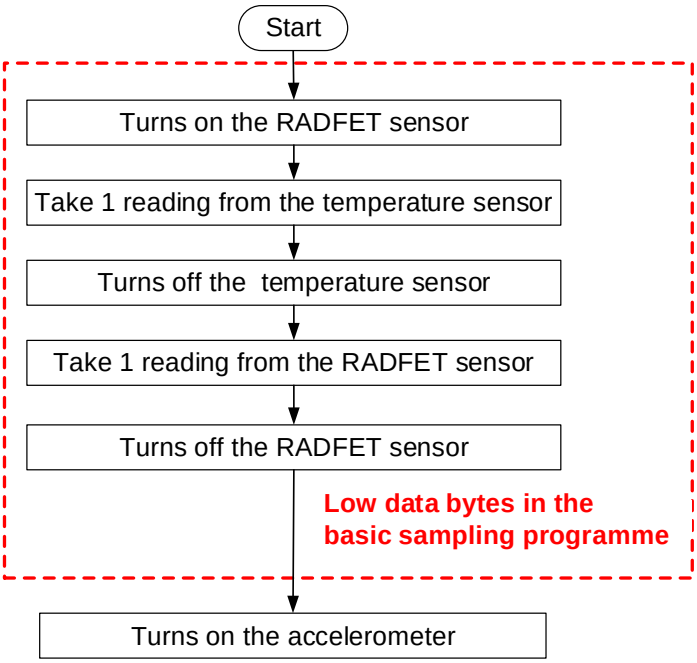

Figure 6.6: The flowchart of the first EH powered WSM reading the sensors with low data bytes in the basic sampling programme

Upon being started, the general purpose input/output (GPIO) function is used to generate a high signal from one GPIO pin to turn on the RADFET sensor, since the switching circuit of the sensor is required drive current to turn on. Furthermore, the WSM uses dn_open () to enable the DP3 pin of DC9003 board

and then used dn_ioctl () function to configure the pin as output, and then uses dn_write () function to drive the GPIO pin high.

Since the RADFET sensor needs time to reach a steady state output, the WSM reads the temperature sensor first to give the RADFET sensor time to get ready for sampling the data. The WSM uses dn_open () to enable the internal ADC pin of DC9003 board and then uses dn_read () to read the output of the temperature sensor, which has 2 bytes of data. After that, dn_close () is used to close the reading temperature function.

Then, the WSM uses dn_open () to enable the ADC 0 pin of DC9003 board and then uses dn_read () to read the output of the RADFET sensor, which is also 2 bytes. After that, the WSM uses dn_close () to close the reading RADFET function and then uses dn_write () function to drive the DP3 pin low to turn off the RADFET sensor. After that, the basic sampling application will proceed with the acceleration measurement.

For the WSMs without the radiation sensor, their basic sampling applications begin with taking 1 reading from the temperature sensor and then go straight to turning on the accelerometer.

After the readings from the sensors with low data byte outputs have been taken, the sensing EAI circuit of accelerometer required a low signal to turn on the accelerometer. Therefore, the WSM uses pin 6 of the DC9003 board to turn on the accelerometer and read the X-, Y- and Z-axis acceleration from its ADC 2, 3, 4 pins, respectively. The application sets the WSM to take a pre-set number of

readings from the accelerometer. In this case, the WSM is set to repeat each data reading process every 10 ms for 14 times to ensure there are enough readings to cover the measured vibration frequencies in the studied case of this thesis. This means the total data acquisition time is 140 ms with a sampling rate of 100 Hz. In each time, the WSM takes a total of three readings (2 bytes of data) each from X-, Y-, and Z-axis of the accelerometer. This results in a total of 84 bytes from the accelerometer.

After the pre-set number of accelerometer sampling function is finished, the WSM measures the current voltage level across the capacitor, $V_{\mathrm{cs-sample}}$ and then compare with V_{judge} which is a pre-set voltage to determine if WSM does the next sampling process. In this case, V_{judge} is set as 2.6 V, since the WSM is able to perform at least 2 times of measurements in the SAM application when the voltage across the 100 mF capacitor is this value, based on the measured energy consumption through experiments in the next Section 6.4.3. If $V_{\mathrm{cs-sample}}$ is higher than V_{judge} , the WSM will perform the SAM application and if $V_{\mathrm{cs-sample}}$ is lower than V_{judge}, the WSM will perform the AAM application with the software EAI.

6.2.3.2 Asynchronous Acceleration Measurements Application

This function is aimed to enable the WSM to achieve a long measurement with the limited energy when $V_{\mathrm{cs-sample}}$ is lower than the V_{judge}. It is used to control the WSM to achieve the AAM application with the software EAI function.

Fig. 6.7 shows the flowchart of the AAM application. Similar with the software EAI in Chapter 4, the function is programmed to set the variable parameter M to 1,

which is used to record the number of times that the WSM had taken the pre-set number of readings from the accelerometer to calculate V_{END}. After that, V_{END} is calculated by using equations 4.3 to 4.7 and then is compared with V_{CS}. In this case, E_{tx-1} +, E_{samp-1} and E_{reset} have been found to be 45 µJ, 19 µJ, and 30 µJ, respectively through the experimental method in Section 4.3.2. In addition, C is set as 0.1, which is the capacitance of the super-capacitor of 100 mF, a is 4 that includes 2 bytes each from the RADFET and the temperature sensor for the first EH powered WSM and is 2 for the other WSMs that have only the temperature sensor, b is 84, and V_{MIN} is set to be 2.5 V, since the voltage reference of the accelerometer is 2.5 V.

It should be noted that, the first comparison is between $V_{\mathrm{cs-sample}}$ and V_{END}. If V_{CS} is higher than V_{END}, M increases by 1 and then the function repeats one cycle of the WSM taking the pre-set number of readings from the accelerometer. After that, the WSM monitors V_{CS} and then calculates a new V_{END} to compare the two voltages again, and then repeats the cycle. If V_{CS} is lower than V_{END}, dn_close () is used to close the reading accelerometer function and then the transmission function is called to transmit all the recorded data. After that, the WSM uses dn_write () to drive the pin 5 to generate a low signal to reset the hardware EAI. As the WSM has been turned off by the hardware EAI, it goes into the non-active phase and the cycle repeats. It should be noted that, the function is also set to transmit all the data and then reset the hardware EAI after the WSM performs 11 cycles of reading from the accelerometer as executed by the AAM. There will be a maximum of 1012 bytes of data where 88 bytes are from the basic sampling application and 924 bytes are from the 11 cycles of readings, which is able to meet most of the monitoring application requirements. Every transmission

interval is set as about 100 ms through the timing function, since the maximum data throughput of the WSN is 36 packets/s [119], which means the maximum data throughput of one WSM is 12 packet/s in the developed EH powered WSN.

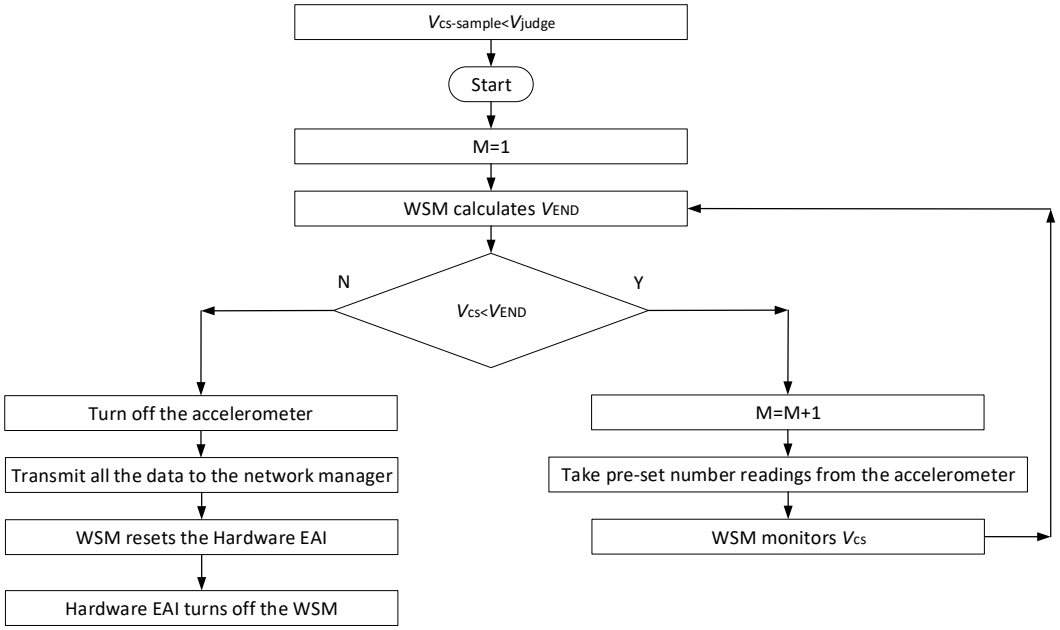

Figure 6.7: The flowchart of the AMM application

6.2.3.3 Synchronous Acceleration Measurements Application

This function is aimed to enable the WSM to repeat a pre-set number of acceleration measurements and then sends them periodically to the network manager in every reporting period, $T_{\mathrm{reportms.}}$ This means the WSM is synchronous to the network where its operation is properly scheduled. It should be noted that this situation happens when the WSM has sufficient energy where $V_{\mathrm{cs-sample}}$ is higher than V_{judge} due to a short network joining time, which means that the energy consumption of the network joining process is low. As a result, the remaining energy of the WSM after it has joined the network allows the WSM to complete tasks with higher energy requirements.

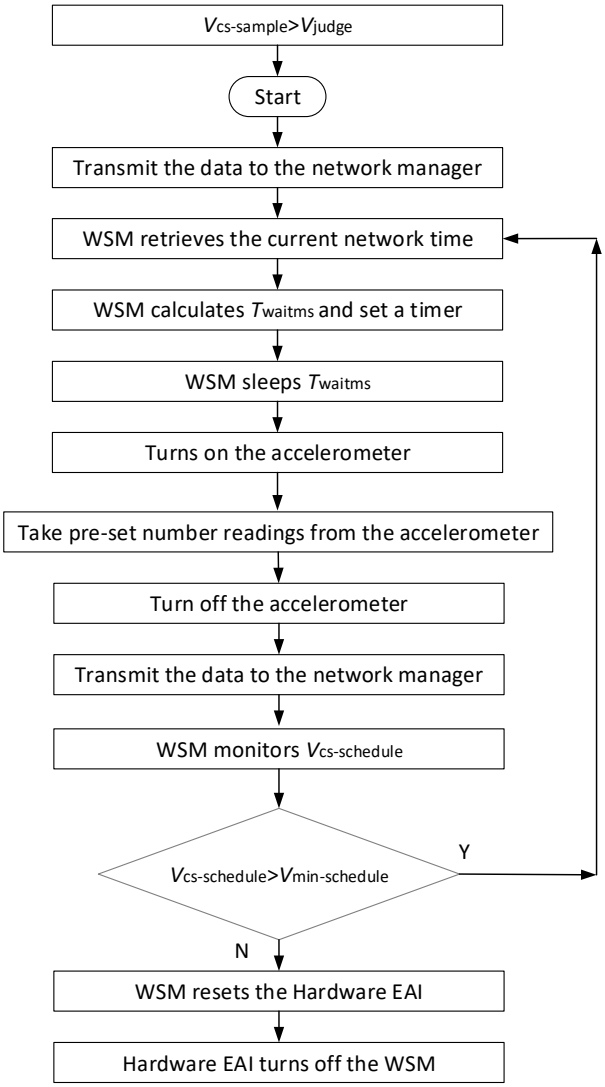

Figure 6.8: The flowchart of the SAM application

Fig. 6.8 shows the flowchart of the SAM application. Upon being started, the WSM transmits the data sampled from the basic sampling application to the network manager. After that, the WSM uses dn_getNetworkTime () to retrieve the current network time from the network manager. The network time contains both current Absolute Slot Number (ASN), which is the number of timeslots since the network start up, represented by a 5 byte integer, and the corresponding Coordinated Universal Time (UTC). The UTC is in the serialised format that includes the number of seconds since midnight of January 1, 1970, represented by a 4 byte integer and is defined as T_{sec}, and the number of microseconds since

the beginning of the current second, represented by a 4 byte integer and is defined as T_{usec}. It should be noted that, the WSM is set to ask the network time after it send the sampled data to the network manager every time to ensure the accuracy of the time synchronisation. Then, the WSM arms a timer, waits for it to expire, and then take a pre-set number of readings from the accelerometer and send them to the network manager. The waiting time, T_{waitms} is calculated by equation 6.4.

$$T_{waitms} = T_{reportms} - (((T_{sec} \times 1000) + (T_{usec} \times 1000)) \,\%\, T_{reportms}) \tag{6.4}$$

It should be noted that the % sign is modulo, T_{waitms} and T_{reportms} are in milliseconds because the timer clock is based on milliseconds [120] and T_{reportms} is set as 5000 ms as an example to show the WSM is able to perform the synchronised measurements with a long time interval in the WSN. This means the operation as programmed in the SAM repeats every 5000 ms that have elapsed as set by T_{reportms} since 00:00:00 Thursday, 1 January 1970. Since the increment of the ASN and UTC time in all the WSMs occur at approximately the same time and the rate with an accuracy of up to microsecond [120], the event of SAM can therefore be assumed to happen at the same time on all the WSMs.

After that, the WSM measures the voltage across the super-capacitor, $V_{\mathrm{cs-schedule}}$ and then compared with $V_{\mathrm{min-schedule}}$ which is the minimum voltage across the super-capacitor to meet the energy requirement for the WSM implementing one measurement cycle to judge whether it has sufficient energy to implement the next measurement cycle or not. If so, the WSM retrieves the

current network time again and repeats the cycle. If not, the WSM reset the hardware EAI to turn off itself, which is similar to that in the AMM application.

Here is an example of how the WSMs achieve the synchronised measurement and transmission after it receives the network time from the network manager. T_{reportms} is set as 5000 ms and assume that the first EH powered WSM obtained the current network time of 2004-09-16T23:59:58.75, which corresponds to the UTC time of 1095379198.750. The second EH powered WSM obtained the current network time of 2004-09-17T00:00:00.25, which corresponds to the UTC time of 1095379200.250. Following this, T_{waitms} of the first EH powered WSM is calculated by 5000- ((1095379198 × 1000) + (0.75 × 1000)) % 5000, which is equal to 1250 and T_{waitms} of the second EH powered WSM is calculated by 5000- ((1095379200 × 1000) + (0.25 × 1000)) % 5000, which is equal to 4750. Therefore, the first EH powered WSM will sleep for 1250 ms and then wake up to turn on the accelerometer to measure at 1095379200.000, which corresponds to the time 2004-09-17T00:00:00.000 and repeats the operation every 5000 ms. Similarly, the second EH powered WSM will sleep for 4750 ms and then wake up to turn on the accelerometer to measure at 1095379205.000, which corresponds to the time 2004-09-17T00:00:05.000 and repeats it every 5000 ms. Therefore, the two EH powered WSM are able to turn on the accelerometer at the same time after 2004-09-17T00:00:05.000, where their measurement operation has been synchronised.

6.3 Experimental Setup

Three WSMs in the EH powered WSN used the same kind of 100 mF super-capacitor and 100% network joining duty cycle. A peak-to-peak strain loading of 600 με at 10 Hz was applied to the vibration energy harvester in the first EH powered WSM and airflow with the speed of about 9 m/s was used to run the airflow energy harvester in the second EH powered WSM. It should be noted that, energy generated from the energy harvesters will not be measured, since this experiment focuses on studying the performance and the energy consumption of the EH powered WSMs during different processes in the WSN. Two source meters were each used for measurements of the first and second EH powered WSM. All the measurements used 200 Hz sampling frequency to allow a longer measurement time.

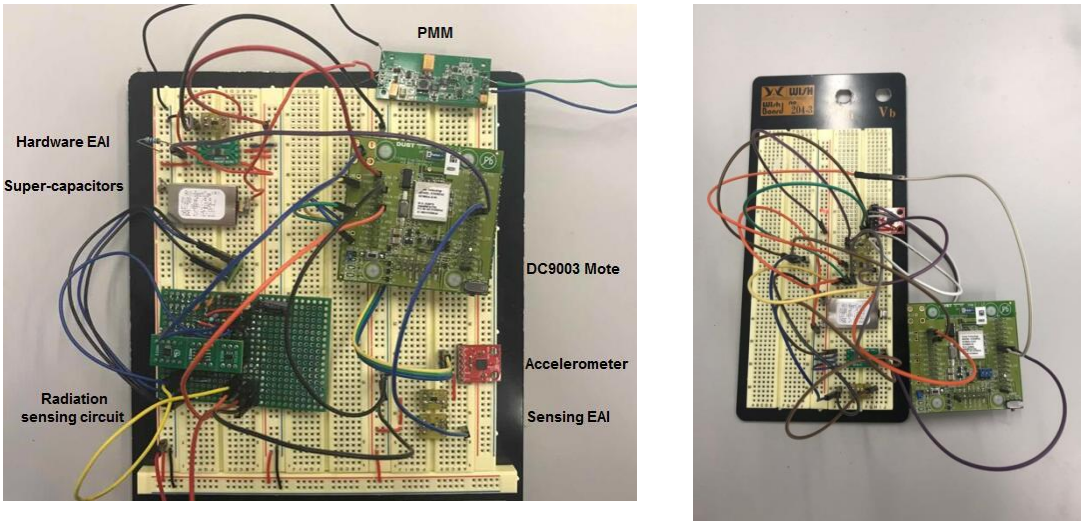

(a) (b)

Figure 6.9: Image of the prototypes of (a) the first EH powered WSM with the radiation sensing circuit that will be powered by the vibration energy harvester and (b) the second EH powered WSM that will powered by the airflow energy harvester

Fig. 6.9(a) and Fig. 6.9(b) show the image of the prototypes of the first EH powered WSM and the second EH powered WSM, respectively, which have been

discussed in Section 6.2. The network manager is the same as the one shown in Fig. 5.5(b).

To study the performances and energy consumption of the studied EH powered WSN with the network energy-aware approach, different test conditions were used. However, in each test, both the Instron testing machine and the portable wind generator were turned on at similar times to ensure that the EH process of the two EH powered WSMs started at a similar time. After that, the battery-powered WSM was turned on right after the energy harvesters have been turned on. The following three typical cases are analysed in the next section:

1. The first studied case is used to show the network energy-aware approach is able to reduce the energy wastage in the event that the network searching of the EH powered WSM is too long. It was done by comparing the current, voltage and energy consumption of the EH powered WSMs without and with the network energy-aware approach when they could not join the network successfully. It should be noted that, the only difference between the two EH powered WSMs is that the EH powered WSM without the network energy-aware approach does not have the network energy-aware approach but still got the other EAIs.

2. The first EH powered WSM has joined the network successfully and then completed the basic sample application. After that, the AMM application was executed because $V_{\mathrm{cs-sample}}$ is lower than V_{judge}.

3. The first EH powered WSM has joined the network successfully and then completed the basic sample application. After that, the SAM application was executed because $V_{cs-sample}$ is higher than the V_{judge}. The second and third EH powered WSM was also used to show that the WSMs in the WSN are able to implement the synchronised accelerometer measurements and transmissions across the network. The stargazer, which is a software that provide a graphical view of the LTC5800 wireless network [121] was used to show the network topology of the proposed EH powered WSN.

6.4 Results and discussions

6.4.1 Verification of Network Energy-aware Approaches for Energy Saving

This section shows the case where the network joining is unsuccessful and how the network energy-aware approach saves energy. Fig. 6.10 shows the measured current, voltage and the calculated energy consumption of the EH powered WSM without and with the network energy-aware approach, respectively.

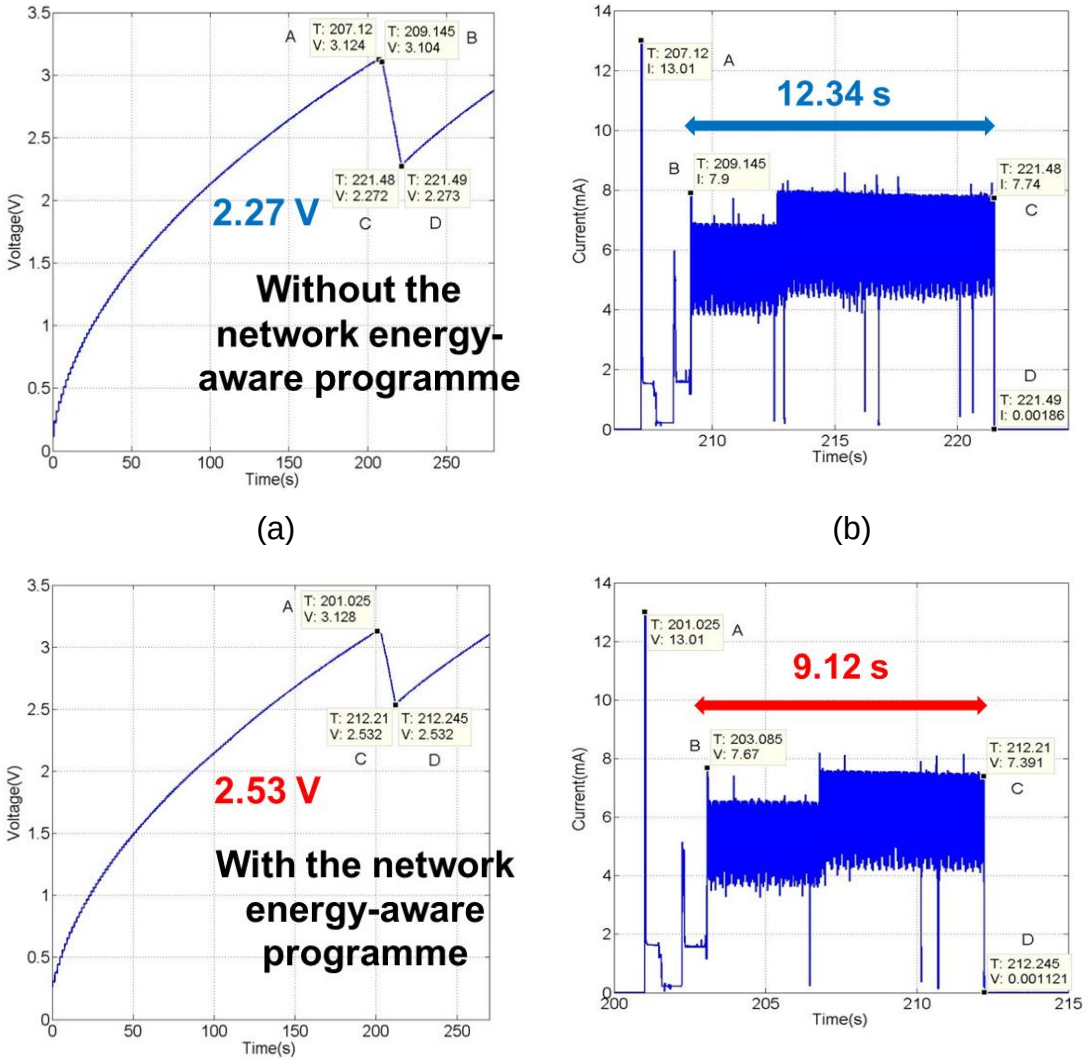

Figure 6.10: Measured V_{cs} and I_w with enlarged view during the active phase of the EH powered WSM without the network energy-aware approach in (a) and (b), respectively and with the network energy-aware approach in (c) and (d), respectively

For the EH powered WSM without the network energy-aware approach, Fig. 6.10(a) shows that, from the beginning at 0 s to about 207 s, the super-capacitor was charged by the PMM with the harvested energy from the MFC and its voltage V_{cs} increased from 0 V to about 3.124 V at point A. After that, the WSM is turned on by the hardware EAI. To better recognise the processes that occur after the WSM becomes active, the measured current as shown in Fig. 6.10(b) will be used in the subsequent analyses. After the WSM has completed the wake up and initialisation process as defined in Section 5.7.1.1 between point A and point B

that last for about 2.03 s, the WSM began to join the network at point B (209.146 s). The WSM spent about 12.34 s between point B and point C (221.48 s) on the search process, including the high-voltage search process and low-voltage search process that caused its voltage V_{cs} to drop from 3.104 V to 2.272 V. After that, the hardware EAI turned off the WSM, since the current V_{cs} is lower than the turn-off threshold voltage of the hardware EAI, which took about 0.01 s and finished at point D (221.49 s) with 2.273 V.

For the EH powered WSM with the network energy-aware approach, Fig. 6.10(c) shows that, from the beginning at 0 s to about 201 s, the super-capacitor was charged by the PMM with the harvested energy from the MFC and its voltage V_{cs} increased from 0 V to about 3.128 V at point A. After the WSM completed the wake up and initialisation process as shown in Fig. 6.10 (d) between point A and point B that last for about 2.06 s, the WSM began to join the network at point B (203.085 s), which is similar to the case without the network energy-aware approach. The voltage across the super-capacitor then increased as energy can be accumulated effectively in the super-capacitor with the hardware EAI that has a low current consumption as discussed in Section 4.4.4.

After that, the network energy-aware programme began. Fig. 6.11 (a) shows that, the WSM first monitored the V_{cs} (3.111 V) at point B and then calculated the current maximum time that the WSM can stay in the search process, $T_{\mathrm{max-low}}$ (8958 ms) through equations 6.1 to 6.3. After 8958 ms has elapsed, the WSM checked whether it has obtained the joining notification or not. Since no notification is received, it repeated the approach, which monitored the V_{cs} (2.545 V) and calculated $T_{\mathrm{max-low}}$ again at 212.04 s. As the calculated $T_{\mathrm{max-low}}$ (168

ms) is higher than 0 ms, the WSM judged that it is able to continue the search process and then set a 168 ms timer. Similarly, after 168 ms, the WSM checked for the joining notification, which again is not received. The approach repeats again at 212.21 s, which is shown as point C (212.21 s). The calculated $T_{\max-\text{low}}$ is -13 ms, which is lower than 0 ms. Therefore, the WSM judged that it has not got the energy to perform the next process even if it is able to complete the search process immediately. After that, the WSM reset the hardware EAI to turn off itself, which spent about 35 ms and finished at point D (212.245 s) with 2.532 V. After that, the capacitor voltage increased just as the case without the network energy-aware approach, which shows that network energy-aware approach works seamlessly with the hardware EAI.

Fig. 6.11(b) compares the measured current between the EH powered WSM without and with the network energy-aware approach from wake up (point A) to the process of the hardware EAI turning off the WSM (point D) in Fig. 6.10(b) and Fig. 6.10(d), respectively. The wake up and initialisation process for both EH powered WSMs are similar, since they use the same related programme. After that, the EH powered WSM with the network energy-aware approach spent about 9.12 s on the search process which is about 3.21 s less than the EH powered WSM without the approach. It should be noted that in this case, spending less time means saving more energy, since all the energy consumed during the search process is wasted because the EH powered WSM was not able to join the network or complete any tasks even if it successfully joined the network.

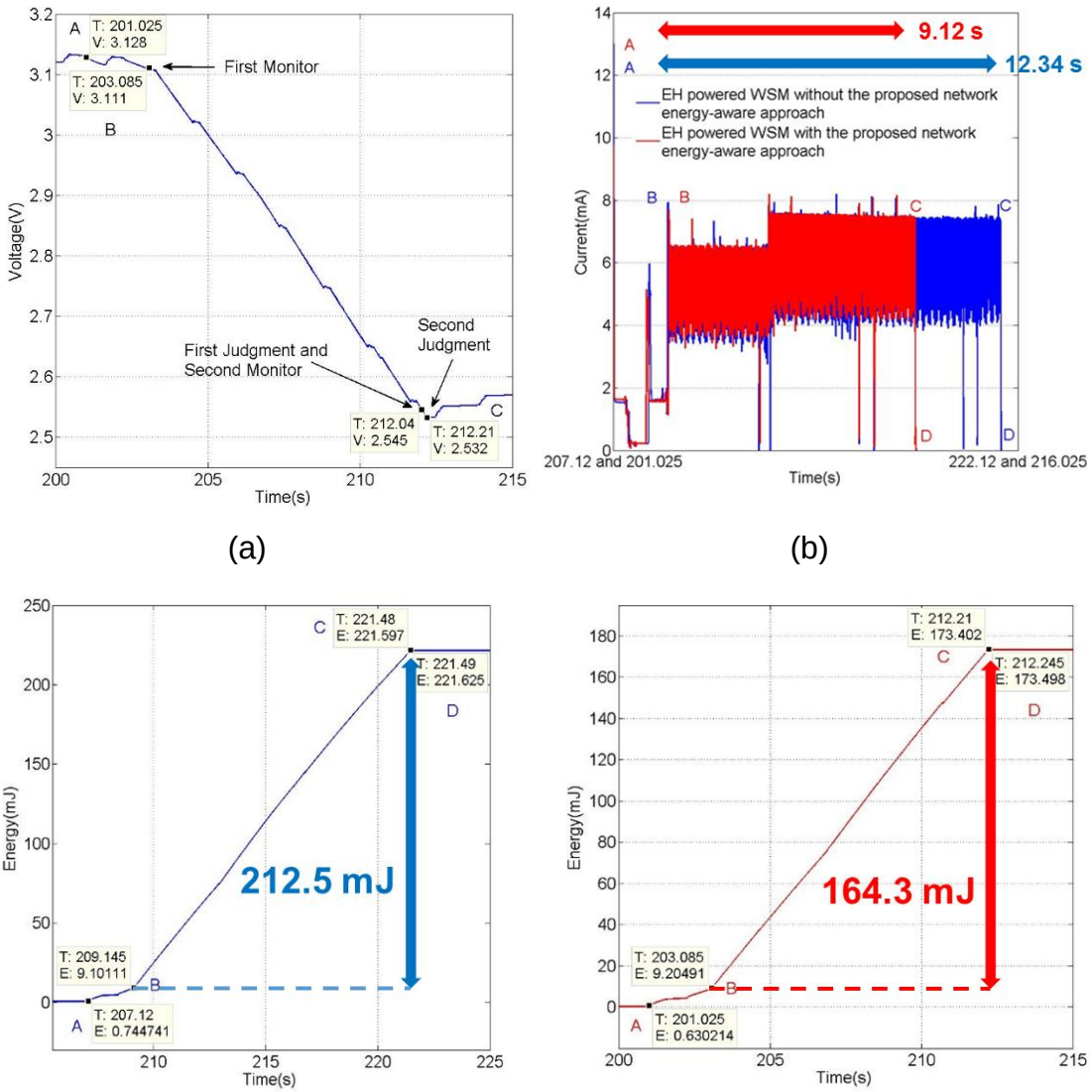

Figure 6.11: The enlarged plots (a) V_{cs} of Figure 6.10(c) and (b) the current comparison between Figure 6.10(b) and Figure 6.10(d) from point A to point D. The calculated results of E_W based on (c) the measured V_{cs} of Figure 6.10(a) and I_w of Figure 6.10(b) and (d) the measured V_{cs} of Figure 6.10(c) and I_w of Figure 6.10(d), respectively.

The EH powered WSM without the network energy-aware approach consumed about 212.53 mJ energy on the search process and resetting the hardware EAI, as shown in Fig. 6.11(c).

On the contrary, the EH powered WSM with the network energy-aware approach consumed a total of about 164.30 mJ on the search process, the network energy-aware programme and resetting the hardware EAI, as shown in Fig. 6.11(d),

which saves about 48.23mJ energy if compared with the EH powered WSM without the network energy-aware approach. This amount of energy saved is quite significant as it could sustain almost the entire high-voltage search process or 219 times of the sensing and transmission, based on the energy analysis in Chapter 5. Since the WSM with the network energy-aware approach resets the hardware EAI earlier at a higher capacitor voltage, the super-capacitor can be recharged to the turn-on threshold voltage of the hardware EAI quicker than the WSM without the network energy-aware approach.

6.4.2 Asynchronous Acceleration Measurements Application

As discussed earlier in Section 6.2, upon a successful network join, the WSM will execute the AAM application if the capacitor voltage is less than 2.6 V after it has completed its basic sampling application. Only the first EH powered WSM with the network energy-aware approach will be analysed here since the AAM is not synchronised, which does not involve other WSMs. The measured voltage V_{cs} and current I_{w} in this case are shown in Fig. 6.12. The voltage profile of V_{cs} as shown in Fig. 6.12(a) is very similar to those in Fig. 6.11(a) and 6.11(c). Therefore, just as before, the measured current I_{w} will be predominantly used for the subsequent analyses. The wake up and initialisation process occurred between point A and point B (210.485 s) as shown in Fig. 6.12(b) is again similar to those in Figs. 6.10(b) and (d) due to the similar related programme used.

After that, the WSM began the network join process with the search process using the proposed network energy-aware approach, which is between point B and point C (219.535 s) in the inset of Fig. 6.12(a) and Fig. 6.12(b). The WSM first

monitored V_{cs} (3.105 V) at point B and then calculated $T_{\mathrm{max-low}}$ to be 8856 ms. After 8856 ms has elapsed, the WSM still has not obtained the joining notification and as a result, it monitored the V_{cs} (2.571 V) again at 219.34 s and calculated $T_{\mathrm{max-low}}$ to be 533 ms, which means the WSM is able to continue the search process. After 533 ms, the WSM has obtained the joining notification and then it stopped the energy-aware program, since the search process has been completed at 219.535 s as shown at point C. After that the WSM spent about 9.47 s on the negotiating process and connecting process, which is the process between point C and point D (229.005 s) in Figs. 6.12(a) and (b).

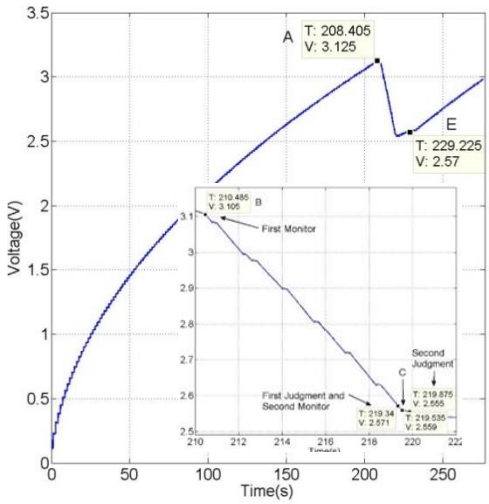

(a)

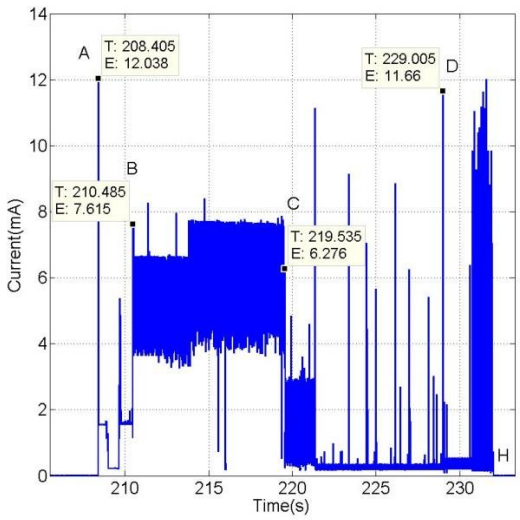

(b)

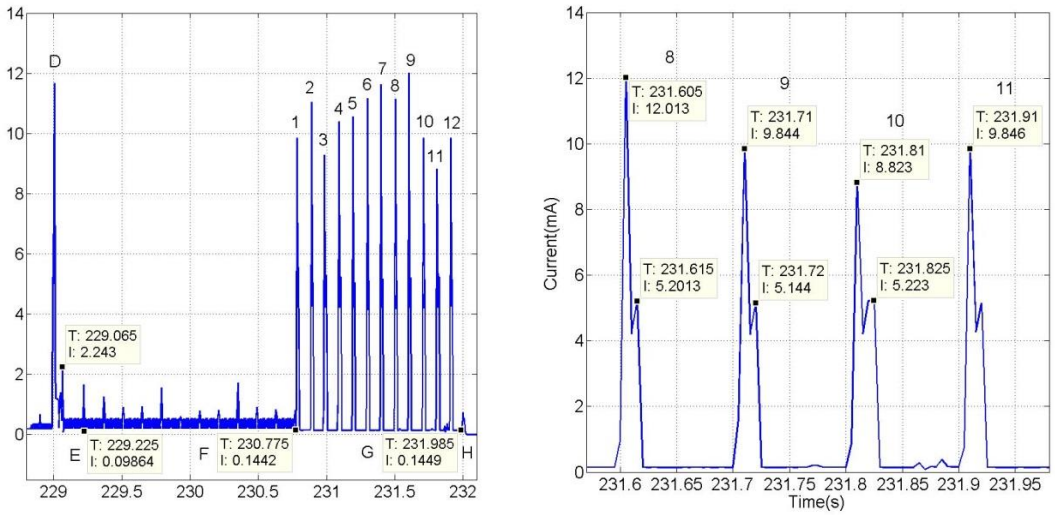

(c) (d)

Figure 6.12: Measured (a) V_{cs} with enlarged view of V_{cs} from 210 s to 225 s as inset and enlarged plots of I_{w} (b) from 205 s to 235 s, (c) from 228 s to 232 s and (d) from 231.6 s to 231.95 s

After the WSM has joined the network successfully, the WSM implemented about 0.22 s of basic sampling application between point D and point E (229.225 s), as shown in Fig. 6.12(c). Then, the WSM judged that it will run the AMM application, since the $V_{\mathrm{cs-sample}}$ as shown at point E is about 2.57 V which is lower than 2.6 V. With the AMM application, the WSM repeatedly take the acceleration measurements for about 1.55 s between point E and point F as shown in Fig. 6.12(c). The current peak of 2.2 mA at 229.065 s is due to the turning on of the accelerometer through the sensing EAI.

After completing the sampling tasks, the WSM sent the data to the network manager through 12 transmission times. Between points G and H, the first transmission has 88 bytes of data from the basic sampling application and each transmission of the following 11 transmissions has 84 bytes of data. This means the WSM has repeated 11 cycles of taking 42 readings (84 bytes) from the 3-axis accelerometer during the AMM application. Fig. 6.12(d) shows the enlarged view of the 8$^{\mathrm{th}}$ to 11$^{\mathrm{th}}$ transmissions as an example to discuss the transmission process.

It can be seen that, the interval between each transmission is approximately 100 ms, which has been set in advance as discussed in Section 6.2.2. After the WSM transmitted the data to the network manager, there is a process with about 5.14 mA of current consumption caused by the WSM waiting for a response from the network manager. If the WSM receives the response, it will finish the current transmission and if not, it will resend the data. Therefore, all the transmissions are successful without the need to resend. After that, the WSM resets the hardware EAI to switch off itself between point G and point H in Fig. 6.12(c) and then it went into non-active phase.

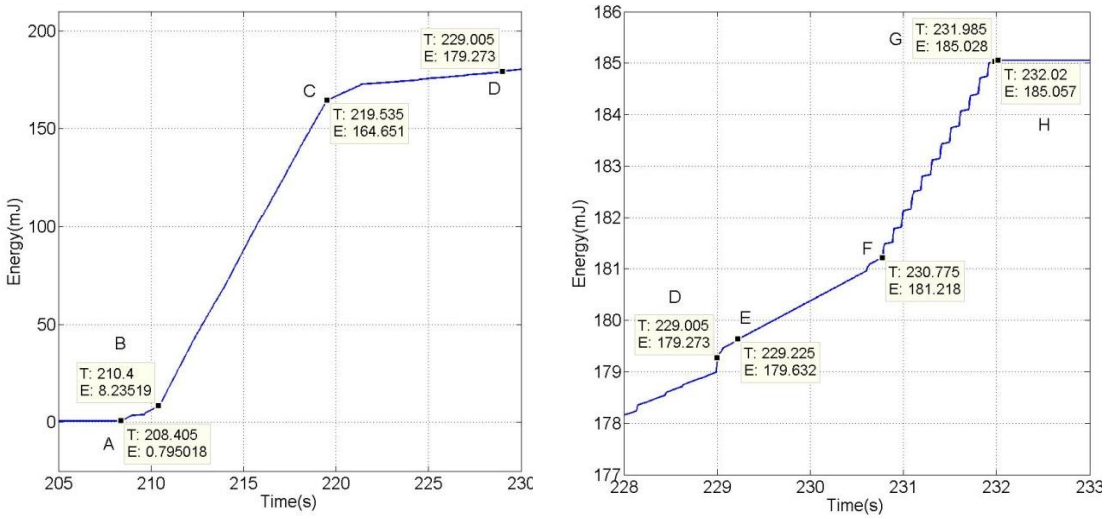

(a) (b)

Figure 6.13: The calculated result of E_W based on the measured V_{cs} of Figure 6.12 (a) and I_w of Figure 6.12 (b) with enlarged view of (a) from 205 s to 230 s and (b) from 228s to 234 s

The average current, average voltage, average power, energy consumption and time of every process separated by any consecutive two points marked by the alphabets of A to H based on the results in Fig. 6.12 and Fig. 6.13 are shown in Table 6.1 It can be seen that, in a total of 23.615 s, the WSM has consumed about 184.26 mJ. The WSM consumed the most energy on the search process during the network joining process which cost about 156.42 mJ in 9050 ms. After the WSM joined the network successfully, it consumed about 1.95 mJ for reading

1012 bytes data in 1770 ms and about 3.81 mJ for transmitting 1012 bytes data in 1210 ms.

Table 6.1: Energy consumption of every process of the first EH powered WSM when it performs AMM application

No.	Process	Average Current (mA)	Average Voltage (V)	Average Power (mW)	Energy (mJ)	Time (ms)
A-B	Wake up and Initialisation	1.25	3.117	3.58	7.44	2080
B-C	Searching Process	6.08	2.838	17.28	156.42	9050
C-D	Negotiating Process and Connected Process	0.61	2.558	1.54	14.62	9470
D-E	Reading data in Basic Sample Application	0.88	2.572	1.63	0.36	220
E-F	Reading data in AMM Application	0.40	2.575	1.02	1.59	1550
F-G	Transmission	1.22	2.582	3.15	3.81	1210
G-H	Resetting Hardware EAI	0.32	2.582	0.83	0.03	35
Total					184.26	23615

6.4.3 Synchronous Acceleration Measurements Application

As discussed earlier in Section 6.2, upon a successful network join, the WSM will execute the SAM application if the capacitor voltage is more than 2.6 V after it has completed its basic sampling application. Both EH powered WSMs and the performance of the EH powered WSN will be analysed here.

6.4.3.1 Operation of the first Energy Harvesting Powered Wireless Sensor Mote

The measured voltage V_{cs} and current I_{w} in this case are shown in Fig. 6.14. Fig. 6.14(a) shows that the voltage profile looks similar to the previous case but with the voltage stops dropping at a higher level and increases at a slower rate afterwards. The WSM began with the wake up and initialisation process as indicated between point A and point B (212.54 s), as shown in Fig. 6.14(b). Then, the WSM with the network energy-aware approach start to join the network, which is similar to the previous case. After the WSM has joined the network successfully, the WSM implemented about 0.22 s of basic sampling application between point D (228.375 s), and point F (228.595 s), as shown in Fig. 6.14(c). Then, the WSM judged that it will run the SAM application, since the $V_{\mathrm{cs-sample}}$ as shown at point E is about 2.74 V, which is higher than 2.6 V.

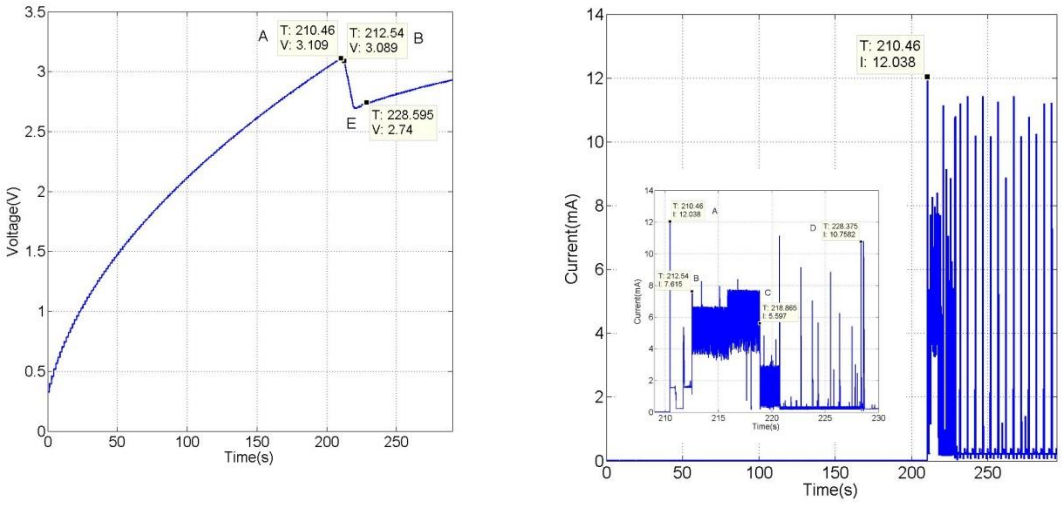

(a) (b)

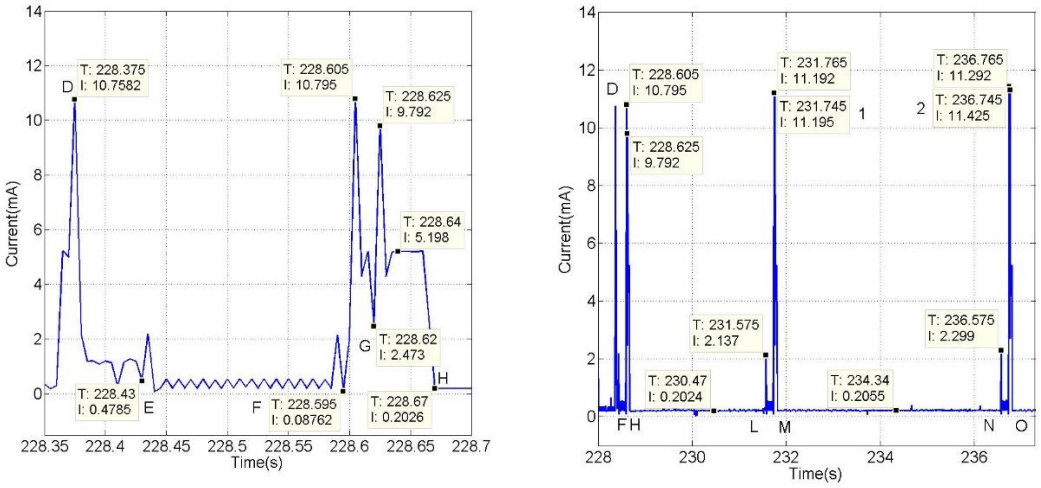

(c) (d)

Figure 6. 14: Measured (a) V_{cs} and measured (b) I_{w} with enlarged view of I_{w} from 210 s to 235 s as inset and enlarged plots of I_{w} (c) from 228 s to 238 s and (d) from 228.35 s to 228.7 s

Fig. 6.14(c) shows three sampling and transmission operations of the WSM running with the SAM application as an example. Fig. 6.14(c) shows the enlarged view of the first operation between point D and H. Between point D and point F, the WSM implemented the basic sampling application. After that, between point F and point G (228.62 s), the WSM transmitted the data from the basic sampling application to the network manager and then waited for a response from the network manager since it was running the SAM application. It should be noted that, the transmission is not based on the network time since it happened before the WSM obtained the network time.

After that, the WSM transmitted a requirement to ask the current network time from the network manager, which is the WSM achieved the 1st network time retrieve and caused a current peak of about 9.8 mA at 228.625 s. Then, it received the ASN and UTC time of the current network from the network manager with about 5.2 mA current consumption.

After that, the WSM went to sleep with the timing function for a duration equals the calculated T_{waitms} between point H and point L (231.57 s) in Fig. 6.14(c). The

WSM then wakes up and turns on the accelerometer at 231.575 s to repeatedly take the 3 readings from the three outputs of 3-axis accelerometer for 14 times every 10 ms. It should be noted that, this measurement is the 1st measurement that is synchronised over the network. Therefore, the following transmission at 231.745 s is marked as 1 in Fig. 6.14(d). The second synchronised transmissions happened at 236.745 s while the network time retrievals happened at 236.765 s. The time interval between successive synchronised operations is 5 s, as defined by T_{reportms} (5000 ms).

The current profiles of the synchronised operations between points L and M as well as points N and O are the same as the current profile shown in Fig. 6.14(b) from point E to point H. The capacitor voltage can be charged up in Fig. 6.14(a) after 228.595 s. This means the average power consumption of the SAM is less than the power from the vibration energy harvester. Thus, the WSM continued to run the SAM application as shown in Fig. 6.15(a) and remained well synchronised as can be seen in Fig. 6.15(b) with the even time gap between successive transmissions.

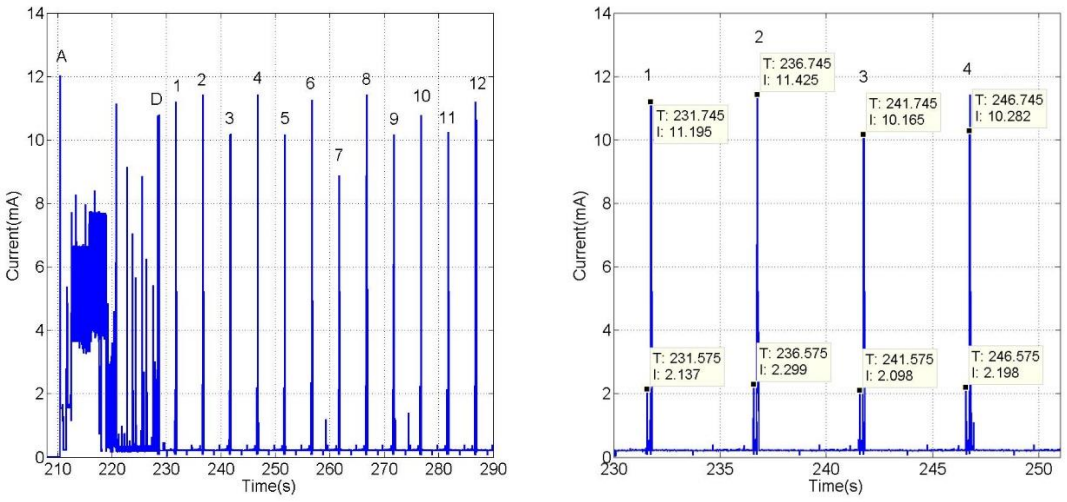

(a) (b)

Figure 6.15: The measured I_{w} (a) during the active phase of the first EH powered WSM from 210 s to 290 s and (b) with enlarged view from 230 s to 250s.

The average current, average voltage, average power, energy consumption and time of every process separated by any consecutive two points marked by the alphabets of A to O based on the results in Fig. 6.14 are shown in Table 6.2. The calculated energy consumption is based on the Fig. 6.14(a) and Fig. 6.14(b). Again, the WSM consumes the most energy on the search process during the network joining process, which cost about 109.50 mJ in 6325 ms. After the WSM has successfully joined the network, it consumed about 0.38 mJ for reading 88 bytes of data during the basic sampling application and about 0.34 mJ for transmitting the 88 bytes data in 25 ms. The network time retrieval process costs about 13.24 mW of power but over a short time of 50 ms, which leads to a low average energy consumption of 0.66 mJ. The energy consumption of the sleeping process with the timing function is about 1.44 mJ, which is very similar to the energy consumption for one cycle of SAM application that reads 84 bytes of data from the accelerometer, turns on and off the accelerometer, transmits the 84 bytes of data, retrieves the network time, monitors the voltage and makes the judgement in 240 ms at 1.47 mJ. Therefore, the overall energy consumption of the WSM that is running the SAM application is higher, mainly due to the higher energy consumption during sleeping with the timing function. This explains the slower capacitor voltage increment rate as observed in Fig. 6.14(a).

Table 6.2: Energy consumption of every process of the first EH powered WSM when it performs SAM application

No.	Process	Average Current (mA)	Average Voltage (V)	Average Power (mW)	Energy (mJ)	Time (ms)
A-B	Wake up and Initialisation	1.23	3.100	3.78	7.87	2080
B-C	Searching Process	5.97	2.904	17.31	109.50	6325
C-D	Negotiating Process and Connected Process	0.62	2.711	1.67	15.90	9510
D-F	Reading data in Basic Sample Application	0.85	2.732	1.71	0.38	220
F-G	Transmission the data in Basic Sample Application	4.95	2.735	13.56	0.34	25
G-H	1st Network time Retrieve	4.83	2.742	13.24	0.66	50
H-L	Sleeping with the timing function	0.21	2.742	0.50	1.44	2900
L-M	1st SAM application	1.87	2.751	6.12	1.47	240
M-N	Sleeping with the timing function	0.21	2.755	0.59	2.81	4760
N-O	2nd SAM application	1.88	2.762	5.03	1.21	240

6.4.3.2 Operation of the second Energy Harvesting Powered Wireless Sensor Mote

The measured voltage V_{cs} and current I_{w} of the second EH powered WSM that was powered at the same time as the first EH powered WSM are shown in Fig. 6.16. Since the airflow energy harvester produces more power than the vibration energy harvester, the super-capacitor was charged up from 0 V to 3.134 V in 122.835 s, which was marked as point A in Fig. 6.16(a). Once the WSM has been powered up, the processes are similar to the first EH powered WSM. The wake up and initialisation process occurred between point A and point B (124.86s).

Then, the WSM with the network energy-aware approach start to join the network, which is similar to the case of the first EH powered WSM. After the WSM has joined the network successfully, the WSM implemented the basic sampling application between point D and point E, as shown in Fig. 6.16(b). Then, the WSM judged that it will run the SAM application, since the $V_{\mathrm{cs-sample}}$ as shown at point E is about 2.972 V, which is higher than 2.6 V. It should be noted that, V_{CS} eventually increased to 3.3 V, which is the maximum output voltage of the PMM because the power from the airflow energy harvester is enough to recharge the super capacitor and supply the power for the operation of the WSM simultaneously.

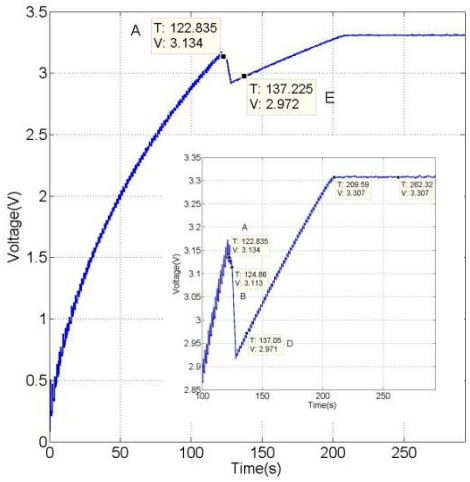

(a)

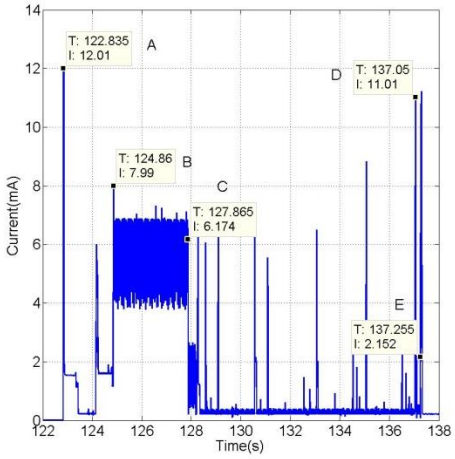

(b)

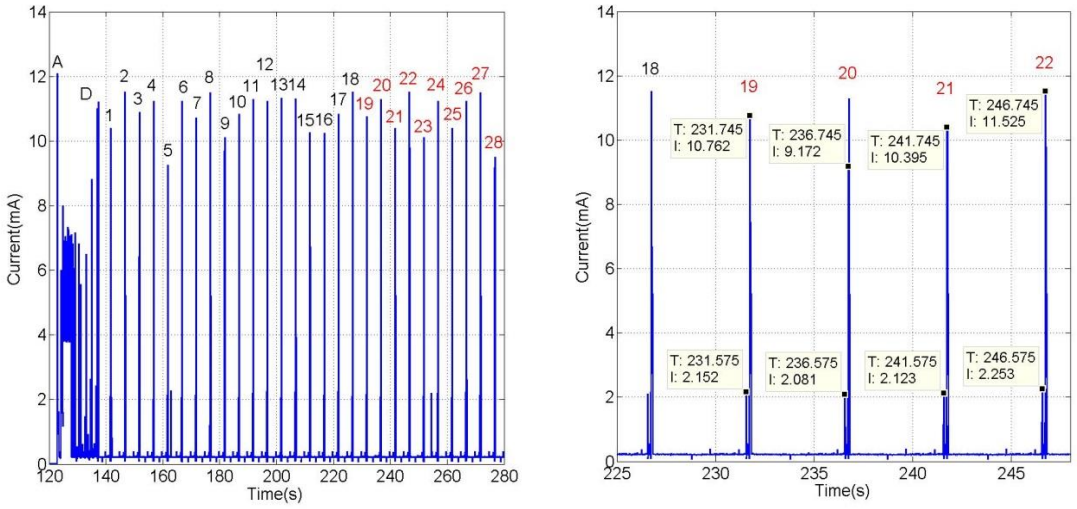

(c) (d)

Figure 6.16: The measured (a) V_{cs} with its enlarged view from 100 s to 299 s in the inset and I_{w} with enlarged view from (b) 122 s to 138 s, (c) 120 s to 280 s and (d) 225 s to 250 s.

The WSM completed the 1st SAM at 141.745 s, which is marked as 1 in Fig. 6.16(c). A total of 28 synchronised transmissions were recorded in this measurement. The WSM synchronised with the first EH powered WSM to measure the acceleration and transmit at the same time in the WSN at its 19th SAM. Fig. 6.16 (d) shows that the 19th to 22th synchronised measurement of the second EH powered WSM happened at 231.575 s, 236.575 s, 241.575 s, and 246.575 s, respectively and the synchronised transmission happened at 231.745 s, 236.745 s, 241.745 s, and 246.745 s respectively. This corresponds to the 1st to the 4th synchronised operation of the first EH powered WSM, which happened at the same time as shown in Fig. 6.15(b). Therefore, it can be seen that, the EH powered WSMs with the proposed energy-aware approaches including the network energy-aware approach, sensing, software and hardware energy-aware approaches in the EH powered WSN are able to achieve a synchronised measurement and transmission. It should be noted that, although three WSMs implement the synchronised accelerometer measurements and transmissions across the network, the network manager may receive the data from them at

slightly different times because they have different communication conditions in the EH powered WSN such as different transmission distances.

6.4.3.3 Operation of the Energy Harvesting Powered Wireless Sensor Network

Fig. 6.17(a) shows the network topology of the proposed EH powered WSN on the stargazer window in three sequences of the joining status of the three WSMs. On the stargazer window, the network manager and the WSMs are identified by the short MAC address of their internal wireless chips, which is the last 2 bytes of their 8-byte long MAC address. The MAC address is unique to each mote and is assigned to the mote at the factory during production. For example, the long MAC address of the first EH powered WSM is 00-17-0D-00-00-60-03-AB and as a result of that it is shown as 03-AB on the stargazer window. With the same rule applies, the network manager, the second EH powered WSM and the battery-powered WSM are identified as 58-33, 06-28 and 23-31, respectively.

The battery-powered WSM (23-31) joined the network first as marked by ‘1’ in Fig. 6.17(a), since the battery is able to power the WSM immediately to wake up and join the network with a steady stream of power supply. Then, it was the second EH powered WSM (06-28) that joined the network on its first network joining attempt, as shown in Fig. 6.16. After that the first EH powered WSM (03-AB) joined the network last on its first network joining attempt, as shown in Fig. 6.14. The order in which the three WSMs join the network depends on the capacitor charging time and the number of attempts to join the network.

Fig. 6.17(b) shows the display window of stargazer that recorded the transmission details from the three WSMs to the network manager. The network manager

received 84 bytes of data from the 3-axis accelerometer in each of the three WSMs in every 5 s in the synchronised measurement.

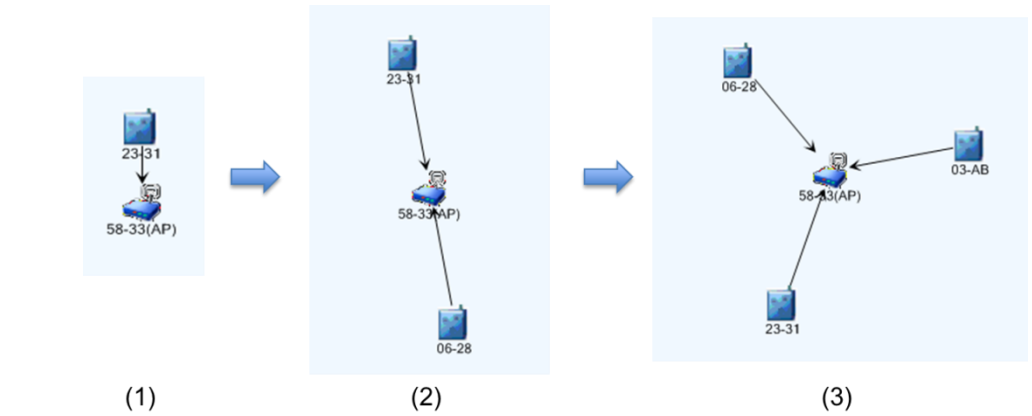

(a)

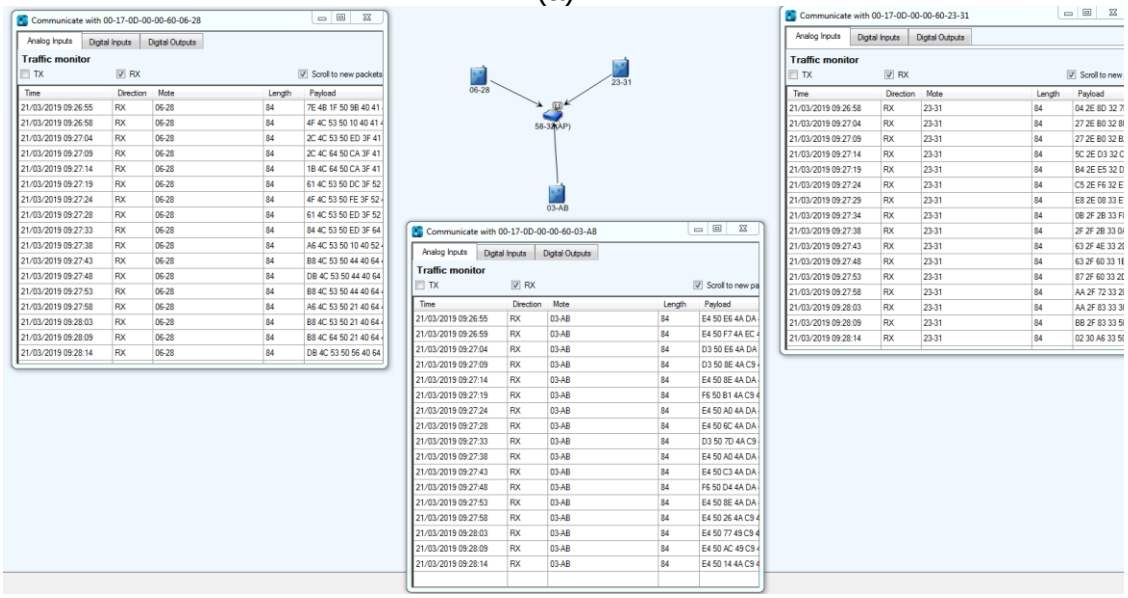

(b)

Figure 6.17: (a) The network topology of the proposed and developed EH powered WSN on stargazer window in three network joining sequences of the three WSMs and (b) The traffic monitor window of stargazer that shows the data from the three WSMs received by the network manager.

6.5 Summary

This chapter has shown how the network energy-aware approach with the network energy-aware approach saves energy during the network joining process of the WSMs that is full of uncertainty, especially in terms of the time and therefore the energy required to complete the network joining process. An EH powered WSN formed by WSMs with the proposed network energy-aware approach was built and tested. The EH powered WSN is a star network and includes one EH powered WSM powered by the vibration energy harvester, one EH powered WSM powered by the air flow energy harvester and one WSM powered by battery. The experimental results show that the network energy-aware approach incorporates all the energy-aware approaches seamlessly. The network energy-aware approach enables (1) the harvested energy to be accumulated in the super-capacitor to deal with the start-up issue of EH powered WSM and (2) allows the EH powered WSM to have a low sleep current with the hardware EAI. (3) Then, once the EH powered WSM with the network energy-aware approach is powered up and began the network joining process, a significant amount of energy can be saved when the attempt to join the network failed. Once the EH powered WSM has joined the network successfully, the different programme applications that incorporate the software EAI, sensing EAI and hardware EAI allow the EH powered WSM to achieve (4) asynchronous operation or (5) synchronised operation based on the energy level left after the WSM has joined the network.

Chapter 7 Conclusions

7.1 Achieved Objectives

The EH powered WSS are gaining increasingly popularity, since they enable the system to be self-powering, long lasting, almost maintenance free, and environmentally friendly. However, the mismatch between the energy generated by the harvesters and the energy demanded by the WSS to perform the required tasks is always a bottleneck as the ambient environmental energy is limited and the WSS is power hunger.

Therefore, the main focus of the thesis for the EH powered WSS (WSMs and WSNs) is to propose, design, implement and test the energy-aware approaches, including hardware EAI, software EAI, sensing EAI, and the network energy-aware approaches to deal with the energy mismatch to carry out required tasks. The main research ideas are to manage the energy flow and reduce the power consumption of the WSM in the EH powered WSS. For these, the thesis has achieved the following objectives.

- **To develop an understanding of WSM power consumption for the development of EH powered WSMs;**

This thesis has reviewed the energy harvesting techniques that can be used to extract energy from different available energy sources, with focus on the power output that can be harvested. It has also reviewed wireless communication technologies, protocols and the off-the-shelf commercial chips, and compared their performance for the EH powered WSS requirements, especially in the

energy consumption of transmission and receive processes. Based on the reviews of the energy harvesting and wireless sensor technologies, a research challenge in the mismatch between energy harvested by harvesting methods and energy demanded by wireless sensor technology is identified. To address the energy mismatch, the thesis has reviewed the energy-saving mechanisms in the WSS, with particular focus on the energy-aware approach.

This thesis has studied a battery powered WSM system and analysed the energy consumption of the WSM. The WSM was implemented with JN5148 microcontroller and two sensors: accelerometer and humidity sensor. The main software was programmed with initialisation function, reading humidity sensor function, reading accelerometer loop function, transmission function and sleeping function. The communication was selected as the ZigBee protocol based on the 2.4 GHz IEEE 802.15.4 standard and was designed to have a fixed channel in non-beacon enabled mode to transmit data. The testing system was designed as one implemented WSM and one base station placed at a distance of 4 m to receive the data from the WSM. The testing set-up was designed to use one DC power source to represent the batteries to power the implemented WSM and use one source meter with a LabVIEW program running on the computer to measure the energy flow through the WSM. The experimental results are then presented and analysed. The most important result of the analysis is that the average energy consumption of the WSM in processing 1 byte is 46.94 µJ /byte, including wake up, sampling and transmission during active time. This experimental analyses has supplied an understanding of the power consumption during sleep and active times, and has formed a basis of the study of EH powered WSS.

• To identify key issues of EH directly powered WSMs and develop smart energy-aware approaches to solve the identified issues, enabled successful EH powered WSMs in one-way communication operations;

This thesis has proposed, designed, implemented and tested the energy-aware approaches, including hardware EAI, software EAI, sensing EAI for energy-harvesting powered WSS. A typically energy harvesting powered WSM was designed to be used to analyse the key issues of existing EH powered WSM through the experimental measurements. The start-up issue and the energy mismatch issue in the system were then identified. Too address these issues, energy-aware approach concepts are proposed and the implementation are developed. The hardware EAI was designed as an interface between the energy storage and the WSMs to monitor the voltage across the energy storage to judge if there is enough energy in the energy storage for the WSMs to perform the pre-programmed tasks and determine when to wake the WSMs up and implemented by an ultra-low power voltage supervisor circuit and N-MOSFET switch circuit. The software EAI was designed as a virtual interface between the MCU and the transceiver to judge whether the energy stored in the energy storage device is enough for the WSM to carry out the next operation and ensure all the measured data is transmitted before the energy becomes too low for the operation of the WSM and implemented by the software energy-aware programme. The Sensing EAI was designed as an interface between the MCU and the sensing unit to turn off the sensors when they are not required during the active time to reduce the power consumption of the sensors in the WSM and implemented by P-MOSFET switch circuit. A piezoelectric vibration powered EH-WSM system with proposed energy-aware approaches was developed to evaluate the effectiveness of the

energy-aware approaches and the enhancement on the performance of the EH-WSM. It has been shown that the energy-aware approaches have enabled the harvested energy to be accumulated in the energy storage device to (1) deal with the mismatch for the operation of the WSM, (2) solve the start-up issue, (3) enable a commercial available WSM with a reduced sleep current from 28.3 µA to 0.95 µA, and (4) enable the WSM operations for a long active time of about 1.15 s in every 7.79 s to sample and transmit a large number of data (388 bytes), rather than a few ten milliseconds and a few bytes.

•To analyse the energy of network behaviour in EH powered WSN and identify issues in the network joining process;

This thesis has studied the energy analyses of the implemented WSM during the network joining process in the EH powered WSN. A star topology EH powered WSN, which comprises one network manager (Linear Technology DC9011A) and three developed WSMs. The WSM was implemented with a strain energy harvester, a PMM, a super-capacitor, hardware EAI and a Linear Technology DC9003 A-B Evaluation/Development Mote. The testing set-up was designed in three steps. The first step was designed to analyse the energy characterisation of the processes when the WSM is joining the network. The second step and third step were designed to analyse the effects of joining duty cycles and the storage sizing on the network joining process, respectively. The experimental results were then presented and analysed, and the key finding are listed below.(1) The network joining process is very power hungry especially for the low-voltage search and high-voltage search processes, with average power of about 17.09 mW and 18.21 mW, respectively. (2) Reducing the network join duty cycle does

not necessarily save the energy required for network joining. (3) Appropriate sizing of the capacitor size is crucial to ensure that the mote is able to join the network from the first attempt. Finally, the main problem was identified that the energy consumption of the WSM joining the network is undetermined because of its randomness. The results have provided an important knowledge and understanding of networking joining processes in energy behaviour to design the energy-aware approaches for EH enabled WSNs through reducing the energy consumption of the implemented WSM.

•To develop network energy-aware approaches to reduce the energy consumption of the WSM joining the network for EH powered WSNs enabled successful EH powered WSMs in network two-way communication operations;

This thesis has proposed, designed, implemented and tested the network energy-aware approaches for EH powered WSN. The network energy-aware approach concept was proposed to save energy during the network joining process of the WSMs that is full of uncertainty, especially in terms of the time. Therefore, the energy-aware approach required to complete the network joining process was implemented by a network energy-aware approach which is able to cover all the possible scenarios of the search process with minimal number of voltage monitoring times while tracing and judging whether the remaining energy of the WSM is sufficient to support the next processes instead of doing a constant monitoring with milliseconds interval. The EH powered WSN formed by WSMs with the proposed network energy-aware approaches was built and tested. The EH-WSN is a star network and includes one EH powered WSM powered by the

vibration energy harvester, one EH powered WSM powered. The experimental results have showed that the network energy-aware approach incorporates all the energy-aware approaches seamlessly. The network energy-aware approach enables the harvested energy to be accumulated in the super-capacitor to deal with the start-up issue of EH powered WSM and allowed the EH powered WSM to have a low sleep current with the hardware EAI. The developed energy-aware approach has been used for EH powered WSN in the lab and can be used for their successful operations. The tested results are given below. Once the EH powered WSM with the network energy-aware approach is powered up and began the network joining process, energy, as an example of 48.23 mJ for a tested case, can be saved when the attempt to join the network failed. Once the EH powered WSM has joined the network successfully, the different programme applications that incorporate the software EAI, sensing EAI and hardware EAI allow the EH-WSM to achieve asynchronous operation and synchronised operation based on the energy level left after the WSM has joined the network.

•To enable EH powered WSNs for structural and environmental monitoring applications.

This thesis has developed the energy-aware approaches which have provided an enabled capability for EH successful powering WSS technologies in the condition of energy mismatch and it can be said that there is potential of the research to be used for wide industrial EH powered WSM and WSN applications. For example, the piezoelectric vibration powered EH-WSM system with proposed energy-aware approaches have enabled the harvested energy to be accumulated in the energy storage device and enabled the WSM operations for a long active

time of about 1.15 s in every 7.79 s to sample and transmit a large number of data (388 bytes), rather than a few ten milliseconds and a few bytes.

7.2 Limitation

- ZigBee over IEEE 802.15.4 is chosen as the wireless communication standards for the study of EH powered WSS in the thesis, since it has the low energy consumption in the short-distance transmission application. The thesis does not has focus on the long-distance wireless communication technologies. Therefore the thesis has a limitation on the transmission distance;

- The thesis focus on enabling the EH powered WSM sample and send data as much as possible during the active time. However, in some other cases, the WSMs are not required to sample and send data all the time during the active time. It only needs to transmit alarms and a small amount of data when the sampled data exceeds the warning value, which requires the WSMs to have the ability to analyse and process the local sampled data. Therefore, the thesis has limitations in meeting the specific applications with event-based alarm features;

- Although the complexity of the network does not affect the function of network energy-aware approaches, large-scale WSM will cause a single WSM to join the network for a long time and increase the failure rate of joining the network. Moreover, although the star network is suitable for the EH powered WSN applications, it is not suitable for the networks with

large-scale WSMs, which will lead to severe channel congestion. Further consideration is needed when developing the network energy-aware approaches for the networks with large-scale WSMs;

- For the real applications, it is recommended that the EH powered WSS with the energy-aware approaches should be developed on a completed end-to-end platform to analyse the data from network servers based on specific application requirements, rather than only show the sampled data in the network manager or base station in the thesis.

7.3 Future Work

7.3.1 Long-distance Transmission Application

In the future, it is recommended to use the developed energy-aware approaches to study the EH powered WSS for the long-distance transmission applications. For example, it is recommended to use the LoRa wireless communication standard to replace the ZigBee over IEEE 802.15.4 wireless communication standard for industrial internet things, since the developed energy-aware approaches are the energy management methods that suit for all EH powered WSS.

7.3.2 Event-driven Methods

In the future, the WSMs in the EH powered WSS are able to add some event-based functions to meet the specific application requirements through software implementation. For example, after the WSM samples the data from the

temperature sensor, it calculates the average or maximum value of the temperature and only transmits the processed data when the temperature is higher than the pre-set fixed value.

7.3.3 Implementation of Real End-to-End Applications

In the future, it is useful to implement the real end-to-end EH powered WSN applications from the WSM to the end users. For example, using EH powered WSMs with the energy-aware approaches collects the environmental data and then transmit the data to the network manager or base station. The network manager or base station then sends the information to network server such as the cloud where the data are analysed by an application server. After that, the application server sends the results or alerts to end user via a mobile phone or a computer.

7.4 Conclusions

The main contributions of this thesis to the research community are the smart mote and network energy-aware approaches **–** which enables a >30 times reduction in sleep power consumption of WSNs for successful EH powering WSNs without the start-up issue in the condition of mismatch between the energy generated by harvesters and demanded by WSNs in both mote and network systems. For EH powered WSM systems, the energy-aware approaches have (1) enabled the harvested energy to be accumulated in the energy storage device to deal with the mismatch for the operation of the WSM; (2) solved the start-up issue and enabled a commercial available WSM with a reduced sleep current from 28.3 µA to 0.95 µA; (3) enabled the WSM operations for a long active time

of about 1.15 s in every 7.79 s to sample and transmit a large number of data (e.g., 388 bytes), rather than a few ten milliseconds and a few bytes.

Moreover, for EH powered WSN systems, on top of energy-aware approached for EH powered WSM, the network energy-aware approaches have additional capabilities for network joining process. Once the EH powered WSM with the network energy-aware algorithm is powered up and began the network joining process, energy, as an example of 48.23 mJ for a tested case, can be saved when the attempt to join the network failed. Once the EH powered WSM has joined the network successfully, the different programme applications that incorporate the software EAI, sensing EAI, and hardware EAI allow the EH powered WSM to achieve asynchronous operation or synchronised operation based on the energy level left after the WSM has joined the network.

Through designs, implementations, and analyses, it has been shown that the developed energy-aware approaches have provided an enabled capability for EH successfully powering WSS technologies in the condition of energy mismatch, and it has the potential to be used for wide industrial applications.

REFERENCES

[1] H. H. Khalili, P. R. Green, D. George, G. Watson, and W. Schiffers, “Wireless sensor networks for monitoring gas turbine engines during development,” *Proc. - IEEE Symp. Comput. Commun.*, pp. 1325–1331, 2017.

[2] Kumar, S. A., & Ilango, P, “The impact of wireless sensor network in the field of precision agriculture: A review,” *Wireless Personal Communications.*, vol. 98, no. 1, pp. 685–698, 2018.

[3] Lan, D., Pang, Z., Fischione, C., Liu, Y., Taherkordi, A., & Eliassen, F, “Latency analysis of wireless networks for proximity services in smart home and building automation: The case of thread,” *IEEE Access*, *7.*, pp. 4856–4867, 2018.

[4] Saleh, N., Kassem, A., & Haidar, A. M, “Energy-efficient architecture for wireless sensor networks in healthcare applications,” *IEEE Access.*, vol. 6, pp. 6478–6486, 2018.

[5] C. Chen, J. Yan, N. Lu, Y. Wang, X. Yang, and X. Guan, “Ubiquitous Monitoring for Industrial Cyber-Physical Systems over Relay-Assisted Wireless Sensor Networks,” *IEEE Trans. Emerg. Top. Comput.*, vol. 3, no. 3, pp. 352–362, 2015.

[6] B. F. Spencer *et al.*, “Recent advances in wireless smart sensors for multi-scale monitoring and control of civil infrastructure,” *J. Civ. Struct. Heal. Monit.*, vol. 6, no. 1, pp. 17–41, 2016.

[7] M. Y. Aalsalem, W. Z. Khan, W. Gharibi, M. K. Khan, and Q. Arshad, “Wireless Sensor Networks in oil and gas industry: Recent advances, taxonomy, requirements, and open challenges,” *J. Netw. Comput. Appl.*,

vol. 113, no. October 2017, pp. 87–97, 2018.

[8] V. J. Hodge, S. O'Keefe, M. Weeks, and A. Moulds, "Wireless sensor networks for condition monitoring in the railway industry: A survey," *IEEE Trans. Intell. Transp. Syst.*, vol. 16, no. 3, pp. 1088–1106, 2015.

[9] S. Sudevalayam and P. Kulkarni, "Energy harvesting sensor nodes: Survey and implications," *IEEE Commun. Surv. Tutorials*, vol. 13, no. 3, pp. 443–461, 2011.

[10] Karray, F., Jmal, M. W., Garcia-Ortiz, A., Abid, M., & Obeid, A. M. " A comprehensive survey on wireless sensor node hardware platforms." *Computer Networks.,* no. 144, pp. 89–110, 2018.

[11] G. Anastasi, M. Conti, M. Di Francesco, and A. Passarella, "Energy conservation in wireless sensor networks: A survey," *Ad Hoc Networks*, vol. 7, no. 3, pp. 537–568, 2009.

[12] M. T. Penella, J. Albesa, and M. Gasulla, "Powering wireless sensor nodes: Primary batteries versus energy harvesting," *2009 IEEE Intrumentation Meas. Technol. Conf. I2MTC 2009*, no. May, pp. 1625–1630, 2009.

[13] S. Akbari, "Energy Harvesting for Wireless Sensor Networks Review," *Proc. 2014 Fed. Conf. Comput. Sci. Inf. Syst.*, vol. 2, pp. 987–992, 2014.

[14] F. K. Shaikh and S. Zeadally, "Energy harvesting in wireless sensor networks: A comprehensive review," *Renew. Sustain. Energy Rev.*, vol. 55, pp. 1041–1054, 2016.

[15] A. S. M. Zahid Kausar, A. W. Reza, M. U. Saleh, and H. Ramiah, "Energizing wireless sensor networks by energy harvesting systems: Scopes, challenges and approaches," *Renew. Sustain. Energy Rev.*, vol. 38, pp. 973–989, 2014.

[16] R. M. Ferdous, A. W. Reza, and M. F. Siddiqui, "Renewable energy

harvesting for wireless sensors using passive RFID tag technology: A review," *Renew. Sustain. Energy Rev.*, vol. 58, pp. 1114–1128, 2016.

[17] X. Tang, X. Wang, R. Cattley, F. Gu, and A. D. Ball, "Energy Harvesting Technologies for Achieving Self-Powered Wireless Sensor Networks in Machine Condition Monitoring: A Review," *Sensors (Basel).*, vol. 18, no. 12, 2018.

[18] S. Sudevalayam and P. Kulkarni, "Energy harvesting sensor nodes: Survey and implications," *IEEE Commun. Surv. Tutorials*, vol. 13, no. 3, pp. 443–461, 2011.

[19] D. Guyomar and M. Lallart, "Recent progress in piezoelectric conversion and energy harvesting using nonlinear electronic interfaces and issues in small scale implementation," *Micromachines*, vol. 2, no. 2, pp. 274–294, 2011.

[20] T. C. Huang *et al.*, "120% Harvesting energy improvement by maximum power extracting control for high sustainability magnetic power monitoring and harvesting system," *IEEE Trans. Power Electron.*, vol. 30, no. 4, pp. 2262–2274, 2015.

[21] N. Kong and D. S. Ha, "Low-power design of a self-powered piezoelectric energy harvesting system with maximum power point tracking," *IEEE Trans. Power Electron.*, vol. 27, no. 5, pp. 2298–2308, 2012.

[22] Wang, W., Cionca, V., Wang, N., Hayes, M., O'Flynn, B., & O'Mathuna, C, "Thermoelectric energy harvesting for building energy management wireless sensor networks," *International journal of distributed sensor networks.*, 9(6), p. 232438, 2013.

[23] Y. K. Tan and S. K. Panda, "Optimized wind energy harvesting system using resistance emulator and active rectifier for wireless sensor nodes,"

IEEE Trans. Power Electron., vol. 26, no. 1, pp. 38–50, 2011.

[24] N. Kong and D. S. Ha, “Low-power design of a self-powered piezoelectric energy harvesting system with maximum power point tracking,” *IEEE Trans. Power Electron.*, vol. 27, no. 5, pp. 2298–2308, 2012.

[25] F. Entezami, M. Zhu, and C. Politis, “How Much Energy Needs for Running Energy Harvesting Powered Wireless Sensor Node?,” *Energy Harvest. Syst.*, vol. 3, no. 3, pp. 197–203, 2016.

[26] N. Fourty, A. Van Den Bossche, and T. Val, “An advanced study of energy consumption in an IEEE 802.15.4 based network: Everything but the truth on 802.15.4 node lifetime,” *Comput. Commun.*, vol. 35, no. 14, pp. 1759–1767, 2012.

[27] T. Rault, A. Bouabdallah, and Y. Challal, “Energy efficiency in wireless sensor networks: A top-down survey,” *Comput. Networks*, vol. 67, pp. 104–122, 2014.

[28] V. A. Marsic, “Wireless Sensor Communication System with Low Power Consumption for Energy Harvesting Technology,” *Sch. Appl. Sci.*, vol. Msc by Res, no. 2, p. 142, 2012.

[29] X. Lu, P. Wang, D. Niyato, D. I. Kim, and Z. Han, “Wireless networks with rf energy harvesting: A contemporary survey,” *IEEE Commun. Surv. Tutorials*, vol. 17, no. 2, pp. 757–789, 2015.

[30] M. Piñuela, P. D. Mitcheson, and S. Lucyszyn, “Ambient RF energy harvesting in urban and semi-urban environments,” *IEEE Trans. Microw. Theory Tech.*, vol. 61, no. 7, pp. 2715–2726, 2013.

[31] L. L. Kazmerski, “Solar photovoltaics R&D at the tipping point: A 2005 technology overview,” *J. Electron Spectros. Relat. Phenomena*, vol. 150, no. 2–3, pp. 105–135, 2006.

[32] T. M. Razykov, C. S. Ferekides, D. Morel, E. Stefanakos, H. S. Ullal, and H. M. Upadhyaya, “Solar photovoltaic electricity: Current status and future prospects,” *Sol. Energy*, vol. 85, no. 8, pp. 1580–1608, 2011.

[33] C. Ó. Mathúna, T. O’Donnell, R. V. Martinez-Catala, J. Rohan, and B. O’Flynn, “Energy scavenging for long-term deployable wireless sensor networks,” *Talanta*, vol. 75, no. 3, pp. 613–623, 2008.

[34] A. Montecucco and A. R. Knox, “Maximum power point tracking converter based on the open-circuit voltage method for thermoelectric generators,” *IEEE Trans. Power Electron.*, vol. 30, no. 2, pp. 828–839, 2015.

[35] A. R. M. Siddique, R. Rabari, S. Mahmud, and B. Van Heyst, “Thermal energy harvesting from the human body using flexible thermoelectric generator (FTEG) fabricated by a dispenser printing technique,” *Energy*, vol. 115, pp. 1081–1091, 2016.

[36] X. Lu and S. H. Yang, “Thermal energy harvesting for WSNs,” *Conf. Proc. - IEEE Int. Conf. Syst. Man Cybern.*, pp. 3045–3052, 2010.

[37] L. A. Weinstein, M. R. Cacan, P. M. So, and P. K. Wright, “Vortex shedding induced energy harvesting from piezoelectric materials in heating, ventilation and air conditioning flows,” *Smart Mater. Struct.*, vol. 21, no. 4, 2012.

[38] D. Zhu, S. P. Beeby, M. J. Tudor, N. M. White, and N. R. Harris, “Novel miniature airflow energy harvester for wireless sensing applications in buildings,” *IEEE Sens. J.*, vol. 13, no. 2, pp. 691–700, 2013.

[39] Z. J. Chew, S. B. Tuddenham, and M. Zhu, “Airflow energy harvesting for high speed vehicles,” *PowerMEMS 2016*, pp. 4–7, 2016.

[40] T. Ruan, Z. J. Chew, and M. Zhu, “Energy-Aware Approaches for Energy Harvesting Powered Wireless Sensor Nodes,” *IEEE Sens. J.*, vol. 17, no.

7, pp. 2165–2173, 2017.

[41] Rome, L. C., Flynn, L., Goldman, E. M., & Yoo, T. D, “Generating electricity while walking with loads,” *Science.*, vol. 309, no. 5741, pp. 1725–1728, 2005.

[42] B. Yang and K. S. Yun, “Piezoelectric shell structures as wearable energy harvesters for effective power generation at low-frequency movement,” *Sensors Actuators, A Phys.*, vol. 188, pp. 427–433, 2012.

[43] Y. Kuang, T. Ruan, Z. J. Chew, and M. Zhu, “Energy harvesting during human walking to power a wireless sensor node,” *Sensors Actuators, A Phys.*, vol. 254, pp. 69–77, 2017.

[44] “ZigBee Alliance, 2014.” [Online]. Available: https://www.zigbee.org/.

[45] ZigBee Alliance, “ZigBee specification document 053474r20,” 2012. [Online]. Available: http://www.zigbee.org/wp-content/uploads/2014/11/docs-05-3474-20-0csg-zigbee-specification.pdf.

[46] P. Baronti, P. Pillai, V. W. C. Chook, S. Chessa, A. Gotta, and Y. F. Hu, “Wireless sensor networks: A survey on the state of the art and the 802.15.4 and ZigBee standards,” *Comput. Commun.*, vol. 30, no. 7, pp. 1655–1695, 2007.

[47] N. Semiconductors, “Data Sheet : JN5148-001-Myy,” 2010. [Online]. Available: https://media.digikey.com/pdf/Data Sheets/Jennic PDFs/JN5148-001-Mxx.pdf.

[48] EMBER, “EM260 ZigBee/802.15.4 Network Processor - 120-1003-000G,” 2006. [Online]. Available: https://datasheet.octopart.com/EM260-RTR-Ember-datasheet-125605.pdf.

[49] Texas Instruments, “CC2430,” 2019. [Online]. Available: https://www.ti.com/lit/ds/symlink/cc2430.pdf.

[50] DIGI International, “XBee™/XBee-PRO™ OEM RF Modules,” 2007. [Online]. Available: http://ftp1.digi.com/support/documentation/manual_xb_oem-rf-modules_802.15.4_v1.xAx.pdf.

[51] “Bluetooth Smart or Version 4.0+ of the Bluetooth specification,” 2019. [Online]. Available: https://www.bluetooth.com/.

[52] M. Siekkinen, M. Hiienkari, J. K. Nurminen, and J. Nieminen, “How low energy is bluetooth low energy? Comparative measurements with ZigBee/802.15.4,” *2012 IEEE Wirel. Commun. Netw. Conf. Work. WCNCW 2012*, pp. 232–237, 2012.

[53] SILICON LABS, “BGM13P Blue Gecko Bluetooth ® Module Data Sheet,” 2019. [Online]. Available: https://www.silabs.com/documents/login/data-sheets/bgm13p-datasheet.

[54] Texas Instruments, “2.4-GHz Bluetooth ® low energy System-on-Chip CC2540F128, CC2540F256,” 2013. [Online]. Available: http://www.ti.com/lit/ds/symlink/cc2540.pdf.

[55] Microchip Technology Inc., “RN4870/71 Bluetooth 4.2 Low Energy Module: Data Sheet,” 2016. [Online]. Available: http://ww1.microchip.com/downloads/en/DeviceDoc/50002489C.pdf.

[56] M. E. R. Laboratories, A. F. Molisch, and J. R. F. Tr, “Channel Models for Ultrawideband Personal Area Networks,” *IEEE wireless communications.*, no. December, pp. 14–21, 2003.

[57] K. Pothuganti and A. Chitneni, “A Comparative Study of Wireless Protocols : Bluetooth, UWB, ZigBee, and Wi-Fi,” *IECON Proc. (Industrial Electron. Conf.*, no. January 2014, pp. 46–51, 2014.

[58] Decawave, “DWM1000 Product Overview,” 2016. [Online]. Available:

https://www.decawave.com/sites/default/files/resources/DWM1000-Datasheet-V1.6.pdf.

[59] Freescale, “XS110 UWB Solution for Media-Rich Wireless Applications,” 2004 [Online]. Available: http://www.uta.edu/rfmems/Telemetry/UWB/UWBFS.pdf.

[60] A. Augustin, J. Yi, T. Clausen, and W. M. Townsley, “A study of Lora: Long range & low power networks for the internet of things,” *Sensors (Switzerland)*, vol. 16, no. 9, pp. 1–18, 2016.

[61] M. Cattani, C. A. Boano, and K. Römer, “An Experimental Evaluation of the Reliability of LoRa Long-Range Low-Power Wireless Communication,” *J. Sens. Actuator Networks*, vol. 6, no. 2, p. 7, 2017.

[62] Semtech, “LoRa^{TM}Modulation Basics Semtech,” 2015. [Online]. Available: https://www.semtech.com/uploads/documents/an1200.22.pdf.

[63] U. Noreen, A. Bounceur, and L. Clavier, “A study of LoRa low power and wide area network technology,” *2017 International Conference on Advanced Technologies for Signal and Image Processing (ATSIP).*, pp. 1–6, 2017.

[64] Anupriya, K., Jerrin Yomas, and S. E. Jubin, “A review on IoT protocols for long distance and low power,” *Int. J. Eng. Sci. Technol*, vol. 5, no. 6, pp. 344–347, 2015.

[65] Microchip, “MICROCHIP RN2483 Low-Power Long Range LoRa® Technology Transceiver Module,” 2019. [Online]. Available: http://ww1.microchip.com/downloads/en/devicedoc/50002346c.pdf.

[66] Semtech, “SEMTECH SX1272/73 - 860 MHz to 1020 MHz Low Power Long Range Transceiver,” 2019. [Online]. Available: https://www.semtech.com/uploads/documents/SX1272_DS_V4.pdf.

[67] LPRS, “easyRadio easyRadio Advanced eRIC-LoRa Long Range Datasheet,” 2018. [Online]. Available: http://www.lprs.co.uk/assets/files/eRIC_LoRa_Datasheet_1v1.pdf.

[68] A. H. El Ahmadi Cheikh, Mostafa Baghouri, “Efficiency Evaluation Metrics for Wireless Intelligent Sensors Applications,” *arXiv Prepr. arXiv*, vol. 1409, p. 7109, 2014.

[69] R. Monthéard *et al.*, “Powering a commercial datalogger by energy harvesting from generated aeroacoustic noise,” *J. Phys. Conf. Ser.*, vol. 557, no. 1, 2014.

[70] Linear Technology Corporation, “LTC5800-IPM - SmartMesh IP Node 2.4GHz 802.15.4e Wireless Mote-on-Chip,” 2013. [Online]. Available: https://www.analog.com/media/en/technical-documentation/data-sheets/5800ipmfa.pdf.

[71] J. Hsu, S. Zahedi, A. Kansal, M. Srivastava, and V. Raghunathan, “Adaptive duty cycling for energy harvesting systems,” *Proceedings of the 2006 international symposium on Low power electronics and design.,* ACM, pp. 180–185, 2006.

[72] R. Torah, P. Glynne-Jones, J. Tudor, T. O’Donnell, S. Roy, and S. Beeby, “Self-powered autonomous wireless sensor node using vibration energy harvesting,” *Meas. Sci. Technol.*, vol. 19, no. 12, p. 125202, 2008.

[73] H. Ba, I. Demirkol, and W. Heinzelman, “Passive wake-up radios: From devices to applications,” *Ad Hoc Networks*, vol. 11, no. 8, pp. 2605–2621, 2013.

[74] S. Misra, M. Pavan Kumar, and M. S. Obaidat, “Connectivity preserving localized coverage algorithm for area monitoring using wireless sensor networks,” *Comput. Commun.*, vol. 34, no. 12, pp. 1484–1496, 2011.

[75] M. Minami, T. Morito, H. Morikawa, and T. Aoyama, “Solar biscuit: A battery-less wireless sensor network system for environmental monitoring applications,” *The 2nd international workshop on networked sensing systems.*, p. 2007, 2005.

[76] M. Y. Cheng, Y. Bin Chen, H. Y. Wei, and W. K. G. Seah, “Event-driven energy-harvesting wireless sensor network for structural health monitoring,” *Proc. - Conf. Local Comput. Networks, LCN*, pp. 364–372, 2013.

[77] Q. Tang, Q. He, M. Li, C. Dong, D. Xu, and X. Li, “Wireless Alarm Microsystem Self-Powered by Vibration-Threshold-Triggered Energy Harvester,” *IEEE Trans. Ind. Electron.*, vol. 63, no. 4, pp. 2447–2456, 2016.

[78] Maraiya, K., Kant, K., & Gupta, N, “Wireless sensor network: a review on data aggregation,” *International Journal of Scientific & Engineering Research., 2*(4), pp.1-6 2011.

[79] N. Kimura and S. Latifi, “A survey on data compression in wireless sensor networks,” *International Conference on Information Technology: Coding and Computing (ITCC'05)*., pp. 8-13 Vol. 2, 2008.

[80] S. Cui, A. J. Goldsmith, and A. Bahai, “Energy-constrained Modulation Optimization,” *IEEE Trans. Wirel. Commun.*, vol. 4.5, pp. 2349–2360, 2005.

[81] F. M. Costa and H. Ochiai, “A comparison of modulations for energy optimization in wireless sensor network links,” *GLOBECOM - IEEE Glob. Telecommun. Conf.*, pp. 1–5, 2010.

[82] G. J. Pappas *et al.*, “ATPC: Adaptive Transmission Power Control for Wireless Sensor Networks,” *ACM Trans. Sens. Networks*, vol. 12, no. 1, pp. 1–31, 2016.

[83] L. H. A. Correia and J. M. S. Nogueira, “Transmission power control

techniques for wireless sensor networks," *NOMS 2008 - IEEE/IFIP Netw. Oper. Manag. Symp. Pervasive Manag. Ubiquitous Networks Serv.*, vol. 51, pp. 1049–1054, 2008.

[84] Xiaoyu Chu and H. Sethu, "Cooperative topology control with adaptation for improved lifetime in wireless ad hoc networks," *2012 Proc. IEEE INFOCOM*, pp. 262–270, 2012.

[85] E. Kranakis, D. Krizanc, and E. Williams, "Directional Versus Omnidirectional Antennas for Energy Consumption and k-Connectivity of Networks of Sensors," *International Conference On Principles Of Distributed Systems.,* pp. 357–368, 2004.

[86] H. N. Dai, "Throughput and delay in wireless sensor networks using directional antennas," *ISSNIP 2009 - Proc. 2009 5th Int. Conf. Intell. Sensors, Sens. Networks Inf. Process.*, pp. 421–426, 2009.

[87] A. P. Subramanian and S. R. Das, "Addressing deafness and hidden terminal problem in directional antenna based wireless multi-hop networks," *Wirel. Networks*, vol. 16, no. 6, pp. 1557–1567, 2010.

[88] D. Kumar, T. C. Aseri, and R. B. Patel, "EEHC: Energy efficient heterogeneous clustered scheme for wireless sensor networks," *Comput. Commun.*, vol. 32, no. 4, pp. 662–667, 2009.

[89] H. Li, Y. Liu, W. Chen, W. Jia, B. Li, and J. Xiong, "COCA: Constructing optimal clustering architecture to maximize sensor network lifetime," *Comput. Commun.*, vol. 36, no. 3, pp. 256–268, 2013.

[90] A. M. Abdal-Kadhim and K. S. Leong, "Electrical power flow of typical wireless sensor node based on energy harvesting approach," *Int. J. Electron. Lett.*, vol. 00, no. 00, pp. 1–11, 2018.

[91] C. Zhang, X. F. He, S. Y. Li, Y. Q. Cheng, and Y. Rao, "A wind energy

powered wireless temperature sensor node," *Sensors (Switzerland)*, vol. 15, no. 3, pp. 5020–5031, 2015.

[92] F. Fei, J. D. Mai, and W. J. Li, "A wind-flutter energy converter for powering wireless sensors," *Sensors Actuators, A Phys.*, vol. 173, no. 1, pp. 163–171, 2012.

[93] Y. Ma, Q. Ji, S. Chen, and G. Song, "An experimental study of ultra-low power wireless sensor-based autonomous energy harvesting system," *Journal of renewable and sustainable energy.*, vol. 9, no. 5, p.054702, 2017.

[94] ROHM SEMICONDUCTOR, "Datasheet Standard CMOS Voltage Detector IC BD48xxx series BD49xxx series," 2013. [Online]. Available: https://www.rohm.com/datasheet/BD48L41G/bd48xxg-e.

[95] Linear Technology Corporation, "LTC3588-1 Datasheet (Rev. B)," 2010. [Online]. Available: https://www.analog.com/media/en/technical-documentation/data-sheets/35881fc.pdf.

[96] S. Chamanian, S. Baghaee, H. Ulusan, O. Zorlu, E. Uysal-Biyikoglu, and H. Kulah, "Implementation of Energy-Neutral Operation on Vibration Energy Harvesting WSN," *IEEE Sens. J.*, vol. 19, no. 8, pp. 3092–3099, 2019.

[97] J. Yick, B. Mukherjee, and D. Ghosal, "Wireless sensor network survey," *Computer networks*, vol. 52, no. 12, pp. 2292–2330, 2008.

[98] Analog Devices, "Accelerometer ADXL335," 2010. [Online]. Available: https://www.analog.com/media/en/technical-documentation/data-sheets/ADXL335.pdf.

[99] Honeywell, "HIH-5030/5031 Series," 2010. [Online]. Available: https://sensing.honeywell.com/honeywell-sensing-hih5030-5031-series-

product-sheet-009050-2-en.pdf.

[100] N. Semiconductors, “IEEE 802.15.4 Stack User Guide v2.6,” 2016. [Online]. Available: https://www.nxp.com/docs/en/user-guide/JN-UG-3024.pdf.

[101] I. Standard, “IEEE Standard for Part 15 . 4 : Wireless Medium Access Control (MAC) and Physical Layer (PHY) Specifications for Low-Rate Wireless Personal Area Networks (WPANs),” *Local Metrop. Area Neworks*, pp. 1–26, 2003.

[102] N. Semiconductors, “JN5148-EK010 Evaluation Kit User Guide,” 2013. [Online]. Available: http://www.glynstore.com/content/docs/jennic/JN-UG-3062-JN5148-EK010-User-Guide.pdf.

[103] N. Semiconductors, “Software Developer’s Kit Installation and User Guide,” 2010. [Online]. Available: https://www.nxp.com/docs/en/user-guide/JN-UG-3064.pdf.

[104] N. Semiconductors, “JN51xx Integrated Peripherals API User Guide,” *System*, 2011. [Online]. Available: http://www.bocon.com.cn/artupfile/2013-12-20/20131220020020019105.pdf.

[105] N. Semiconductors, “JN51xx Flash Programmer User Guide,” 2012. [Online]. Available: https://www.nxp.com/docs/en/user-guide/JN-UG-3007.pdf.

[106] Keithley, “Multi-Channel USB and USB / GPIB Programmable DC Power Supplies,” 2013. [Online]. Available: https://www.mouser.com/ds/2/403/2220_2230DataSheet_0-934564.pdf.

[107] Keithley Instruments Inc, “Series 2600B System SourceMeter ® Instruments,” 2013. [Online]. Available:

https://static.rapidonline.com/pdf/1164906_an_en_01.pdf.

[108] A. S. Weddell, M. Magno, G. V. Merrett, D. Brunelli, B. M. Al-Hashimi, and L. Benini, “A Survy of Multi-Source Energy Harvesting Systems,” *2013 Design, Automation & Test in Europe Conference & Exhibition (DATE).*, pp. 905–908, 2013.

[109] Wilkie, W. K., Bryant, G. R., High, J. W., Fox, R. L., Little, B. D., Mirick, P. H., ... & Jalink, A, “NASA Langley Research Center Macro-Fiber Composite Actuator (LaRC-MFC): Technical Overview,” 2007. [Online]. Available: https://ntts-prod.s3.amazonaws.com/t2p/prod/t2media/tops/pdf/LAR-TOPS-209.pdf.

[110] M. Pozzi, S. Guo, and M. Zhu, “Harvesting energy from the dynamic deformation of an aircraft wing under gust loading,” *Heal. Monit. Struct. Biol. Syst. 2012*, vol. 8348, no. April 2012, p. 834831, 2012.

[111] A. Giuliano, V. Marsic, and M. Zhu, “Implementation and testing of an elastic strain powered wireless sensing system for energy-autonomous applications,” *2012 IEEE International Conference on Green Computing and Communications*, pp. 681–684, 2012.

[112] Z. J. Chew and M. Zhu, “Microwatt power consumption maximum power point tracking circuit using an analogue differentiator for piezoelectric energy harvesting,” *J. Phys. Conf. Ser.*, vol. 660, no. 1, 2015.

[113] Linear Technology Corporation, “LTC2935, Ultra-Low Power Supervisor with Power-Fail Output, Selectable Thresholds,” *Technology*, 2007. [Online]. Available: https://www.analog.com/media/en/technical-documentation/data-sheets/2935fa.pdf.

[114] Linear Technology Corporation, “DC9000 SmartMesh IP Starter Kit.” , 2016. [Online]. Available: https://www.analog.com/media/en/technical-

documentation/product-information/2PB_DC9000fc.pdf.

[115] T. Watteyne, J. Weiss, L. Doherty, and J. Simon, “Industrial IEEE802.15.4e networks: Performance and trade-offs,” *IEEE Int. Conf. Commun.*, vol. 2015-Septe, no. April 2012, pp. 604–609, 2015.

[116] A. Somov, Z. J. Chew, T. Ruan, M. Zhu, and S. P. Platt, “Ultra-low-power RADFET sensing circuit for wireless sensor networks powered by energy harvesting,” *Proc. IEEE Sensors*, pp. 1–3, 2017.

[117] Tyndall National Institute, “TY1003 Technical Data,” 2015. [Online]. Available: https://www.tyndallworks.com/contentfiles/P-Channel-RADFET-1003-DS.pdf.

[118] M. Chew, ZJ; Tuddenham, SB; Zhu, “Airflow energy harvesting with high wind velocities for industrial applications,” *J. Phys. Conf. Ser*, vol. 773, p. 12091, 2016.

[119] Linear Technology Corporation, “SmartMesh IP User ’ s Guide.” 2016. [Online]. Available: https://www.analog.com/media/en/technical-documentation/user-guides/SmartMesh_IP_User_s_Guide.pdf.

[120] Linear Technology Corporation, “SmartMesh IP Manager API Guide.” 2016. [Online]. Available: https://www.analog.com/media/en/reference-design-documentation/design-notes/SmartMesh_IP_Mote_Serial_API_Guide.pdf.

[121] Linear Technology Corporation, “SmartMesh IP Tools Guide.” 2016. [Online]. Available: https://www.analog.com/media/en/technical-documentation/user-guides/SmartMesh_IP_Tools_Guide.pdf.